Man-made noise measurement programme

Article *in* IEE Proceedings - Communications · July 2005

DOI: 10.1049/ip-com:20045025 · Source: IEEE Xplore

2 authors, including:

Adrian Wagstaff
MASS Consultants Ltd
5 PUBLICATIONS **26** CITATIONS

SEE PROFILE

Man-Made Noise Measurement Programme (AY4119)

Final Report

Issue 2

September 2003

Prepared By:

A J Wagstaff	N Merricks
Principal Consultant	Consultant

Approved By:

M W Biggs
Project Manager

Authorised By:

M J Ashman
Real-Time Systems Manager

Mass Consultants Limited
Grove House, Rampley Lane
Little Paxton, St Neots, Cambs PE19 6EL
National Tel: 01480 222600 Fax: 01480 407366
International Tel: +44 1480 222600 Fax: +44 1480 407366
E-mail: systems@mass.co.uk

EXECUTIVE SUMMARY

The background noise level of the electromagnetic spectrum in the 40 MHz to 3 GHz region is dominated by Man-Made Noise (MMN) produced by a wide variety of equipment. Electric motors, car ignition systems, neon lights and many other devices produce sparks as part of their normal mode of operation. These spark discharges radiate across a wide frequency range and can interfere with radio receivers; the effects worsening as receiver bandwidth is increased. As well as these impulsive noise sources, there are also a great many (intentional and unintentional) sources of narrowband signals. Television viewers and radio listeners regularly experience the effects of MMN, although they don't always recognise it as such.

Measuring the level of the MMN activity can give useful information to receiver designers, researchers and to those concerned with allocating the RF spectrum. Currently the levels of MMN are documented in the ITU-R recommendation [P.372]. The graphs in that document are based on measurements made in the 1970s and earlier using narrowband equipment in the United States. Because technology has moved on considerably since then and because Electromagnetic Compatibility (EMC) regulations have changed, there is concern that the [P.372] document may now be out-of-date and even misleading. Such concerns can only be addressed by measuring today's MMN levels in the UK.

A feasibility study was commissioned by the RA in 2001 to look at the state of MMN research and identify a way forward. That study ([Shukla01]) reported that [P.372] should be updated and that, in order to do so, a new, wider bandwidth measurement system could be built, based on disk array recorder technology. The RA subsequently commissioned the present study to build the measurement system and set it to work via eight one-day surveys.

The present programme of work included the building of a Noise Measurement Facility (NMF), which allows the Intermediate Frequency (IF) output of a spectrum analyser to be digitised and recorded on a disk array. The IF can then be analysed via a suite of C++ programs and MATLAB scripts. This approach has yielded some surprising and interesting results.

The recorded MMN data can be analysed in many different ways. The majority of our analysis has been based on using the Amplitude Probability Distribution (APD), which is a graphical representation of the amount of received power in the environment. From these graphs we have estimated the power levels of the MMN after assuming that it comprises two dominant and distinct components: White Gaussian Noise (WGN) and Impulsive Noise (IN).

The distinction between WGN and IN is an important concept in MMN studies and they have quite different characteristics. It is important to recognise that they are only statistical models and that the measured MMN sometimes exhibits features that are not included in these models. Nonetheless, the WGN and IN models allow MMN levels to be measured and documented via ITU-R recommendations.

Our findings suggest that the majority of the overall MMN noise power, in all environments, is contained in the WGN component and that this appears to be higher than [P.372] would suggest.

For many purposes it is the level and characteristics of IN that are significant and this is not well documented in [P.372]. We have found that a first-order model of the IN can be used to effectively characterise the IN, in a form that would be suitable for use in the ITU-R standard. This model captures the most important aspects of the IN by just using a mean and standard deviation. There is even a suggestion that the mean IN voltage density alone may be sufficient for many purposes.

This report therefore describes the progress made during this study and outlines ideas for further work.

CONTENTS

LIST OF FIGURES

ACKNOWLEDGEMENTS

MASS would like to thank Neil Waby, John Airs, David Bacon, David Eden and Tom Marten of the Radiocommunications Agency for their contributions to this study, including the use of the RA van and the anechoic chamber at Whyteleafe.

Many thanks to Chris Jenkins of Arrow Electronics for kindly arranging access to their plant in Bedford and also for the use of his back garden in Blunham. Similarly, our gratitude is extended to the IEE for the use of their headquarters in London.

1 INTRODUCTION

This final report covers the activities conducted by Mass Consultants Ltd. under contract AY4119 for the Radiocommunications Agency (RA). The programme has involved building a wideband measurement system and using it to measure the levels of Man Made Noise (MMN) at a number of sites in the UK.

The Noise Measurement Facillity (NMF) allows the Intermediate Frequency (IF) output from a spectrum analyser to be digitised and recorded onto a disk array. The NMF allows approximately 3 hours of IF to be recorded with a maximum bandwidth of 10 MHz.

Analysis of the data has been performed using a suite of C++ programs and MATLAB scripts. This report summarises our findings, comparing the MMN levels at the different locations and across the spectrum.

An approach to simulating MMN is described, together with representative levels for each kind of environment. This uses a simplified model with just two components: WGN and class B IN.

The main body of this report is broken down as follows:

Section 2	Literature Review
Section 3	Noise Environment Measurement
Section 4	Theory and Modelling
Section 5	Results
Section 6	Conclusions
Section 7	Further Work

The remainder of the document covers the abbreviations, definitions and references.

2 LITERATURE REVIEW

The electromagnetic noise environment results from the combination of a number of different types of source. Figure 1 is taken from [Hagn] and shows a classification of these sources.

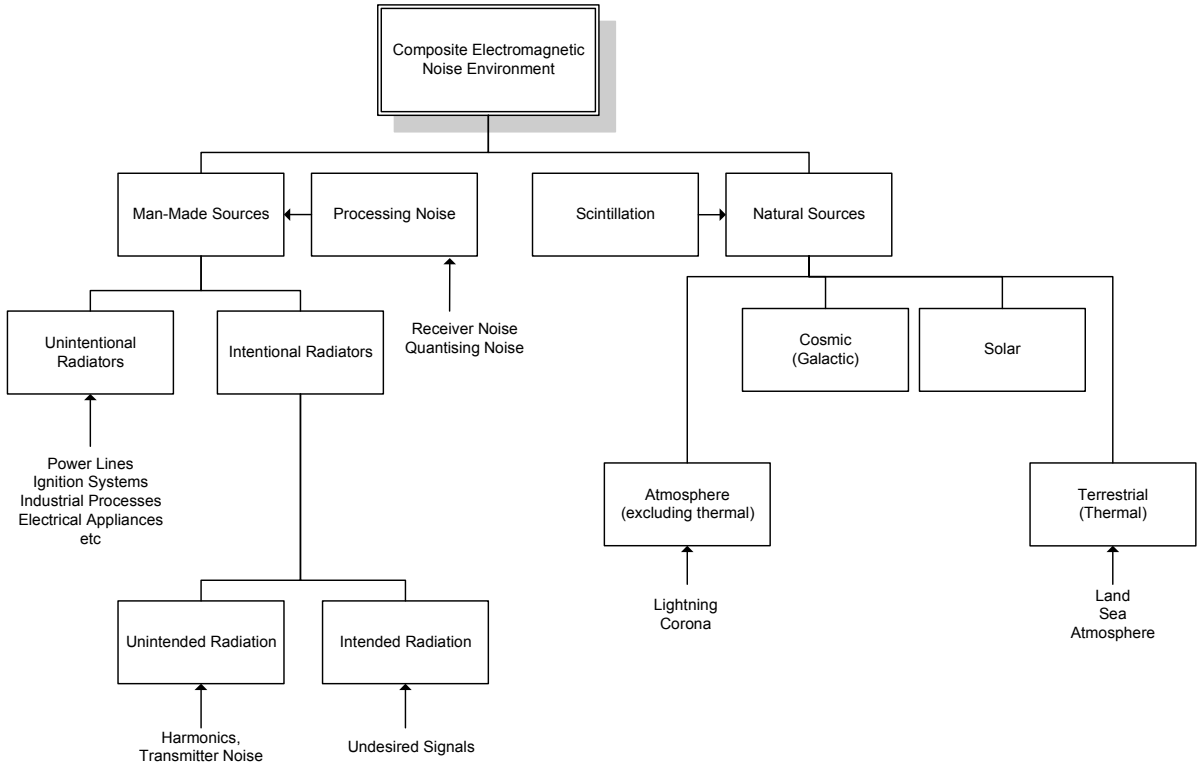

Figure 1 Electromagnetic Noise Sources

Thus, the electromagnetic noise environment results from a combination of intentional and unintentional, man-made and natural sources.

The proportion of each type of noise observed depends on antenna pointing angle (if directional) and frequency. Furthermore, the receiver noise figure and measurement bandwidth have large effects on the absolute and relative levels of noise observed.

Noise sources are not evenly distributed across the spectrum. Figure 2 shows how, at lower frequencies, atmospheric radio noise is the dominant source. Galactic, solar and sky noise noise can all be detected in addition to MMN. In the VHF and UHF regions, the Man Made Noise sources tend to dominate, so these regions are easier for studying MMN levels.

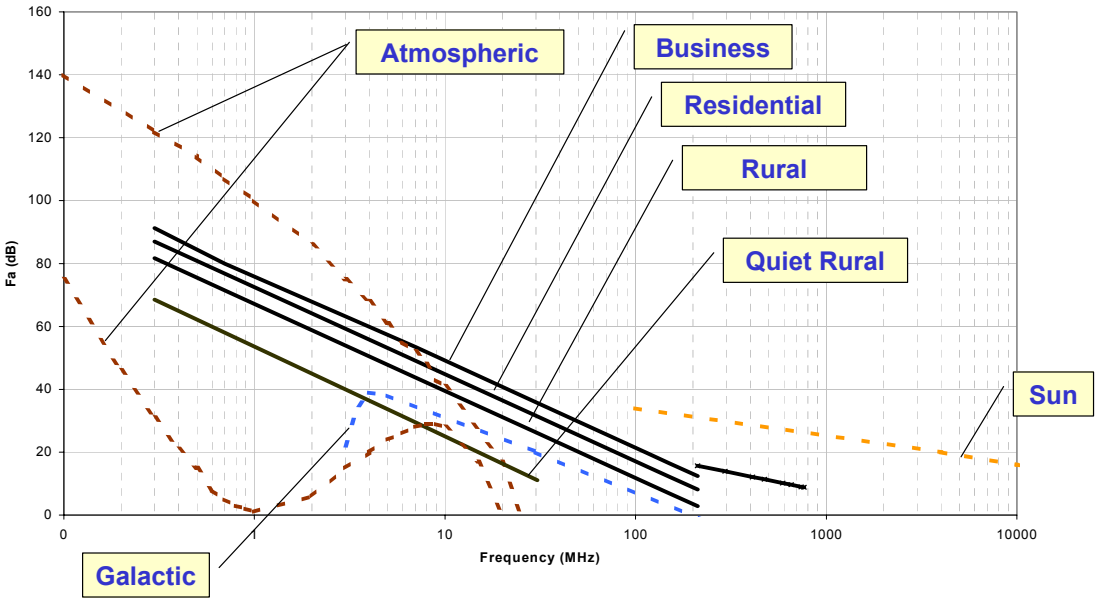

Figure 2 Noise distribution with Frequency

The levels in Figure 2 are taken from the ITU-R recommendation [P.372], which contains descriptions of the various types of electromagnetic noise.

The black lines are the current, standard levels of WGN due to MMN. It will be seen that these are categorised by the ITU-R are Business, Residential, Rural and Quiet Rural. The Business category is described with two lines and a breakpoint at about 200 MHz.

2.1 MAN-MADE NOISE MODELS

The noise model developed by Middleton in [Middleton75], [Middleton76], [Middleton78a] and [Middleton78b] is perhaps the most comprehensive theory of electromagnetic man-made noise currently in use. This work uses a mathematical description of the underlying physical processes involved in noise generation to aggregate the total noise environment present at a particular location. Although attractive due to its description of a noise environment in terms of physically significant parameters (such as emitter density), the model is very complex and this limits its usefulness in practical applications

Middleton's model considers electromagnetic noise as two main components: White Gaussian Noise (WGN) and Impulsive Noise (IN). The IN is further classified by Middleton as comprising that which could interfere with typical receiver systems in different ways:

Class A	Interference is spectrally comparable to, or less than, the IF filter of the receiver being considered. Class A noise may be thought of as structured noise, possibly generated by communication systems, which is probably not of interest to the receiver being considered.
Class B	Interference is broadband compared to the IF filter of the receiver being considered. Class B noise is typically made up of very short impulses that are very wideband and are frequently man-made in origin. The class includes impulses from automotive ignition circuits, thermostats, lighting, etc.
Class C	This is the sum of class A and class B interference.

Many other papers have been published casting varying degrees of light on the analytical study of man-made noise, some addressing quite specific aspects of the analysis. Particularly relevant are Spaulding's paper on bandwidth scaling [Spaulding62] and Sheikh's investigation of frequency dependence [Sheikh83].

Other works describe the analysis methods in more general terms, notably Parsons [Parsons92], Jeruchim et al. [Jeruchim92] and the feasibility study by DERA [Shukla01]. Most relevant to the present study however is [Achatz98] by the National Telecommunications and Information Administration (NTIA) in which they develop a simplification of the Middleton noise model that takes just the class A and B definitions. This model has been reviewed and is believed to provide a strong basis on which to carry out noise analysis and modelling for class B noise. The emphasis is on the use of APD graphs to derive statistics in a form suitable for computer simulation. These statistics are readily documented via the ITU [P.372] recommendation and suggest that the majority of man-made noise in the environment is class B in nature. Rather than use the Middleton approach of considering the underlying physics of the noise, the NTIA make the assumption

that the noise can be modelled by simply fitting known functions to measured data and the parameters of those functions become the measure of that environment.

[Achatz98] provides a clear and concise introduction to the theoretical analysis of noise signals. The notation used in that report has been adopted throughout this report.

2.2 MAN-MADE NOISE MEASUREMENTS

Studies that have attempted to characterise the electromagnetic environment have been reviewed and compared with the results of the present study.

The most up-to-date of these are published by the NTIA ([Achatz98] and [Achatz01]) in which both the WGN and IN noise environments are characterised. They use a measurement bandwidth of around 30kHz over a range of frequencies and locations. The emphasis is on the use of the Amplitude Probability Distribution (APD) and parameters obtained by curve fitting to such graphs.

Another important source of MMN measurements has been those made by Parsons. These were dominated however by pulse counting methods and narrow bandwidth receivers. This approach tended to bias the results, as it ignored the WGN and other components of the MMN, as well as seeing only the strongest impulses. The emphasis was on vehicular noise and results tended to be presented in terms of Noise Amplitude Distribution (NAD) graphs, which are cumbersome to compare between surveys. NAD graphs can be useful in some cases, but are potentially misleading and should be used with care.

Other common graphical representations of MMN have been the Pulse Interval Distribution (PID), Pulse Duration Distribution (PDD) and Average Crossing Rate (ACR). Each of these has its uses, but should be used with care, especially when trying to convert to different bandwidths. Section 3.1.2 gives descriptions of the various graphical representations in common use.

In this study we have analysed the WGN and IN components, but have not yet considered the other components. The measured levels of WGN are compared with those given in [P.372], which is currently the definitive description of MMN characteristics. Also, a more succinct approach to IN measurement is presented that should make it easier to compare IN levels in future surveys.

3 NOISE ENVIRONMENT MEASUREMENT

This section describes the NMF hardware and software and also the surveys carried out during this study.

3.1 NOISE MEASUREMENT FACILITY

The NMF has been designed, built, tested and set to work during this programme. It is based on the MASS DART-30 recording system and uses a spectrum analyser as a receiver. Programs have been written that allow the data to be statistically analysed to extract the MMN characteristics. The data processing is described in Section 3.1.2.

3.1.1 Hardware

The equipment used in the NMF (Figure 3) comprises:

- Schaffner bilog CBL6143 antenna
- 5m RF cable
- Rohde & Schwarz FSU3 spectrum analyser
- IF cable
- DART-30 recording system, which includes a 12-bit 30 MS/s ADC card and a 700 GB RAID disk array
- Laptop PC (for field work)
- Desktop PC (for analysis) with LTO tape drive

The system uses the 20.4 MHz IF output from the spectrum analyser and allows for a range of bandwidth settings, up to a maximum of 10 MHz. This output is spectrally inverted throughout the analyser's RF range, which extends from 20 Hz to 3.6 GHz. The spectrum analyser has a 20 dB RF pre-amplifier, which should always be used when taking noise measurements in order to minimise the system noise figure, which is typically 4 dB. A block diagram of the NMF is shown in Figure 4.

Figure 3 NMF Hardware

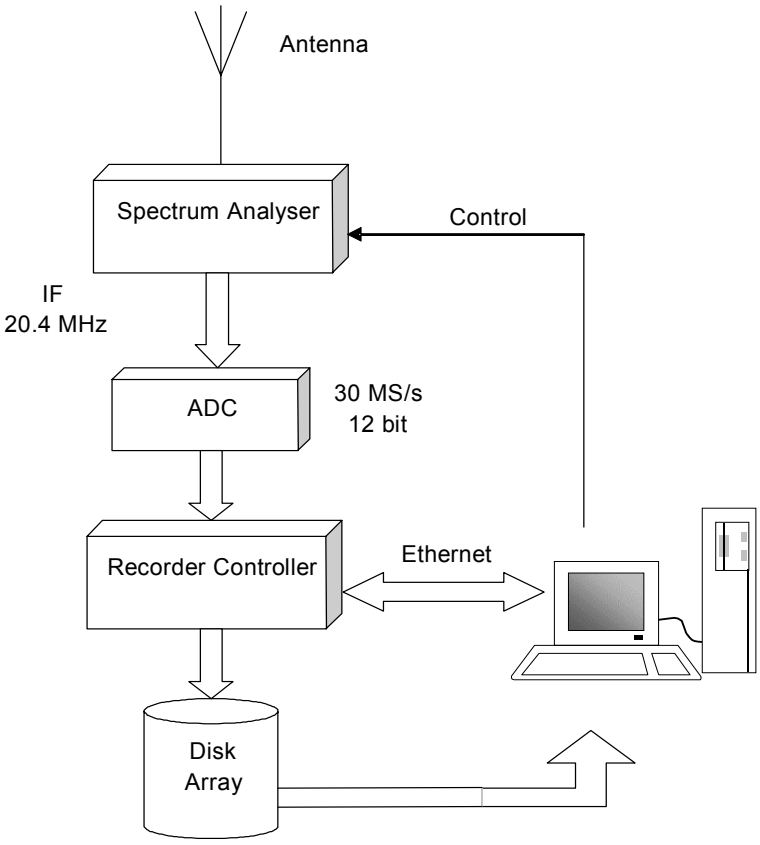

Figure 4 NMF Block Diagram

The sampling scheme used in the NMF is illustrated in Figure 5. Undersampling is used to 'fold' the IF output, which ranges across 20.4 ± 5 MHz, down to a baseband range of 9.6 ± 5 MHz.

This scheme has the advantage that there is no need to downconvert the IF to baseband and, at the same time, helps to reduce the data storage requirements. Furthermore, there are two spectrum inversions, which ensures that the baseband spectrum is upright and therefore readily examined by Fourier transform analysis.

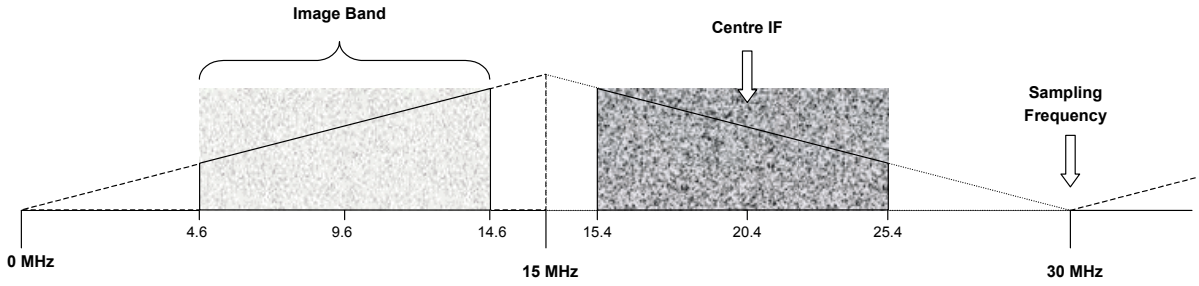

Figure 5 NMF Sampling Scheme

The raw data has been archived onto LTO tapes for future reference. Each tape holds 100 GB uncompressed or approximately 200 GB compressed.

3.1.2 Software and Data Processing

The NMF software comprises a suite of programs that allow the user to record digitised IF, archive it to tape and analyse it statistically. Figure 6 is an example of the main test controller used when making recordings.

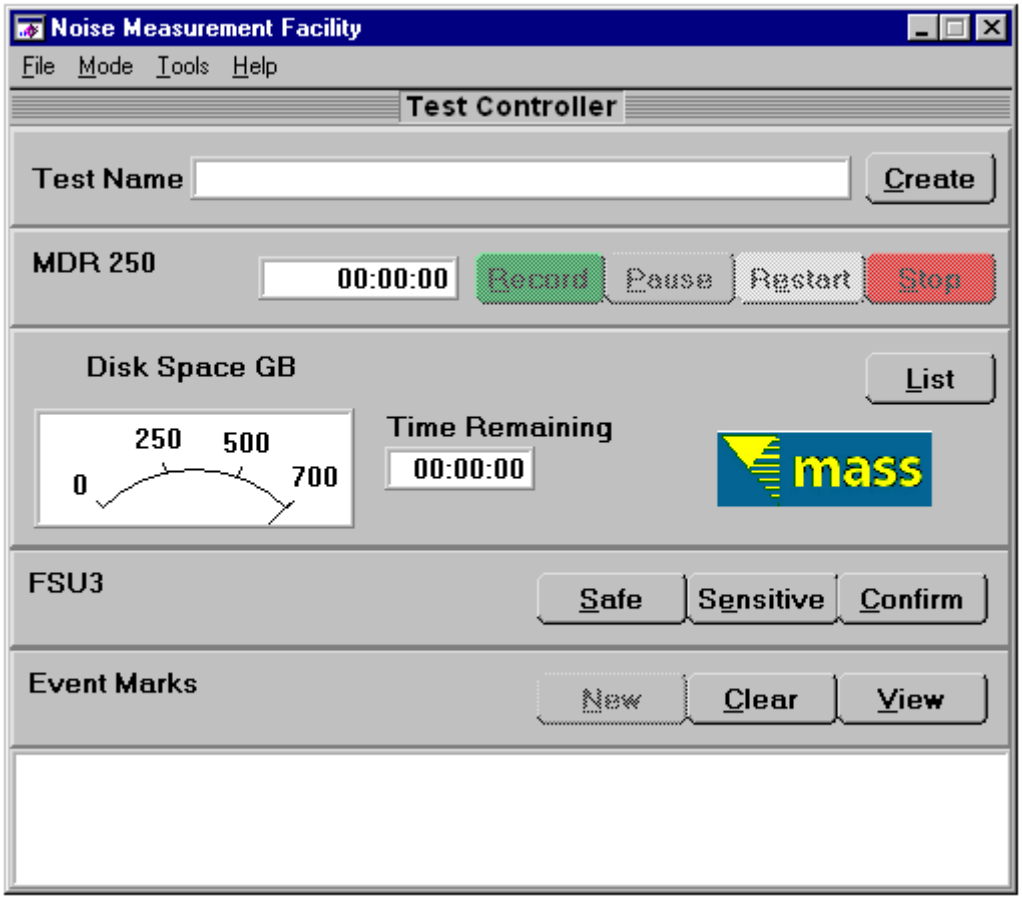

Figure 6 Test Controller Window

For convenience of data handling, each recording is 30 seconds long, which gives file sizes of just under 2 GB. These can be read into C++ programs or MATLAB routines. As described below, all the files from the survey have been processed to create smaller files that can be used to draw APD graphs and NAD graphs.

3.1.2.1 Amplitude Demodulation

Each binary file is first amplitude demodulated to obtain the voltage amplitude of the IF. There are many GB of data and so a simple, fast demodulation algorithm was devised to perform this task. Figure 7 is an example of how this fast 'maximum riding' algorithm compares with IQ and Hilbert demodulation.

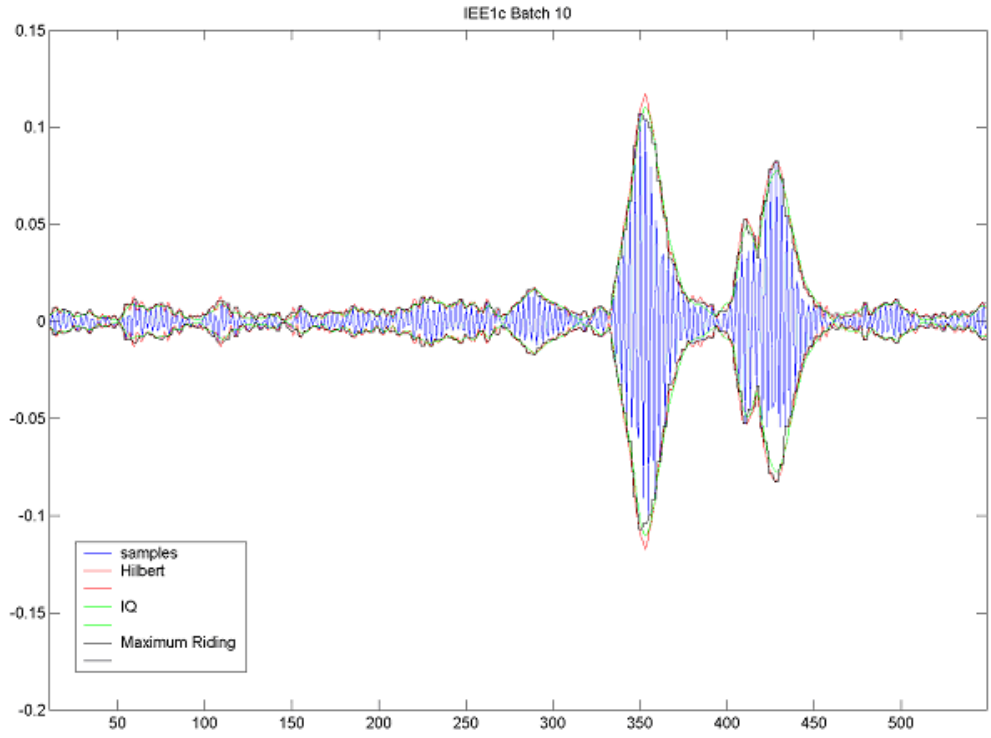

Figure 7 Comparison of Demodulator Outputs

3.1.2.2 Histograms

The demodulated data are quantised in the range 0 to 2047, corresponding to the positive 12-bit ADC levels. These data are then histogrammed, the results being stored in files, one for each recording.

These histograms (e.g. Figure 8) are simply representations of how often each voltage amplitude occurs during a recording.

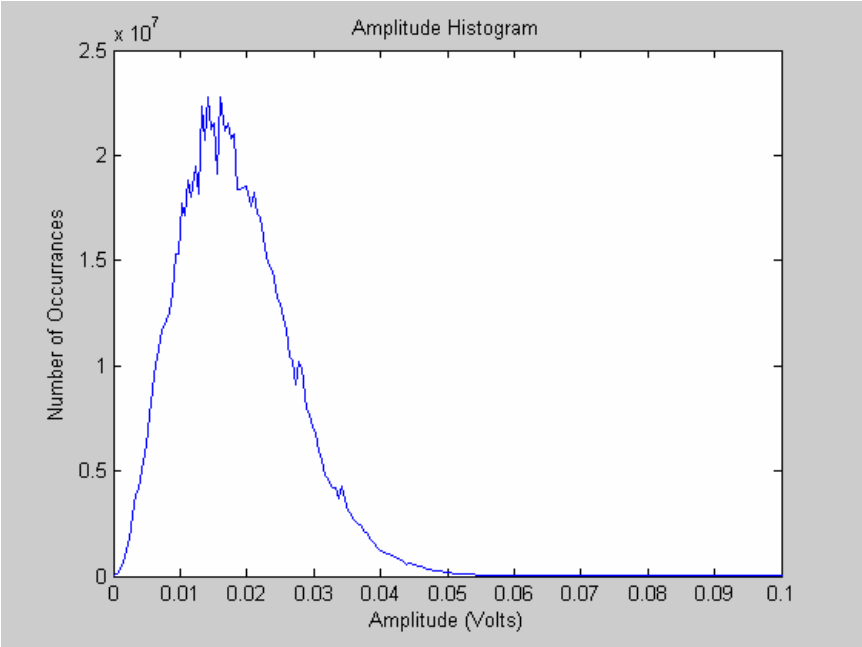

Figure 8 Example of an amplitude histogram

3.1.2.3 APD Graphs

APD graphs (e.g. Figure 9) can be produced from the histogram files. The APD is a way of displaying the cumulative histogram such that Rayleigh and power Rayleigh distributions appear as straight lines, which is convenient for noise analysis. The theory behind the APD representation is explored in Section 4.

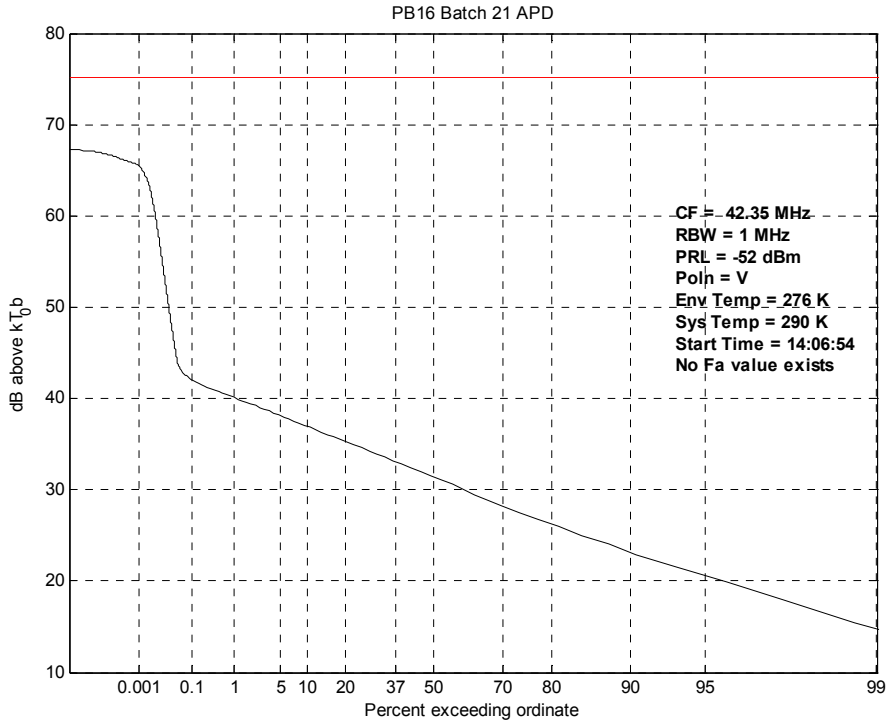

Figure 9 Typical Amplitude Probability Distribution (APD) graph

It is important to understand the scaling of the APD. The horizontal scale (abscissa) shows the probability of exceeding a given power on the vertical scale (ordinate).

The ordinate scaling is in terms of power relative to the thermal noise level and is therefore proportional to bandwidth. It is therefore 'correct' for the WGN power, which scales linearly with bandwidth. WGN appears as a downward sloping line on the right hand side of the APD.

IN, on the other hand, appears as the raised section on the left hand side of the APD. The power in the IN is proportional to the square of bandwidth, so this section will be more pronounced if the measurements have been made with a wider bandwidth.

The far left hand end of the APD has a plateau region, which represents very low probability, high amplitude IN. This region has not been used in our analyses.

The FSU3 spectrum analyser incorporates APD-like displays and these were evaluated for their usefulness during the study.

Two standard displays are available:

- APD (Amplitude Probability Distribution)
- CCDF (Complementary Cumulative Distribution Function)

The former display plots the probability of occurrence against the amplitude level and the latter plots the probability that the mean signal power will be exceeded.

From these definitions, there is an immediate source of potential confusion in that the APD graphs used in MMN analysis are analogous to the FSU3's CCDF display and not the APD display. The APD display on the analyser is the probability distribution rather than the cumulative distribution.

An example of the CCDF display is shown in Figure 10.

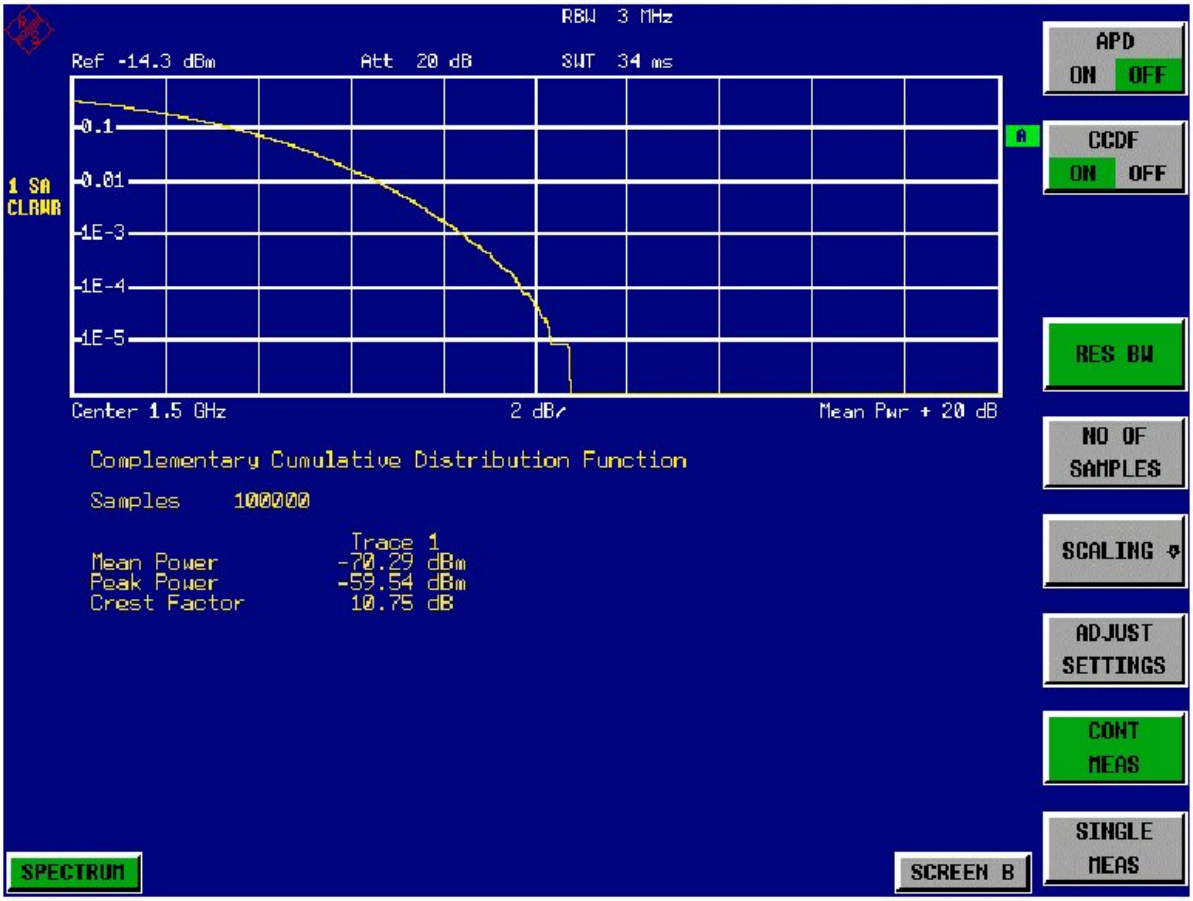

Figure 10 Example of FSU3 CCDF Display

The FSU3's CCDF display is not Rayleigh scaled, so the WGN appears as a curved line rather than a straight line. The axes are also swapped, but this is not a problem for its interpretation.

It would require a much longer memory for the CCDF display to be useful for making measurements of MMN.

This display was not used for making measurements during the study. With modification, however, it could form the basis of real-time analysis functions in future measurement systems.

3.1.2.4 Pulse Extraction

Pulse Descriptor Words (PDW) are extracted from the binary data by amplitude demodulating and applying a detection threshold obtained by inspection of the APD graph. The PDW is a collection of three numbers characterising pulse Time Of Arrival (TOA), Pulse Amplitude (PA) and Pulse Width (PW).

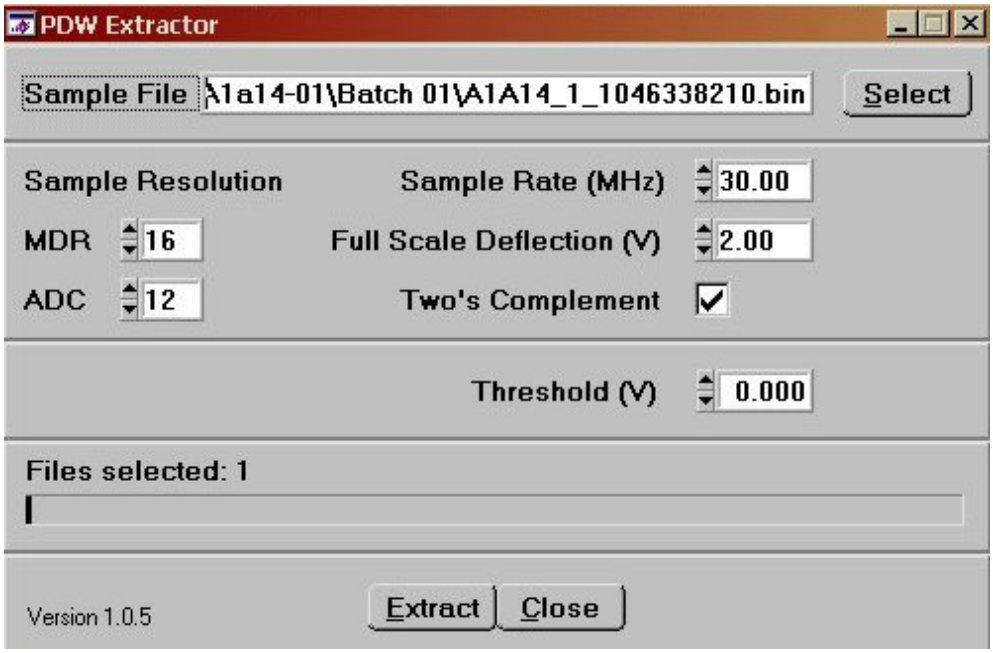

Figure 11 PDW Extractor Program

The PDWs are generated by a 'pulse extractor' application (Figure 11), which looks through the raw data for samples with amplitudes above a user-defined threshold. These are assumed to be class B impulses.

3.1.2.5 NAD Graphs

The resulting PDW files can be used to generate NAD graphs (e.g. Figure 12). The abscissa of the NAD is the impulse rate and the ordinate is the spectrum amplitude in units of dB(μV/MHz). If the impulses are assumed to be class B, then this ordinate scaling is correct for the IN component of the MMN, because the IN voltage is proportional to bandwidth.

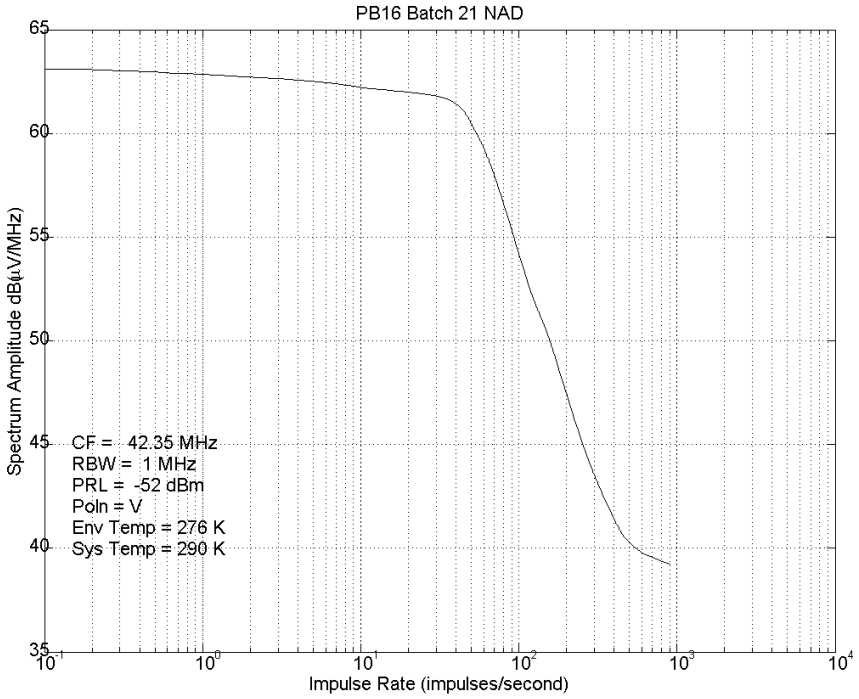

Figure 12 Typical Noise Amplitude Distribution (NAD) graph

The principal advantage of the NAD over the APD is in its use for setting up impulse generators that are calibrated in dB(μV/MHz).

The NADs exhibit broadly the same graphical features as the APDs, but are less amenable to statistical analysis. In Figure 12 the steeply sloping line corresponds to the Weibull IN line on the APD. In practice the line is seldom straight as measurements tend to be dominated by a few nearby MMN sources.

The plateau on the left hand side corresponds to the plateau on the APD and represents the very low probability, high amplitude impulses. If these are class B, then, with longer measurement periods one would see the plateau rise. If they are class A, then increasing the measurement time should not cause the plateau to rise.

Towards the right hand side of the NAD one sees some WGN starting to appear, which causes the line to lift slightly. Some voltage peaks in the data are inevitably due to WGN and these are indistinguishable from the 'true' IN. If one sets a lower pulse detection threshold then more PDWs are generated from the WGN. These WGN PDWs cannot be

used sensibly, as the WGN is not impulsive in nature and its voltage is not proportional to bandwidth.

3.1.2.6 Other Graphs

Researchers have used a variety of graph types for analysing noise, but the APD and NAD predominate and have become the *de facto* standard representations. This section covers some of the other graph types briefly.

3.1.2.6.1 Pulse Interval Distribution (PID)

The PID graph plots the Pulse Interval (PI) against the probability that the ordinate is exceeded. This abscissa is scaled in a similar manner to the APD, so that Rayleigh and Weibull distributions will appear as straight lines. The ordinate (PI) is scaled logarithmically.

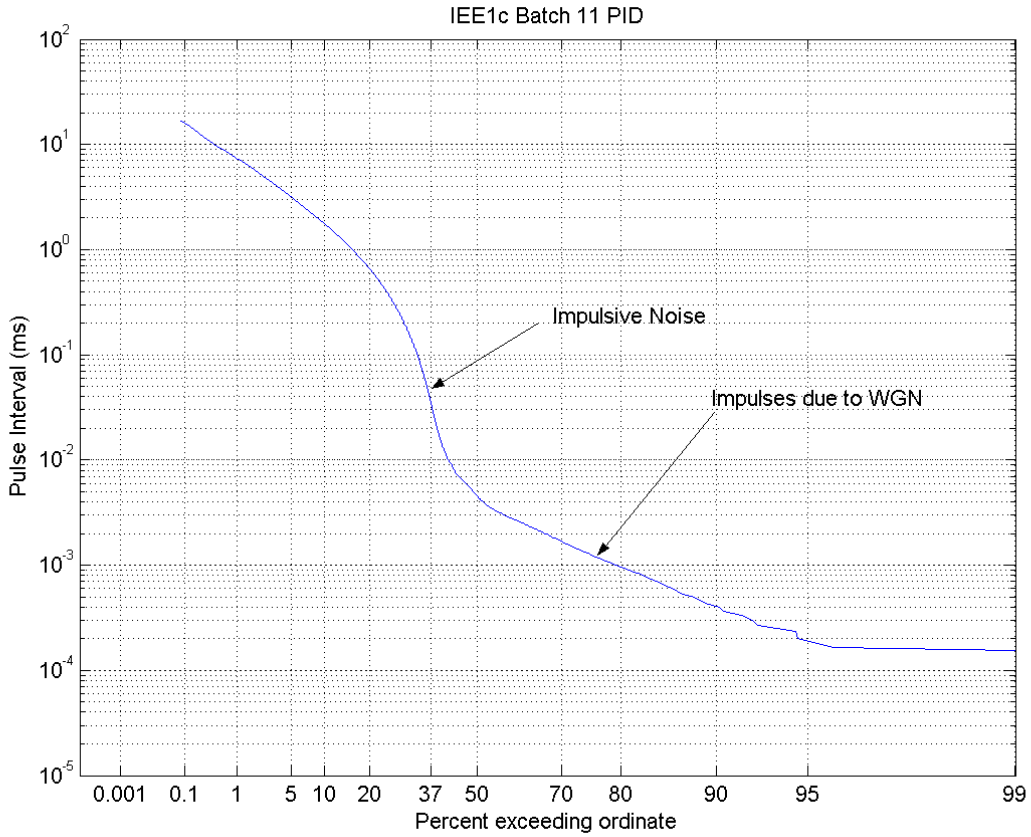

Figure 13 Example of PID Graph

As with the APD and NAD, the PID is a cumulative histogram, but its weakness is that it is sensitive to the detection threshold used by the pulse extractor. The NAD is therefore a much more useful representation than the PID if the pulse rate / interval is to be studied.

PID graphs can be produced from PDW files. An example is shown in Figure 13, on which the regions of IN and impulses due to WGN are indicated.

3.1.2.6.2 Pulse Duration Distribution (PDD)

The PDD graph shows the Pulse Duration (PD) logarithmically on the ordinate and the probability that the ordinate is exceeded on the abscissa. As with the APD and PID, the abscissa is 'Rayleigh-scaled'.

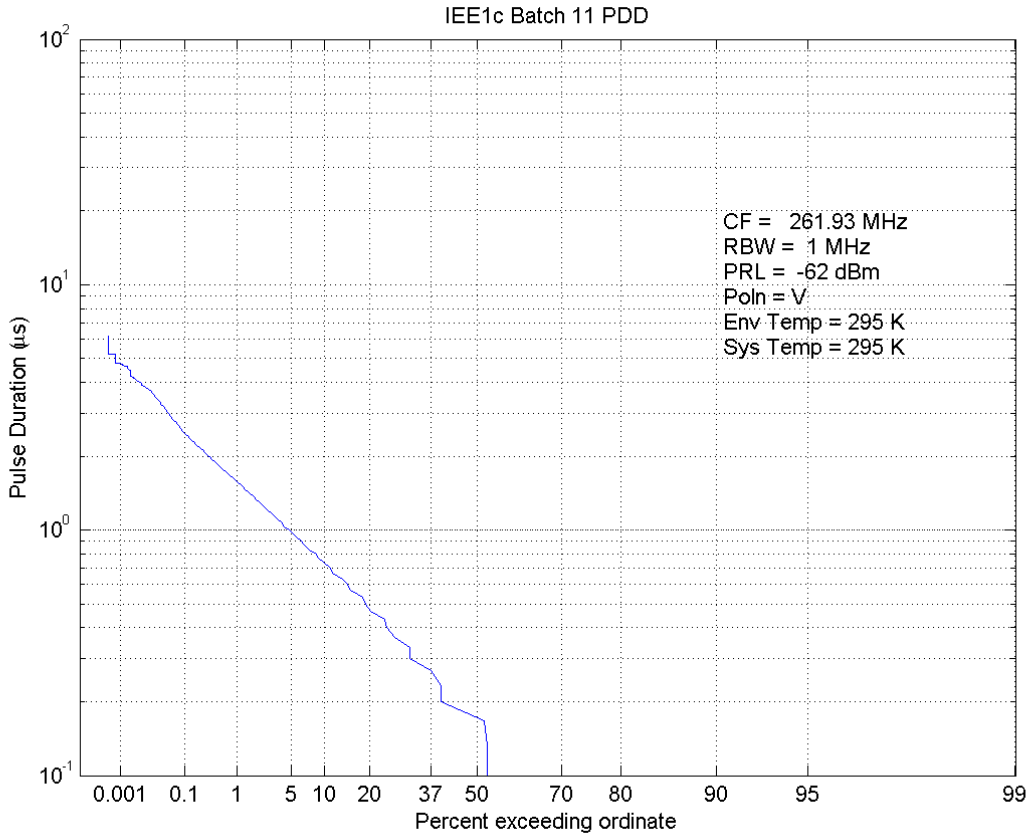

Figure 14 Example of PDD Graph

As the majority of the impulses are band-limited, the PDDs tend to be straight lines. An example is shown in Figure 14.

As with the PID, the major shortcoming of the PDD is that it is affected by the choice of threshold in the PDW extractor. Thus, if the threshold is lowered to the point that impulses due to WGN are included, then there will be a higher proportion of minimum PD impulses, which means in turn that the PD will be reduced.

A further weakness of this representation is that its form varies depending on the measurement bandwidth. A suggested improvement is therefore to plot PD x Bandwidth on the ordinate, which results in a normalised graph.

Figure 15 shows the PID scaled in this way, with the PD multiplied by the measurement bandwidth on the abscissa.

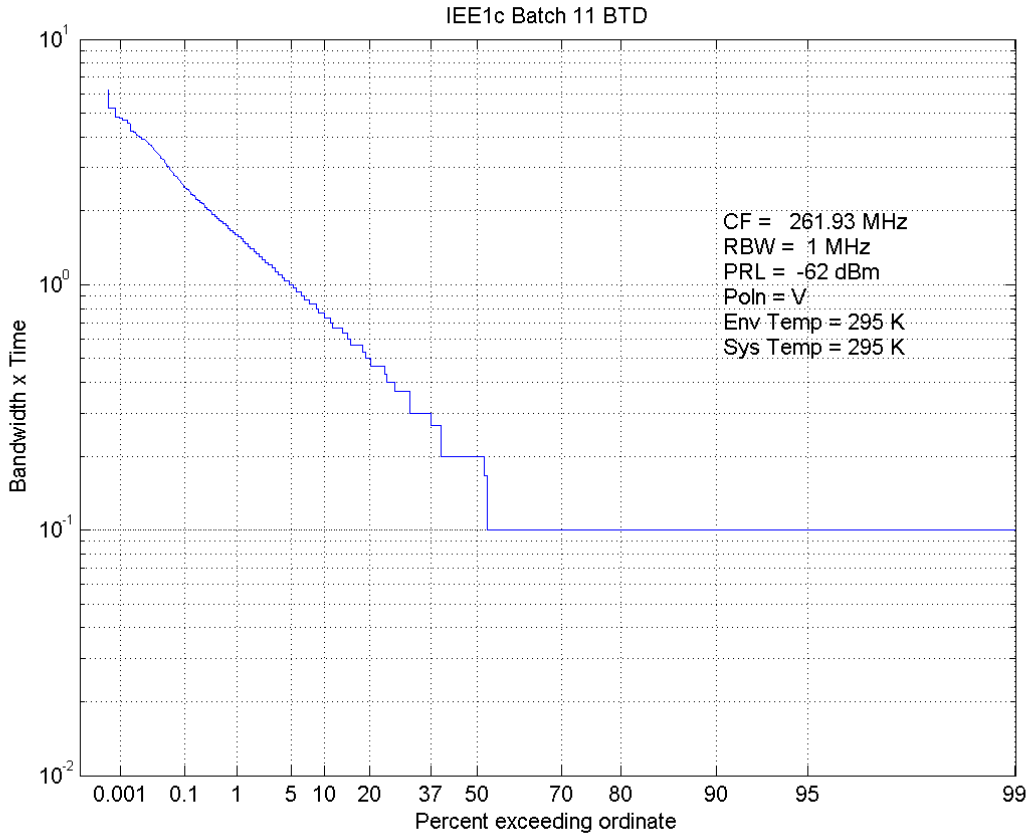

Figure 15 Example of PDD with Rescaled Ordinate

The form of the PDD will depend on the algorithm used for calculating PD. The existing PDW extractor simply calculates the PD at the threshold crossing points, which means that the PD depends on the amplitude of the impulse. This could be alleviated by using the 3 dB points to define the PD, although this would be a significantly slower algorithm to run against large quantities of data.

A final observation of the PDD is that it requires a degree of oversampling to be used. With Nyquist sampling or undersampling, the time quantisation becomes very noticeable at low PDs. For this reason a maximum measurement bandwidth of 5 MHz should be used on the NMF if this representation is to be used.

3.1.2.6.3 Average Crossing Rate (ACR)

The ACR graph appears in papers such as [Parsons83] and appears to be a precursor of the NAD.

On this representation, the abscissa is the number of impulses per second that exceed the ordinate, which is the same as the abscissa of the NAD. The ordinate in this case however is the power in dB above kT_0B, rather than the spectral amplitude used on the NAD. The move to using spectral amplitude rather than impulse power seems to have been motivated purely by its usefulness in configuring impulse generators, which are commonly calibrated in spectral amplitude.

If the IN is assumed to be class B, then the ACR does not scale correctly with bandwidth, whereas the NAD does. As the NAD is now the preferred representation in many papers and books, the ACR has not been used in the present survey.

3.1.2.7 PDW Graphs

It is possible to plot the PDW parameters, TOA, PA and PW against each other using the NMF software. These graphs can reveal useful insights into the nature of the IN.

An example is shown in Figure 16, which is a histogram of the PAs in a batch of recordings.

The important feature to be observed here is that there are a considerable number of pulses in the 'spike' on the left of the graph. These impulses are at low amplitude, just above the detection threshold.

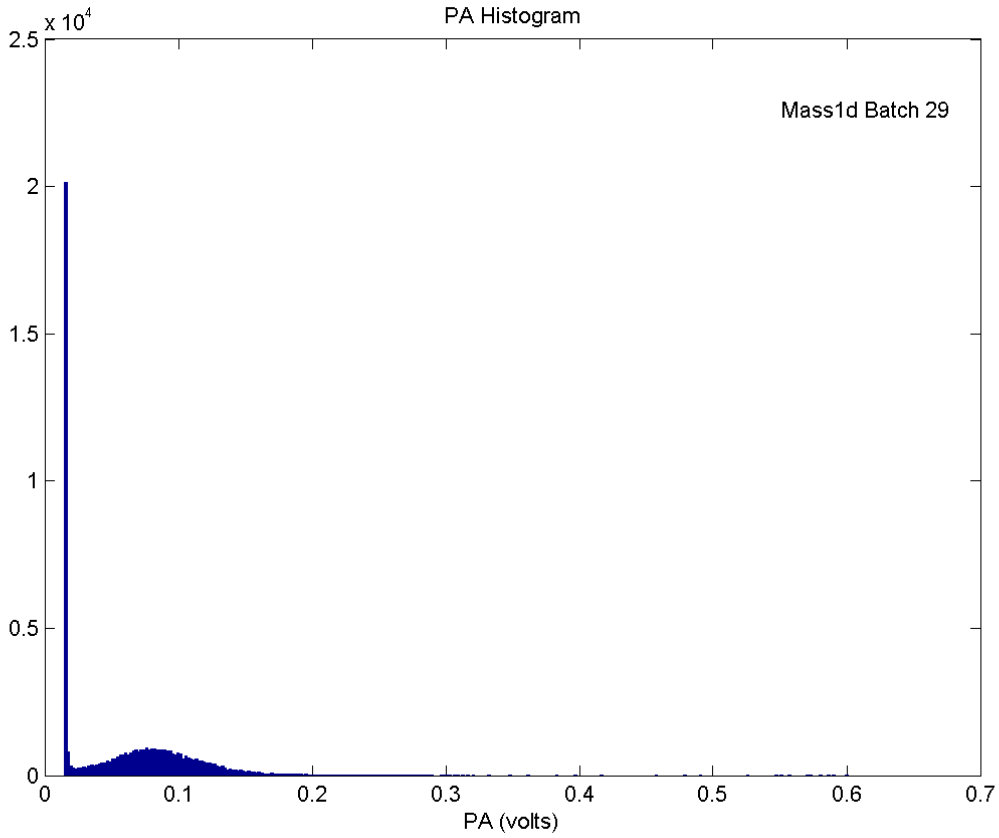

Figure 16 Typical PA Histogram

These lower amplitude PDWs are the result of WGN rather than IN, which forms the remainder of the impulses. There will always be a mixing of WGN and IN and it will never be possible to set a detection threshold that picks out all the IN without incorporating some PDWs that are due to WGN.

It is a reasonable conjecture that the PDWs due to WGN will tend to have relatively short Pulse Widths (PW) because the probability of the WGN remaining at high power for a long duration is low.

The PW histogram for this batch is shown in Figure 17 and, indeed, a preponderance of low PW impulses is seen, which supports the above conjecture.

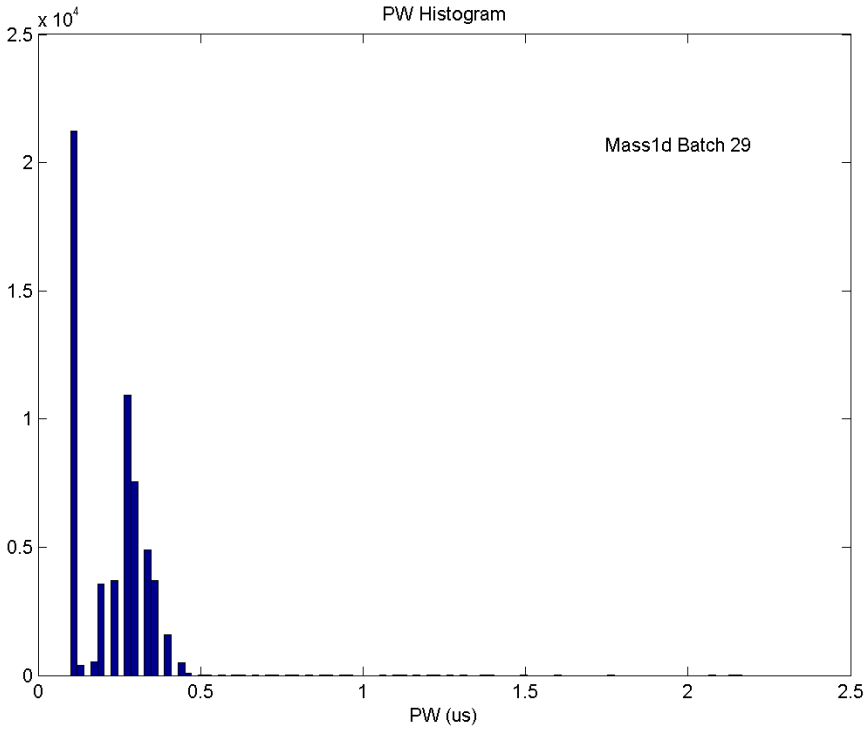

Figure 17 Typical PW Histogram

It is therefore possible to remove a large proportion of the WGN PDWs by applying a threshold to the PW as well as the PA.

Figure 18 and Figure 19 are the 2D and 3D scattergram plots of PW vs PA for the same batch of recordings. It can be seen that the WGN PDWs are indeed confined to the low PA, low PW region.

A further feature that becomes apparent is that there is an increase in PW as the PA increases. This is a side effect of using a simple PDW detection algorithm, which calculates the PW at the threshold crossing point. Stronger impulses will be wider at the threshold crossing points, so the PWs are larger.

This effect could be corrected by calculating the PW at the 3dB points rather than the threshold. We have not done this, as we believe that all previous pulse counting methods have used simple threshold crossing detector circuits.

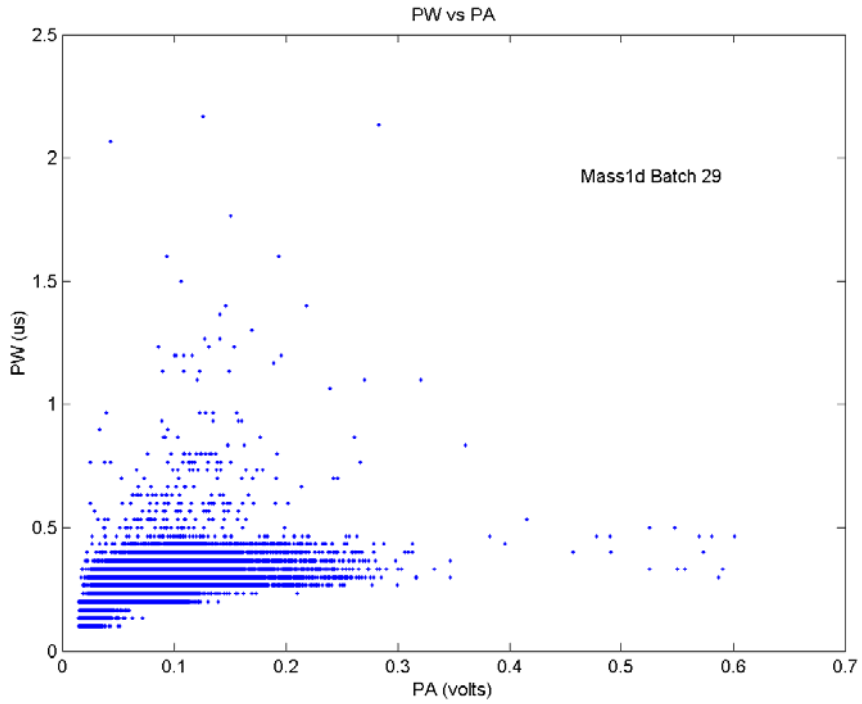

Figure 18 Typical PW vs PA Scattergram

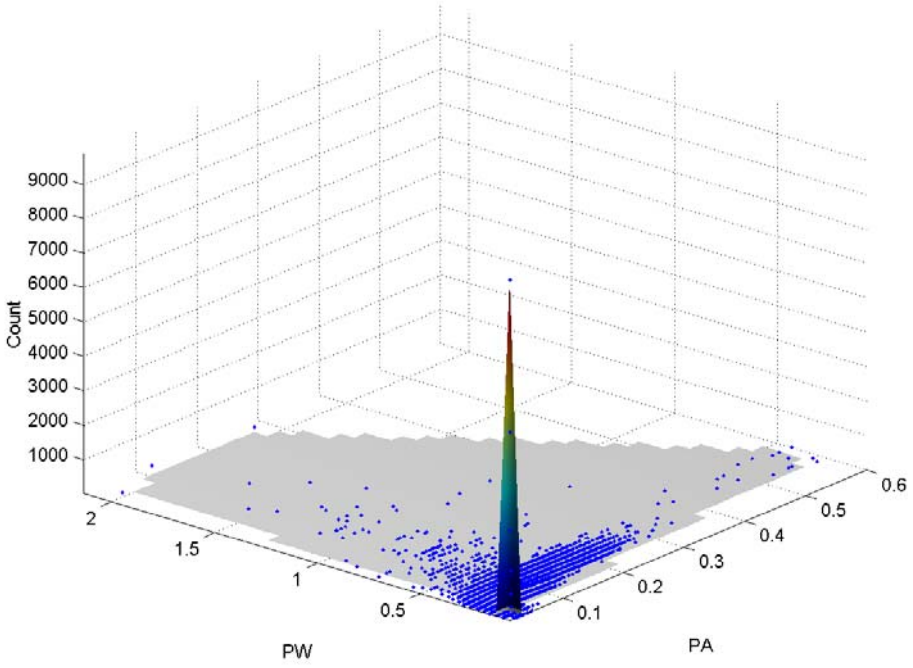

Figure 19 Typical PW vs PA 3D Scattrgram

3.2 MEASUREMENTS

The project has included surveys at eight different locations. In each case the recording was limited to one working day.

In practice the 700GB disk array was never filled completely, as significant amounts of time were needed searching for gaps in the spectrum at which to record. Approximately 4TB of data is now held on 42 LTO tapes.

Over 500 graphs were produced from the survey data. Appendix A contains a set of APDs and NADs that have been selected for comparison within frequency bands.

3.2.1 Frequencies

Figure 20 shows the frequency and bandwidth coverage across all eight sites.

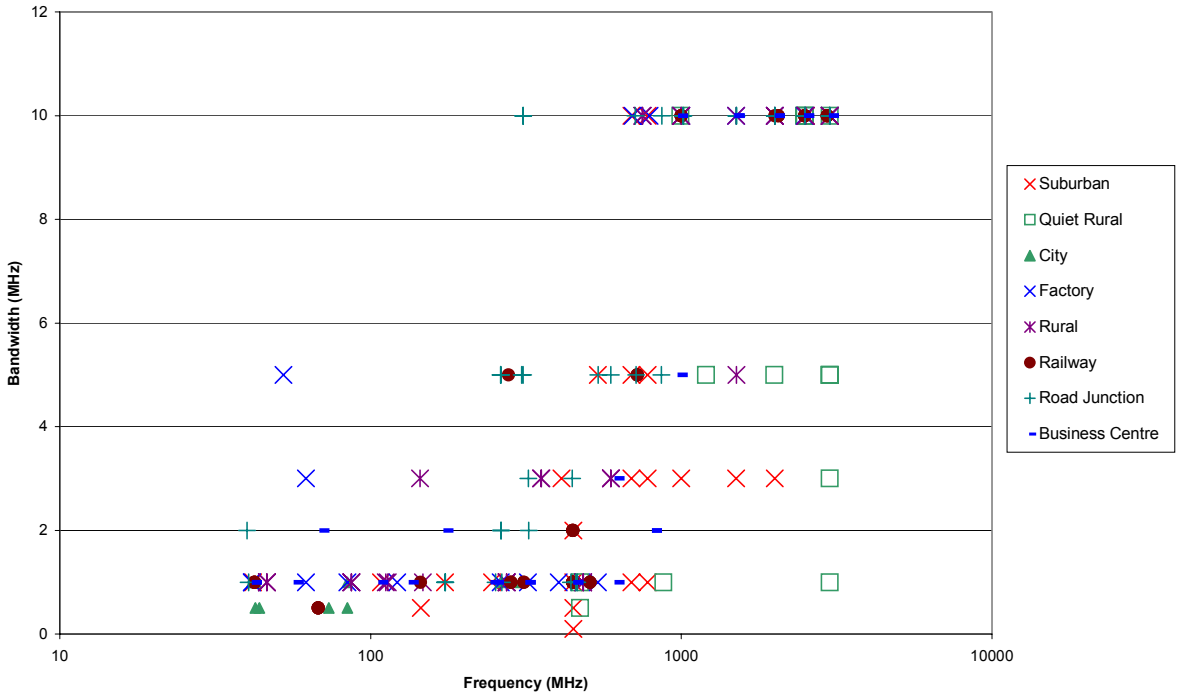

Figure 20 Measurement Coverage

It will be seen that the higher bandwidths were only used at the higher frequencies (>500MHz), where the gaps in the spectrum are wider.

With hindsight it is now possible to state that a preferred measurement bandwidth of no less than 1 MHz and preferably 2 MHz should have been used. Coherent signals that are not too strong can be removed during post-processing and bandwidths above 1 MHz have the advantage that they allow IN to be clearly resolved and measured.

3.2.2 Measurement Sites

MASS was unable to find any standard definitions of site categories recognised by official bodies (Government Agencies, etc). The following table gives the *ad hoc* definitions that were therefore used, the selected sites and a mapping to the [P.372] categories:

Category	[P.372] Category	Definition	Site
Road Junction	-	Location close to motorway or main A-road, covering both slow and fast moving traffic and traffic changing speed (i.e. accelerating or braking)	A1/A14 Junction, Huntingdon
City Centre	Business	Centre of large city in proximity to light industry, offices and public transport systems (road / train / underground)	IEE Headquarters, Savoy Place, London
Factory Estate	Business	Concentration of industrial units and factories undertaking light to medium industrial activities	Arrow Electronics, Bedford
Business Centre	Business	Modern business centre containing a concentration of office automation equipment (PCs, fax machines, photocopiers, telephones, etc)	Silicon Valley Ltd, Lightwater
Railway	-	Location close to railway system, preferably with a variety of electrically-hauled traffic (express, commuter & freight)	GNER car park, Peterborough Railway Station
Suburban	Residential	Mainly residential area on the outskirts of a town / city	Grove House, St. Neots
Rural	Rural	Countryside location, but with evidence of human activity (small groups of houses and shops, minor roads)	103 High St, Blunham (private residence)
Quiet rural	Quiet Rural	Countryside location, but with little or no evidence of human habitation	Plummer Park, Grafham Water

Table 1: Site Category Definitions

3.2.3 Power Supplies

At five of the sites mains power was available. However, the RA van (Figure 21) was used for the Railway, Quiet Rural and Major Road Junction surveys, with the antenna mounted on the roof. This van has a diesel generator, batteries, charger and an inverter.

Figure 21 NMF Antenna on Roof RA Van

A series of tests were performed at Railway and Quiet Rural locations to try and examine the effects of different power supply configurations on the results obtained by the NMF.

The overall conclusion from these tests was, however, that it was not possible to fully attribute noise levels to the power supplies, unless the environment could be screened in some way. This would have to be done using a large shielded chamber, or at some very deserted location.

4 THEORY AND MODELLING

This section consists of four parts:

- Section 4.1 is a restatement of the theory presented in the [NTIA98] and [P.372] reports and is included for its usefulness in understanding the noise model.
- Section 4.2 is a description of how noise is modelled in this study.
- Section 4.3 describes how the model parameters are extracted from measured data.
- Section 4.4 shows how the model performs against measured data.

4.1 BACKGROUND AND TERMINOLOGY

4.1.1 Noise Representations

A noise voltage is a function of time that can be described statistically with the use of random variables. The time-varying noise voltage *v(t)* is represented as a passband signal modulated on a carrier frequency f_c thus:

$$v(t) = \mathrm{Re}\left\{\hat{v}(t)e^{j2\pi f_c t}\right\} \tag{1}$$

where $\hat{v}(t)$ is the noise voltage complex baseband signal centred about 0 Hz that can be represented in Cartesian or polar form as:

$$\hat{v}(t) = x(t) + j\,y(t) = \sqrt{x(t)^2 + y(t)^2}\,e^{j\arctan\left(y(t)/x(t)\right)} \tag{2}$$

where *x(t)* and *y(t)* are the baseband signal real and imaginary components respectively.

The instantaneous noise power is defined as

$$w = \left|\hat{v}(t)\right|^2 \tag{3}$$

The average noise power is defined as

$$w_0 = E\{w\} \tag{4}$$

where $E\{\}$ denotes the expected value of its argument.

In this report, as in the [Achatz98] report, the noise power is normalised by the average noise power due to black body radiation and thermal noise that is present in all radio systems. This average noise power is kT_0b where k = 1.38 x 10^{-23} JK^{-1} is Boltzmann's constant, T_0 = 290K is the absolute temperature and b is the receiver noise equivalent bandwidth.

Furthermore, the standard convention is used that variables in upper case are the decibel equivalents of those in lower case, e.g. $W = log_{10}(w)$. In this format W is known as a *figure* and w is known as a *factor*.

4.1.2 White Gaussian Noise Statistics

A random statistical process can be characterised in terms of a Probability Density Function (PDF) which can take many different forms according to the type of process being modelled. In the case of WGN, by definition, the voltage is modelled by a Gaussian distribution with zero mean and a uniform Power Spectral Density (PSD). In terms of polar co-ordinates, the WGN amplitude is Rayleigh distributed and the phase is uniformly distributed. If a long enough measurement is made, then an amplitude histogram will approximate to the PDF.

Assuming a mean power level of w_{0g} and a random noise variable, w_{RV}, the power PDF for WGN (from [Achatz98]) is:

$$p_g(w_{RV}) = \frac{1}{w_{0g}} e^{\frac{-w_{RV}}{w_{0g}}} \tag{5}$$

For any distribution, the Cumulative Distribution Function (CDF) is defined as:

$$P(w_{RV} \le w) = \int_0^w p(w_{RV}) dw_{RV} \tag{6}$$

where w is the noise power independent variable. In radio engineering, the APD function is used rather than the CDF, as it indicates the probability that the power exceeds a given level. The APD function is related to the PDF by:

$$A(w) = P(w_{RV} > w) = \int_w^\infty p(w_{RV}) dw_{RV} \tag{7}$$

If the noise is WGN distributed according to equation (5), then the APD function is:

$$A_g(w) = e^{\frac{-w}{w_{0g}}} \tag{8}$$

4.1.3 Average White Gaussian Noise Power

A noise power measurement system consists of an antenna, antenna matching circuit, transmission line and receiver. The receiver is further divided into a filter and gain stage. The most appropriate reference point for an overall operating noise factor of this system is the input of a theoretical equivalent loss-free antenna. This is defined in the [P.372] recommendation in terms of the noise factors and loss factors of various stages in the system (see Figure 22). For receivers free from spurious responses, the desired noise factor is given by:

$$f_a = f - (f_c - 1) - l_c(f_t - 1) - l_c l_t(f_r - 1) \tag{9}$$

where f is the measured system noise factor defined as[1],

$$f = w_{0g} \tag{10}$$

f_c is the noise factor associated with the antenna circuit losses,

$$f_c = 1 + (l_c - 1)\left(\frac{t_c}{t_0}\right) \tag{11}$$

f_t is the noise factor associated with the transmission line losses,

$$f_t = 1 + (l_t - 1)\left(\frac{t_t}{t_0}\right) \tag{12}$$

and:

f_r: noise factor of the receiver

l_c : antenna circuit loss (available input power / available output power)

l_t : transmission line loss (available input power / available output power)

t_c : actual temperature (K) of the antenna and nearby ground

t_t : actual temperature (K) of the transmission line.

[1] This equivalence is not true when measuring in the presence of spurious signals. See section 4.3.1.

If $t_c = t_t = t_0$ then equation (9) becomes:

$$f_a = f + 1 - f_c f_t f_r \tag{13}$$

and f_a is thus available from knowledge of the system parameters.

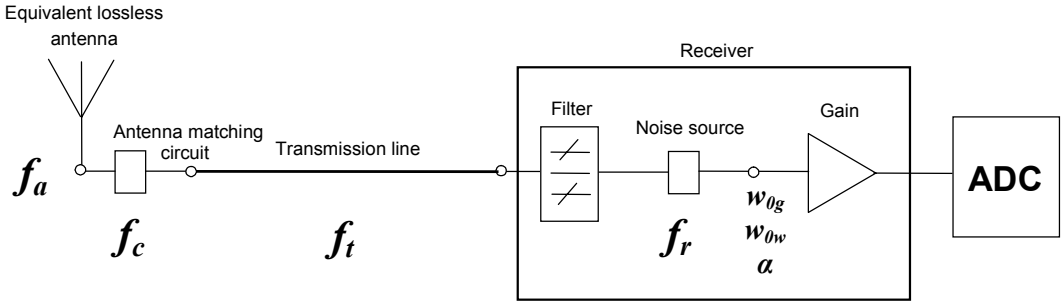

Figure 22 Representation of Idealised Receiver

It is apparent that f_a is estimated at the notional lossless antenna terminals, but all the other parameters are estimated at the output of the receiver and are not adjusted for losses and receiver noise. This is a matter for further investigation.

4.1.4 White Gaussian Noise on the APD Graph

Starting with equation (8), the APD function for WGN may be expressed as:

$$A_g(w) = e^{\frac{-w}{w_{0g}}} \tag{14}$$

This implies that,

$$w = w_{0g} \ln\left(\frac{1}{A_g(w)}\right)$$

$$\therefore 10\log(w) = 10\log(w_{0g}) + 10\log\left(\ln\left(\frac{1}{A_g(w)}\right)\right) \tag{15}$$

The last term is zero when

$$A_g(w) = e^{-1} \approx 0.368 \tag{16}$$

Thus at a cumulative probability of (approximately) 37%:

$$10\log(w) = 10\log(w_{0g})$$

(17)

It is important to realise that this result has nothing to do with the way that data is plotted on the APD plots, rather it is purely a ramification of the Rayleigh distribution. Thus a value for w_{0g} can be obtained by reading the power level at the 37% point on the APD graph.

It is also important to note that this estimate will only be accurate if the WGN component is truly Gaussian. Section 4.3.1 describes the more accurate method of determining the mean power level used in this project, which is robust in the presence of coherent signals.

The abscissa of an APD plot does not present $A_g(w)$ linearly or even scaled as $\log(\ln(1/A_g(w)))$, as we have already noted that $\log(\ln(1/A_g(w))) = 0$ when $A_g(w) \approx 0.368$. However, it may be evaluated that the abscissa actually presents $A_g(w)$ scaled as $1-\log(\ln(1/A_g(w)))$.

In this scaling it is important to appreciate that a "unity distance" along the "linear" abscissa actually corresponds to the distance between the 0.0045 and the 36.8, the 36.8 and 90.5, and the 90.5 and the 99.0 percentiles, as these points correspond to the points at which $1-\log(\ln(1/A_g(w))) = 0, 1, 2$ and 3, respectively.

As the APD plot actually plots W versus $1-\log(\ln(1/A_g(w)))$, equation (14) must be re-cast in order to present it in the form in which it actually appears on an APD plot, i.e. as:

$$10\log(w) = -10\left[1 - \log\left(\ln\left(\frac{1}{A_g(w)}\right)\right)\right] + 10\left[1 + \log\left(w_{0g}\right)\right]$$

(18)

From this equation, it is apparent that Rayleigh Noise, when displayed on an APD plot, is characterised by a gradient of –10, i.e. a drop of 10 dB on the ordinate over a unity abscissa distance.

4.1.5 Impulsive Noise Statistics

It has been found that an effective analysis can be performed by assuming that only class B IN is present in the environment.

Under the class B assumption, the shapes of individual impulses are of little importance. To quote from [Parsons92]: "Any two impulses are indistinguishable if they provide the same spectrum amplitude over the frequency range of interest." The amplitude envelope of each impulse is purely dictated by the impulse response of the receiver.

The class B IN is modelled as a series of impulses that are Poisson distributed in time and have a Weibull power distribution (also known as a Power Rayleigh distribution). This power distribution is convenient as it plots as a straight line on the APD graph. A simple line fit to this region therefore allows one to produce statistical parameters to quantify the amount of IN present. It is important to note that this is a simplification of the Middleton noise model. Although it is a simplification, it is very suitable for analysing survey data and produces parameters that are easy to use for simulation purposes.

Assuming a random noise variable, w_{RV}, the Weibull power PDF (from [MATLAB01]) is:

$$p_w(w_{RV}) = a.b.{w_{RV}}^{b-1}.e^{-a{w_{RV}}^b} \tag{19}$$

where a and b are the parameters of the distribution.

Using the definition in equation (7), the corresponding APD function for an independent variable, w, is:

$$A_w(w) = e^{-aw^b} \tag{20}$$

Equation (20) may be recast in terms of parameters w_{0w} and α, which may be evaluated directly from the APD graph:

$$A_w(w) = e^{-\left(\frac{w}{w_{0w}}\right)^{1/\alpha}} \tag{21}$$

where,

$$a = \frac{1}{{w_{0w}}^{1/\alpha}}$$
$$b = \frac{1}{\alpha} \tag{22}$$

This implies that:

$$w = w_{0w}\left(\ln\left(\frac{1}{A_w(w)}\right)\right)^{\alpha} \tag{23}$$

$$\therefore 10\log(w) = -\alpha.10.\left[1-\log\left(\ln\left(\frac{1}{A_w(w)}\right)\right)\right]+10.\left[\alpha+\log(w_{0w})\right] \tag{24}$$

As with the WGN distribution, the term $\alpha.10\log\left(\ln\left(\frac{1}{A_w(w)}\right)\right)$ is zero when:

$$A_w(w) = e^{-1} \approx 0.368 \tag{25}$$

Thus at a cumulative probability of (approximately) 37%:

$$10\log(w) = 10\log(w_{0w}) \tag{26}$$

So we see that the parameters w_{0w} and -10α are the 37% power and the gradient respectively of the impulsive part of the APD graph.

In practice the values of w_{0w} and α can be readily obtained by fitting a line to the steepest part of the APD graph, but are not in themselves particularly helpful. As the amount of IN increases, w_{0w} tends to decrease and α increases. The meaning of w_{0w}, in particular, is counter-intuitive and it is also a small number that is sensitive to errors in estimating the line gradient.

It is therefore more useful to estimate the mean and standard deviation of the IN noise power. These parameters are more intuitive than either a and b, or w_{0w} and α. They are also less sensitive to estimation errors.

[MATLAB01] reveals the mean and standard deviation of the Weibull distribution to be:

$$m_w = w_{0w}\Gamma(1+\alpha) \tag{27}$$

$$s_w = w_{0w}\sqrt{\Gamma(1+2\alpha)-\Gamma^2(1+\alpha)} \tag{28}$$

where $\Gamma(\ )$ denotes the gamma function defined as:

$$\Gamma(a) = \int_0^\infty e^{-t}t^{a-1}dt \tag{29}$$

The m_w and s_w parameters, given in equations (27) and (28), are the mean and standard deviation of the IN power assuming a Weibull model for the class B noise.

These parameters can be usefully represented in decibel form as:

$$M_w = 10.\log_{10}(m_w) \tag{30}$$

$$S_w = 10.\log_{10}(s_w) \tag{31}$$

Both parameters are obtained from the APD graph in units of dB above kT_0b. These are rescaled to voltage densities in units of dB(μV/MHz) so that they scale linearly with bandwidth.

4.2 NOISE SIMULATION

The MMN simulation assumed in this study requires the summation of two noise components, one for the WGN and one for the class B IN.

4.2.1 White Gaussian Noise Simulation

The model for the WGN component is simply,

$$g_k e^{j\theta_{gk}} \tag{32}$$

where

$$g_k = \sqrt{f_a}\left(-\ln u_{gk}\right)^{1/2} \tag{33}$$

is the Rayleigh distributed amplitude which comes from equation (8), u_{gk} is a uniformly distributed random variable with a range from 0 to 1 and θ_{gk} is a uniformly distributed phase between 0 and 2π. The simulation time index is k.

4.2.2 Impulsive Noise Simulation

The IN model has to take into account the Poisson distributed pulse arrival times. The mean impulse rate is γ and therefore the probability of a pulse occurring in time interval Δt is therefore $\gamma \Delta t$. Therefore, the presence of a pulse is determined by:

$$\chi_k = \begin{cases} 1 & with\ probability\ \gamma \Delta t \\ 0 & with\ probability\ 1 - \gamma \Delta t \end{cases} \tag{34}$$

In the simulation, Δt is the time-step increment (1 / Sample Rate) and γ is taken to be the bandwidth of the simulation. This is based on the arbitrary assumption that the mean impulse rate occurs at the mean amplitude but works well for the measured data examined in this study. Equation (34) assumes a class B environment, because each impulse only lasts for one time step. The model for IN then becomes,

$$b_k \chi_k e^{j\theta_{wk}} \tag{35}$$

where, using equation (21),

$$b_k = \sqrt{w_{0w}}\left(-\ln u_{wk}\right)^{\alpha/2} \tag{36}$$

and the random variables u_{wk} and θ_{wk} are not correlated with those for the WGN model.

4.2.3 Combined Noise Model

The sum of the WGN and IN models leads to the model for the total class B noise environment as,

$$\hat{v}_k = g_k e^{j\theta_{gk}} + b_k \chi_k e^{j\theta_{wk}} \tag{37}$$

and $\hat{v}_k$ is the instantaneous complex noise voltage waveform.

4.2.4 Sample Rate

The sample rate effectively sets the bandwidth for the simulation. To avoid any issues of bandwidth scaling (see section 4.3.3), the sample rate for the simulation is always set to twice the bandwidth of the measurement from which the simulation parameters have been extracted. This has the added benefit of not having to add a digital filter to the model.

4.3 NOISE MEASUREMENT PARAMETER EXTRACTION

The noise parameters have been estimated by analysing the APD graphs. Figure 23 is the same APD graph shown in Figure 9, but with indications of the salient features.

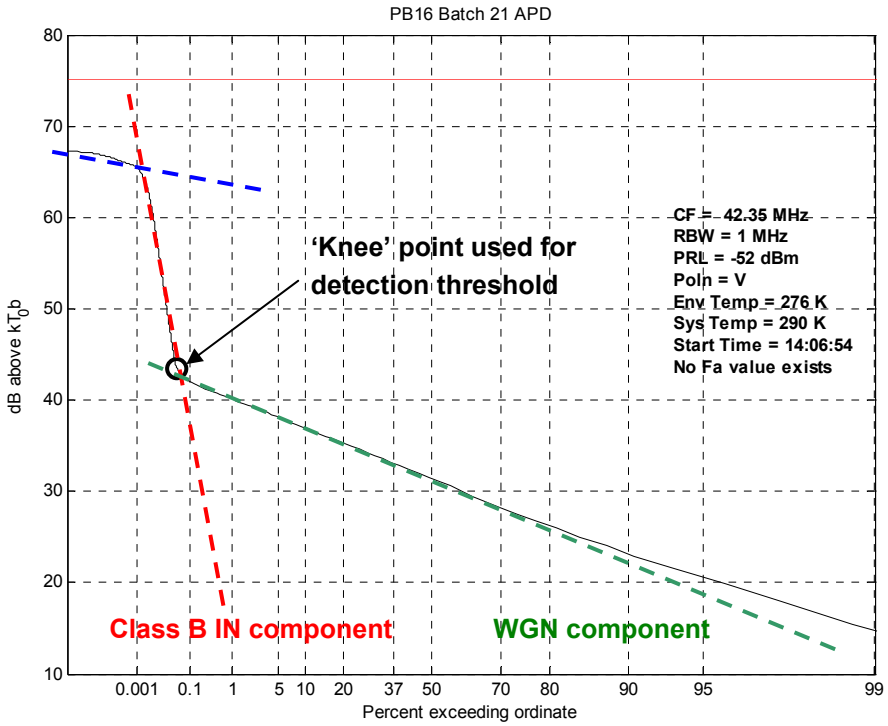

Figure 23 APD graph showing salient features

The following features are shown:

- The WGN component, the level of which is estimated using the green dashed line.
- A 'knee' point, which is obtained by visual inspection and establishes the threshold for PDW extraction.
- The class B IN component, which is approximated by the red dashed line in our analyses.
- Also shown, as a blue dashed line, is that which would have been used by the NTIA for modelling the IN. This is where our approach differs significantly from the NTIA, in that we have used the point of steepest gradient to define the class B IN estimate.

4.3.1 White Gaussian Noise Parameter Extraction

The noise environment may be characterised by three parameters, f_a (or w_{0g}), w_{0w} and α. The first of these may be approximated by reading the 37% power on the APD graph and making the necessary adjustment for system noise in equation (13). This actually gives w_{0g} (or W_{0g} because the APD graph is scaled in dB) instead of f_a. However, this approximation is very poor when measuring in the presence of spurious signals which are non-Gaussian. In this case, an algorithm which delves in-between these signals to reach the true Gaussian component has been developed. This uses the Welch transform to obtain a fine-grain power spectrum from which the 'noise floor' can be measured. The algorithm includes measures to ensure that it is robust to momentary wideband signals. When an f_a value is unavailable for any reason, w_{0g} is the next best approximation.

In the presence of Nakagami-Rice distributed noise (i.e. that due to continuous signals) the w_{0g} extraction from the APD graph is best performed by fitting a straight line of gradient –10 to the Gaussian part of the APD graph (the green line in Figure 24). The point of contact of the fit line with the measured curve is below the 37% point so as to avoid contamination by any Nakagami-Rice component.

4.3.2 Impulsive Noise Parameter Extraction

The NTIA have used three parameters to characterise the impulsive noise component, w_{0w}, α and γ. In this study the number of IN parameters has been reduced to two by setting γ equal to the simulation bandwidth. The remaining two parameters may be evaluated by fitting a straight line to the impulsive part of the APD graph. An example of the fit is shown in Figure 24.

α is immediately available from the gradient of the red line in the figure and w_{0w} is evaluated by solving equation (23) at the point of maximum gradient. The plateau section of the APD graph would, were one to record for a very long time, tend to rise as increasingly high amplitude impulses were observed. The plateau section is then a poor indicator of the IN level. We have used a straight line fit to the region around the maximum gradient and this has led to consistent results across all the survey data.

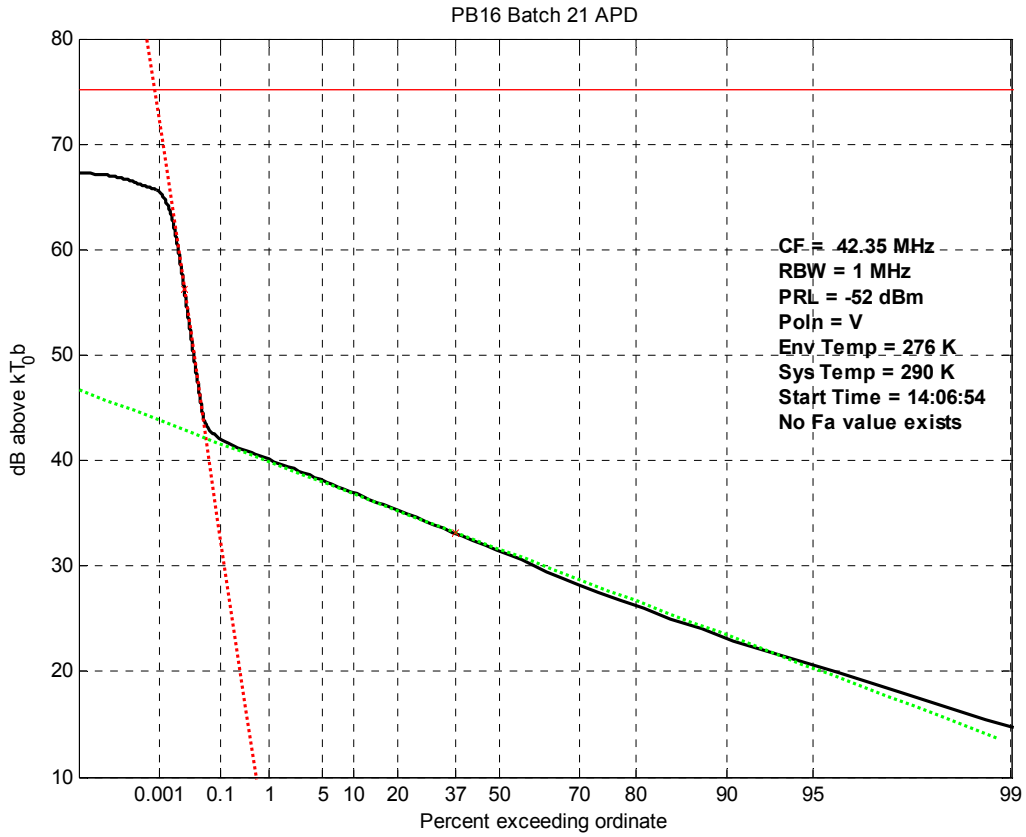

Figure 24 APD parameter extraction fit lines.

4.3.3 Influence of Receiver Bandwidth

It has been found that using bandwidths of 1 MHz and greater means that the probability of impulses overlapping in time is extremely small. This has important ramifications for the interpretation of the APD graphs and, to a lesser extent, the NAD graphs.

Earlier studies typically used much narrower bandwidths. This caused the impulses to spread significantly in relation to the average impulse rates observed. At narrow measurement bandwidths therefore, the IN line on the APD graph tends to flatten out and it is not easy to convert an APD graph to a different bandwidth. [Spaulding62] describes a technique for mapping APD graphs from one bandwidth to another. The technique is awkward to apply, although it could be automated in software.

In our tests however the influence of measurement bandwidth is much reduced and we believe that, in our results, the IN line on the APD graph is asymptotically approaching the 'true' line. This is a very useful observation as a result of which it is recommended that all future measurements be made with a bandwidth of at least 1 MHz and preferably 2 MHz.

4.4 ALGORITHM PERFORMANCE

Equation (37) can be evaluated once the noise parameters have been extracted. The resulting simulated time-history may be run back through the APD graph calculation routines to show a comparison of the measured APD function and the simulated APD function. An example of the match between measurement and simulation is shown in Figure 25.

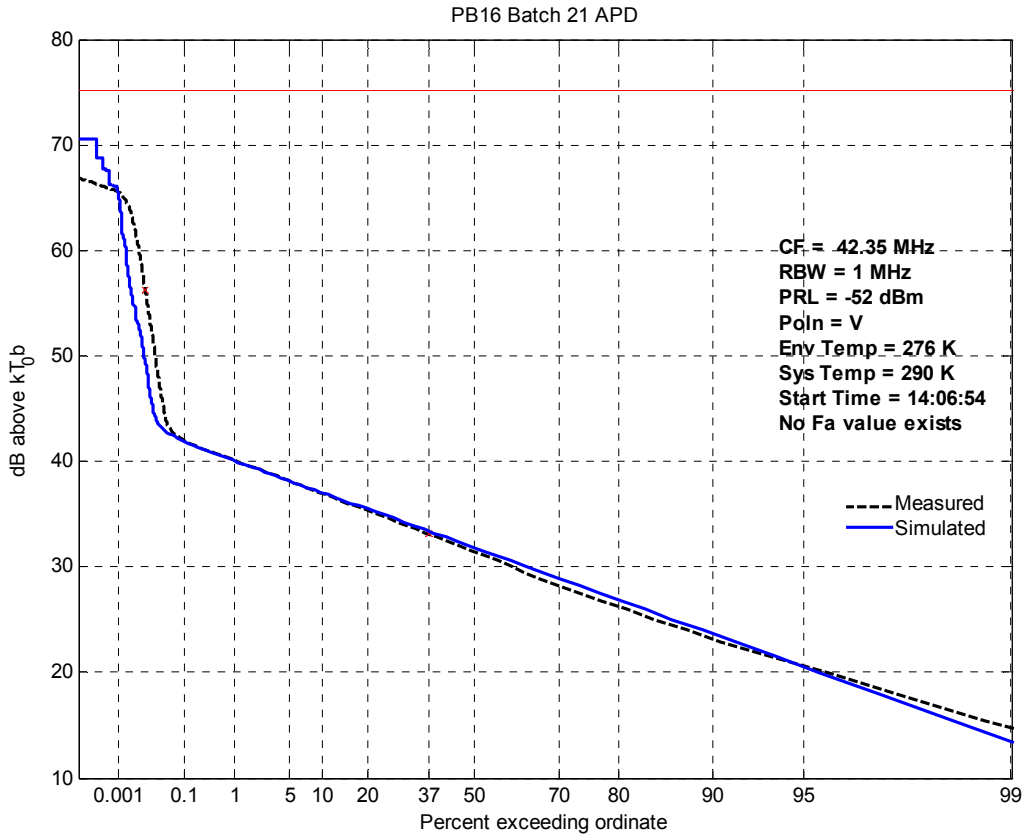

Figure 25 Comparison of measured and simulated APD functions

When class A emitters are present then the algorithm either ignores them, as shown in Figure 26, or it models them as class B emitters.

The algorithm also tries to match the straight line fit to the Weibull distributed fit-line, but inevitably fails at very low probabilities as this would require a very large number of samples. Figure 26 was generated using 10^6 samples.

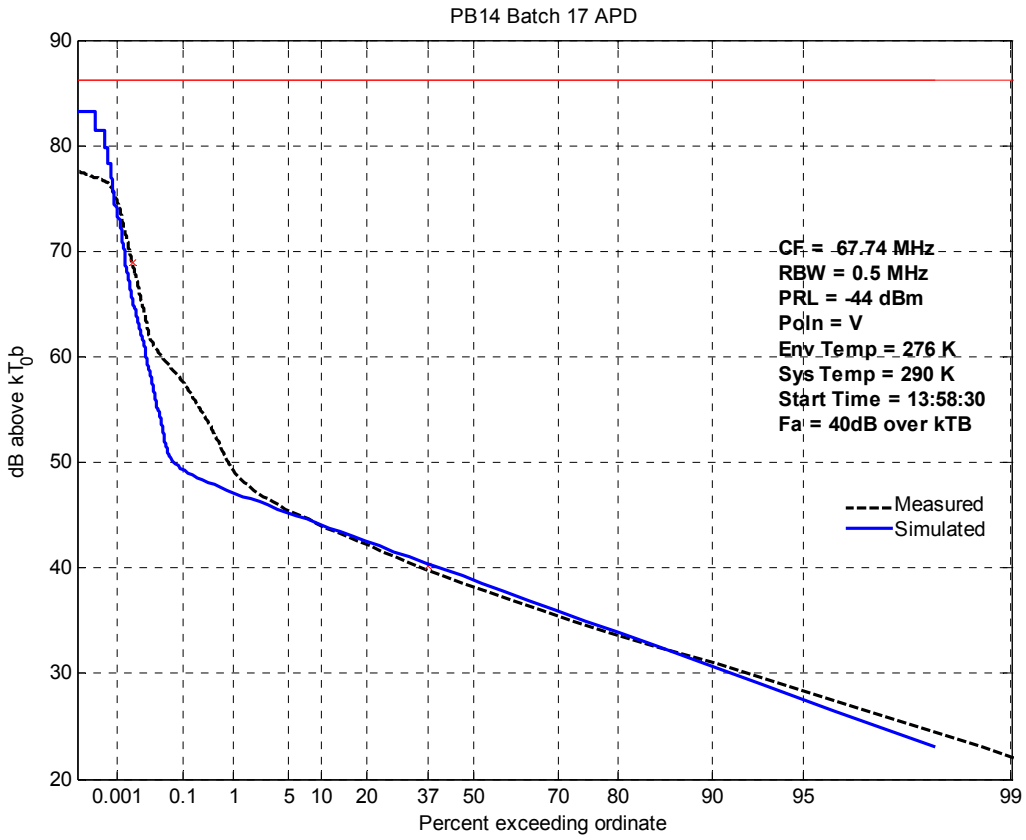

Figure 26 Algorithm performance in the presence of class A emitters

As explained in Section 4.3.1, f_a has been estimated using an algorithm based on the Welch transform. This algorithm cannot always find a value of f_a lower than that derived from the graph, but when it can then the measured and simulated APD functions may differ as shown in Figure 27.

In this example, the f_a algorithm has found a mean WGN power lower than suggested by the APD 37% point. The measured and simulated WGN part of the APD functions diverge at higher probabilities. This is due to a Nakagami-Rice distributed noise component present in the measurement, which is not modelled by the simulation.

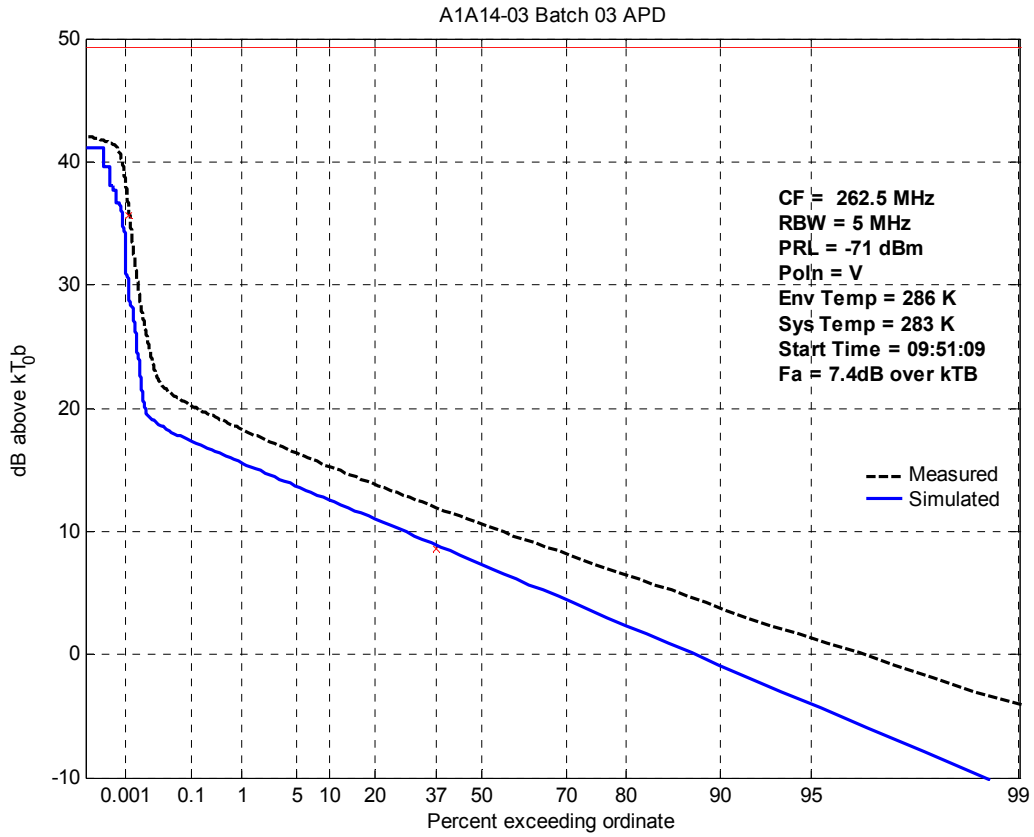

Figure 27 Simulated APD when Fa value exists

4.5 WAVELETS

[Shukla01] proposed that the Wavelet Transform (WT) be used for analysing the IN component of MMN.

If the class B model is assumed to apply to all the MMN, then such analysis would not produce any meaningful results from the data recorded on the NMF. The measurement bandwidth is, by definition, significantly less than that of the impulses themselves. The observation of each impulse is therefore simply the convolution of the receiver's impulse response with a vanishingly short impulse.

Wavelets would only be of use where class A is present. Inspection of the data suggests that this actually happens in a very small percentage of the PDWs. Usually it is the case that the long PDWs are actually due to a number of impulses occurring in a burst and being blurred together by the receiver's impulse response.

Further work could be carried out to search through all the longer PDWs to ascertain whether a wavelet analysis would be of significant use. However, it is currently felt that more benefit would be obtained by using the class B model and seeking to improve the Poisson time distribution to include impulse bursts.

4.6 UWB

The use of UWB is not fully sanctioned in the UK at present, although it is possible that these kinds of transmission will become legal within the foreseeable future. Were this to be the case then it is likely that UWB would appear very similar to the IN component currently observed.

If this were the case, then the analysis methods would probably need refinement to allow UWB to be separated from the IN due to MMN. Wavelets may be one of the ways ahead should this become an issue, but it is also likely that such transmissions will be recognisable by their pulse repetition rates and largely constant amplitudes.

5 RESULTS

The results of the survey are presented in terms of the WGN components (Section 5.1), the class B IN components (Section 5.2) and a comparison of the two (Section 5.3).

5.1 WHITE GAUSSIAN NOISE

This section summarises the Gaussian noise levels measured in terms of the F_a values.

The external noise figure, F_a, is defined in [P.372] and describes the level of Gaussian noise in the environment. It is not clear in that reference however, whether F_a is the median of the distribution or the mean. There is therefore ambiguity in the definition.

Each of the component terms used to calculate F_a is a noise factor or loss and it makes sense to assume that these are obtained as mean values. The corollary of this assumption is that the intention of [P.372] was to imply that F_a is calculated as a mean rather than a median. The plots given in [P.372] are therefore the medians of a set of mean values.

The results of our surveys are plotted in Figure 28, which also shows the lines given in [P.372]. Note however that the latter are medians, whereas the results from this survey are regression lines to a limited number of observations and should therefore be considered estimates of the means. It would be necessary to visit the same sites several times to obtain median lines that are fully comparable with the [P.372] lines.

With this caveat in mind, it is still possible to draw conclusions from these results:

1. All the plots show the same trend for F_a to decrease linearly with log frequency, which agrees with the [P.372] model.

2. Overall however, the results from this study are higher than the [P.372] lines.

3. In none of the cases were there significant differences between the polarisations. Therefore, the lines drawn in Figure 28 were obtained by combining both sets of measurements.

4. The highest values of F_a were obtained at the City Centre, Factory Estate and Business Centre. There were a large number of emission sources in these environments. As well as cars, factory machines and office equipment were present. Much of the MMN from these devices would appear as Nakagami-Rice in form when seen individually. When seen in large numbers however, these signals combine incoherently and would appear on the APD graph as a raised WGN level, with an occasionally dominant Nakagami-Rice component.

5. The Suburban and Major Road Junction exhibited low levels of WGN. The conclusion drawn is that there were very few emitters in these locations apart from the ‘target’ ones. The Major Road Junction surveyed carries a high traffic density, but is surrounded by fields, so there were few emitters apart from the road vehicles. The Suburban site would have had a much lower population density than the City Centre and Factory Estate during the day, so there would have been fewer emitters present.

6. The Rural case showed surprisingly high values of F_a at lower frequencies and a much sharper drop-off with increasing frequency than seen in the other environments. Previous researchers have commented on the amount of variability in F_a and it is possible that these results are a reflection of such variability. It is also possible that the particular location used was not a 'typical' rural location.

Equation (11) in [P.372] defines an approximation for the median level of MMN as:

$$F_{am} = c - d \log f \tag{38}$$

where F_{am} is in dB and f is the frequency in MHz.

The table below summarises the [P.372] values and the results of the mean measurements made in this study.

ITU Category	*c*	*d*	Study Category	*c*	*d*
Business	76.8	27.7	City Centre	111.6	36.1
			Factory Estate	104.5	34.4
			Business Centre	89.5	28.4
Residential	72.5	27.7	Suburban	60.8	20.8
Rural	67.2	27.7	Rural	141.0	54.5
Quiet Rural	53.6	28.6	Quiet Rural	62.3	20.6
			Road Junction	48.7	16.6
			Railway	77.3	26.2

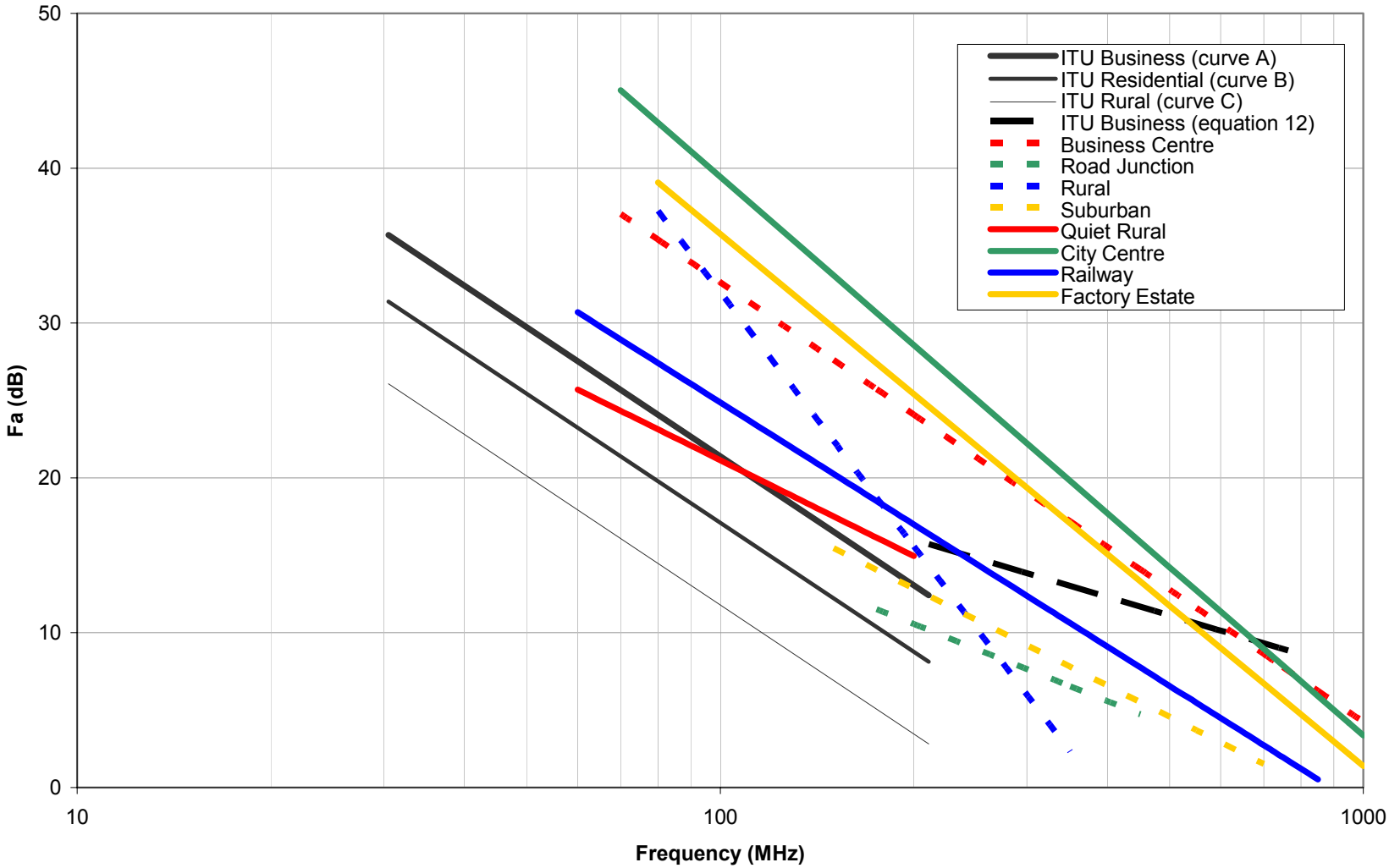

Figure 28 *Fa* versus Frequency

5.2 IMPULSIVE NOISE

The graphs on the following pages summarise the findings with respect to class B IN.

5.2.1 Mean IN Voltage Density

Figure 29 is a graph of the mean IN voltage density, M_w, against frequency. It has been found that M_w falls off with log(frequency) following a linear relationship. This conveniently means that a relationship similar to that used for F_{am} in [P.372] may be used. The following is therefore proposed:

$$M_w = g - h \log f \tag{39}$$

where M_w is in dB(μV/MHz) and f is in MHz. The measured coefficients are:

Site Category	*g*	*h*
City Centre	79.3	32.9
Factory Estate	96.8	40.8
Business Centre	56.6	32.6
Suburban	45.9	21.9
Rural	104.1	53.3
Quiet Rural	65.7	39.3
Road Junction	69.8	34.3
Railway	91.4	39.3

It will be seen that the mean IN voltage density falls in a similar way to the WGN power. Above 1 GHz the mean IN voltage density is low and long recordings are needed to measure it reliably. It is recommended that recordings should last at least 10 minutes when trying to measure IN above this frequency.

The mean IN voltage density is concluded to be a more meaningful and useful parameter than W_{0w}, which tends to fall when the level of IN increases. The W_{0w} parameter can only be interpreted properly when the value of α is also considered, a high value of α implying a high level of IN.

It should be noted however that M_w cannot be compared directly with F_a for two reasons. Firstly, M_w applies at the output of the receiver rather than the output of the antenna. For this reason it would be worth considering the use of a mean IN voltage density parameter referenced to the same point as F_a.

Secondly, M_w scales with the square of the measurement bandwidth if regarded as a power, whereas F_a scales linearly with bandwidth. For this reason, M_w is more correctly regarded as voltage density.

5.2.2 Standard Deviation

Figure 30 graphs the standard deviation of the IN, S_w, against frequency. In most cases there is a good linear relationship such that S_w falls with log frequency.

Assuming a relationship of the form:

$$S_w = m - n \log f \tag{40}$$

where S_w is in dB(μV/MHz) and f is in MHz, the measured coefficients are:

Site Category	*m*	*n*
City Centre	106.5	32.4
Factory Estate	116.3	35.6
Business Centre	50.8	11.5
Suburban	126.9	41.0
Rural	130.4	51.2
Quiet Rural	100.9	45.6
Road Junction	128.8	40.8
Railway	142.0	44.8

The estimation of S_w is quite sensitive to the number of impulses detected. For this reason, it is recommended that all future measurements be taken for periods of more than 5 minutes in quiet locations.

Whilst both M_w and S_w are necessary to fully describe the Weibull distribution assumed for class B noise, an empirical relationship appears to exist that may be useful in simplifying simulations of IN. Figure 31 is a scatterplot of the two parameters for all the data and it may be seen that there is a correlation between them.

At individual sites, better correlations exist between M_w and S_w. It appears that it may be possible to link the two IN parameters using linear relationships with parameters unique to the environments. No physical explanation is currently proposed for this relationship, but it is considered significant enough to warrant further investigation in future studies.

The dashed line on Figure 31 is an overall regression that may be useful for simulation purposes. Using that line it would be possible for a developer to lookup just the two M_w coefficients (g and h) pertinent to the type of location to be simulated. A reasonably representative value of S_w could then be inferred within the simulation function.

An important corollary of this empirical relationship is that the value of M_w can be used as an indicator of IN level without involving a measure of spread such as S_w. This could be a useful simplification for comparing environments.

5.2.3 Polarisation

At the start of the project there was a suggestion that the level of IN may vary with polarisation, especially at the railway site.

Figure 32 shows all the data graphed as mean impulsive noise against frequency. From the regression lines it will be seen that there is a slight tendency for vertical polarisation to receive slightly higher IN voltage density than the horizontal polarisation. The correlations are not strong however, so it is suspected that this may be more to do with differences in antenna patterns than actual differences in the environment.

5.2.4 Train Type

There was a discernible difference between the IN levels observed between different types of train, as shown in Figure 33. Electric trains exhibited a higher M_w than the diesel types.

In a number of cases there were more than one train close to the NMF and these have been placed in the 'Mixed' category in Figure 33. Understandably, the levels of IN in these cases are variable, but tend to be higher than when just one train is present.

It would be possible to analyse the data to locate the point of closest approach in each case. From this it would be possible to determine the maximum IN level. This is a possible area for further work.

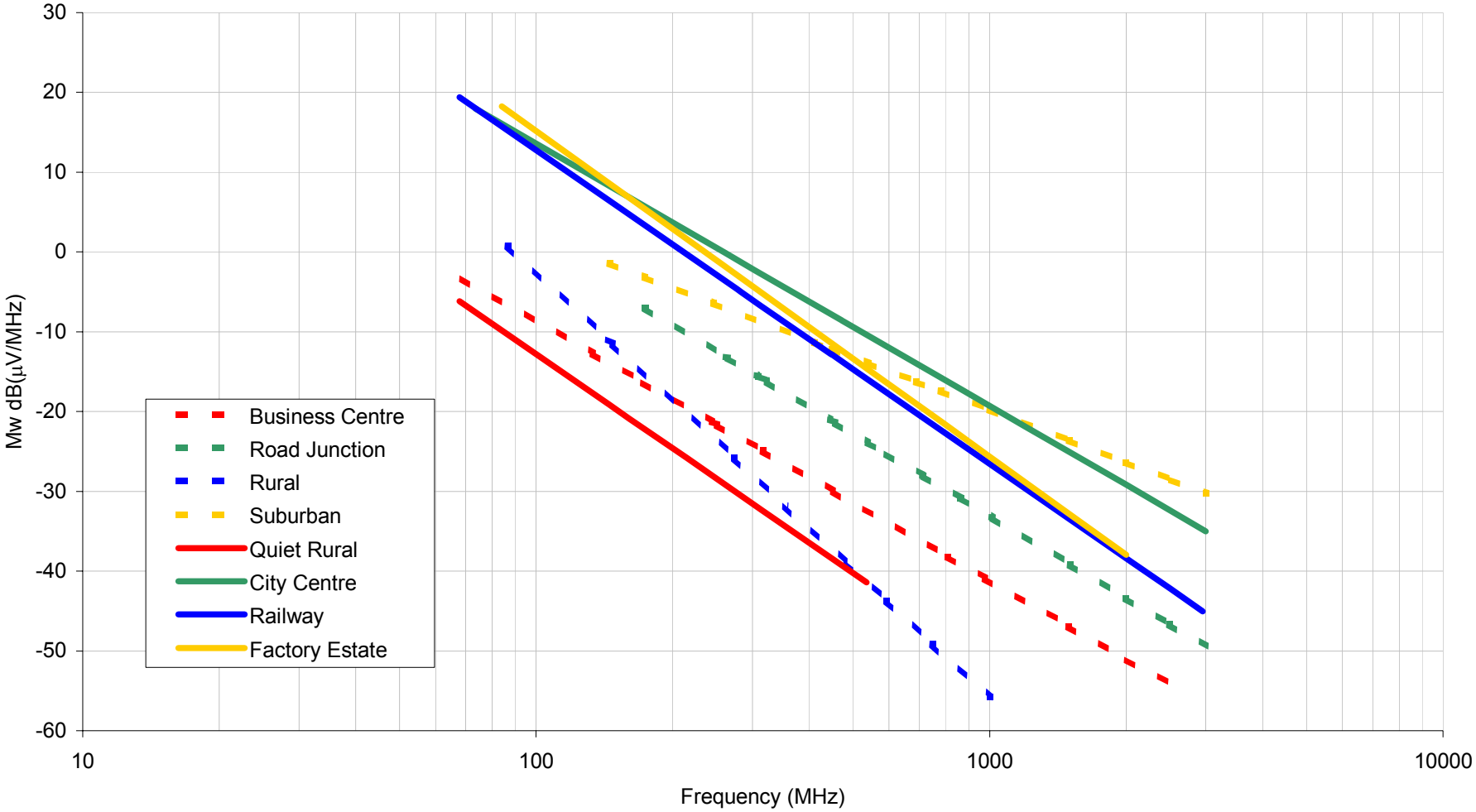

Figure 29 Mean IN Voltage Density versus Frequency

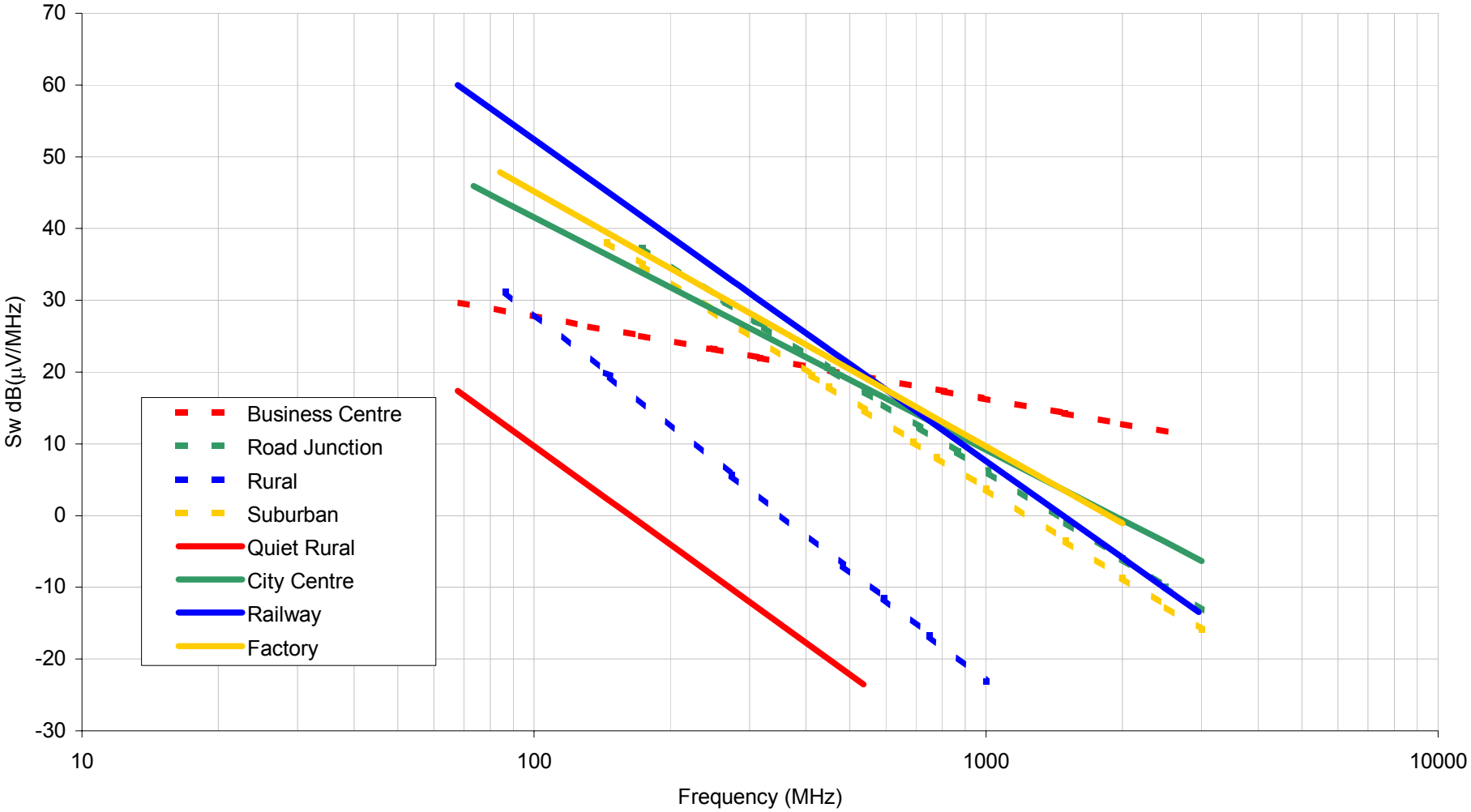

Figure 30 Standard Deviation of IN Voltage Density versus Frequency

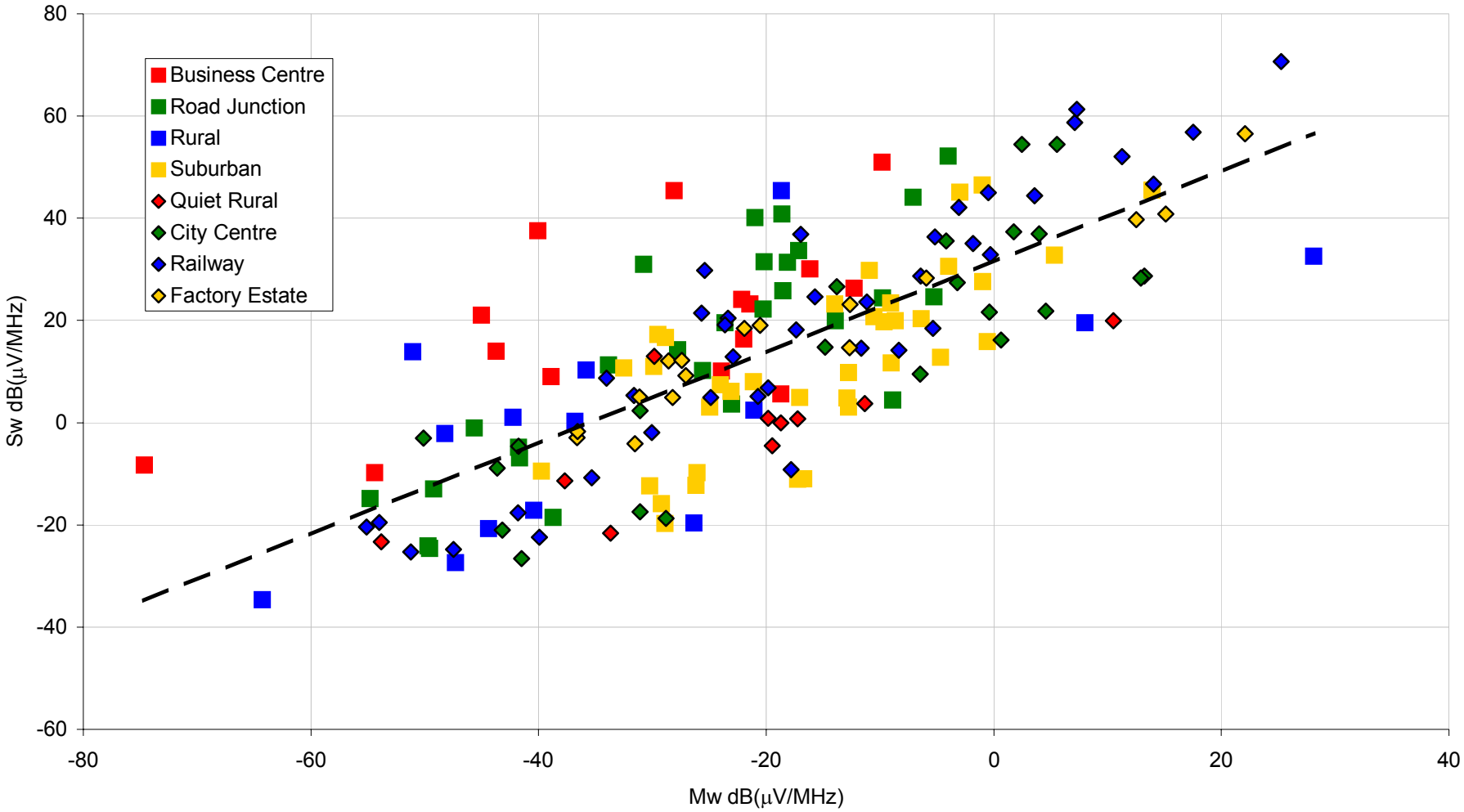

Figure 31 IN Standard Deviation versus Mean – All Sites

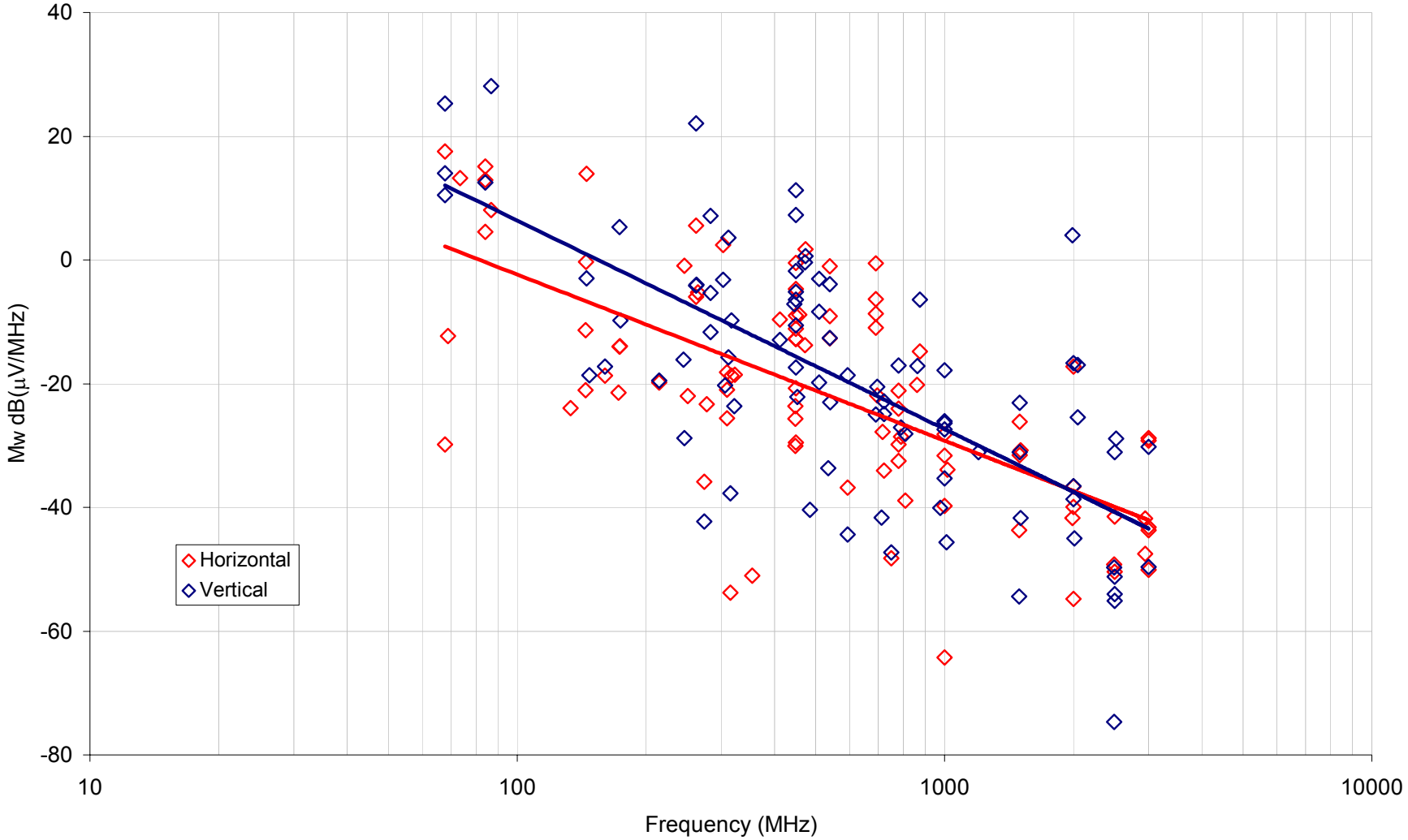

Figure 32 Effect of Polarisation on IN

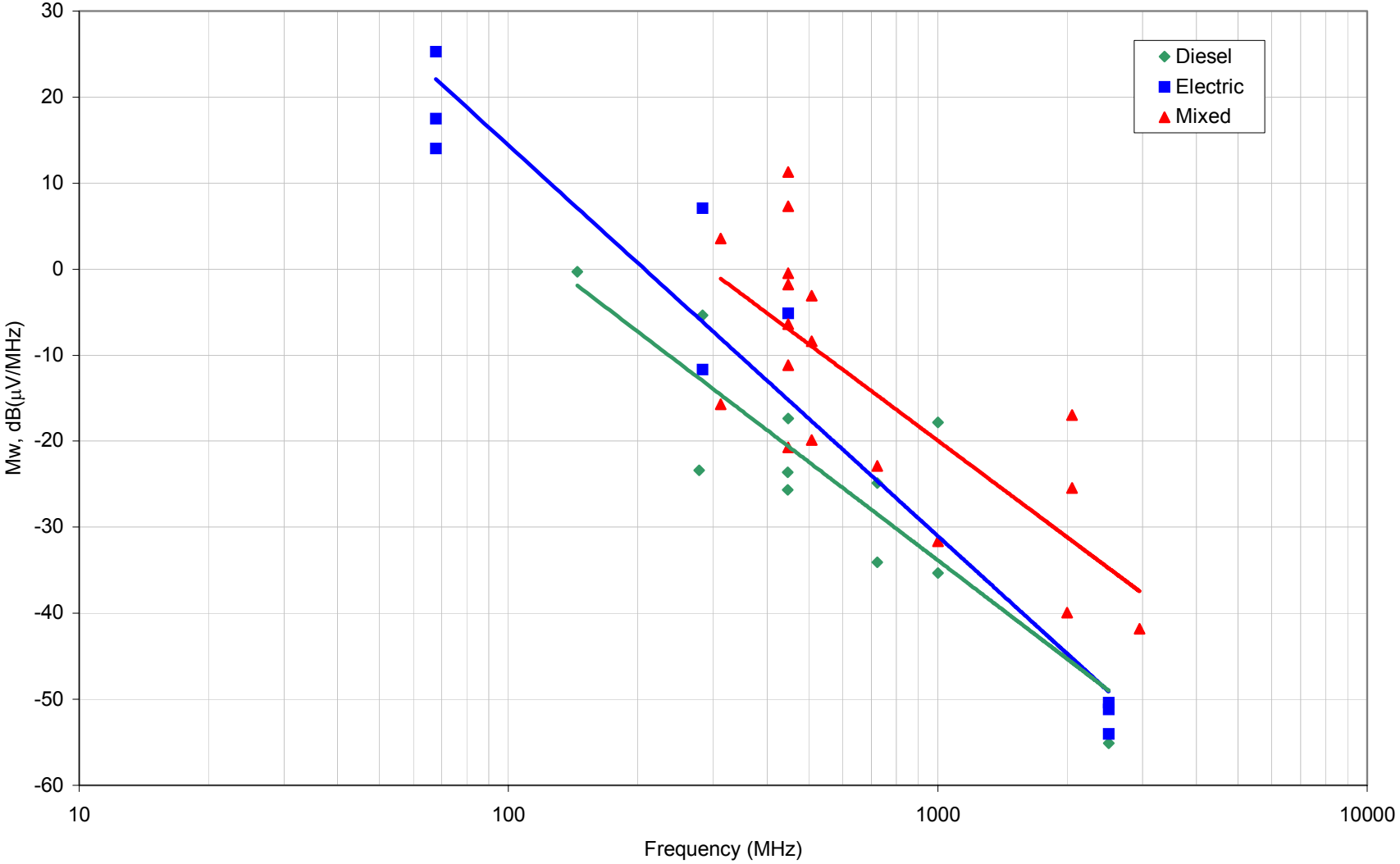

Figure 33 Mean IN Voltage Density versus Frequency by Train Type

5.3 COMPARISON OF WGN AND IN

When comparing WGN and IN it should be remembered that they are displayed in different units. This is because the power in the two components does not scale the same with bandwidth. The power level of WGN increases linearly with bandwidth, whereas the power level of IN squares with bandwidth. Hence the WGN is described in terms of dB above kT0b and the IN is shown as a voltage density in dB(μV/MHz). At higher bandwidths we can therefore expect the IN to become more significant.

Figure 34 and Figure 35 are graphs of M_w against F_a for all frequencies and at 200 MHz respectively. Following the observations above concerning the empirical relationship between M_w and S_w, we have assumed that it is reasonable to compare the class B IN and WGN levels without referring to S_w.

M_w has been estimated at the output of the receiver (see Figure 22), whilst F_a has been estimated, in accordance with [P.372], at the output of a lossless antenna. The comparison between these parameters may be considered reasonable however, provided one assumes that the measurement system does not itself contribute IN in the same way that it contributes WGN.

The City Centre and Factory Estate stand out as having high values of both types of noise, whilst the Rural and Quiet Rural had low values of each. Note however that Figure 28 suggests that the Rural site has much higher values of F_a at lower frequencies.

The Road Junction, Suburban and Railway sites exhibited relatively higher levels of IN compared to WGN, whilst the Business Centre was the opposite.

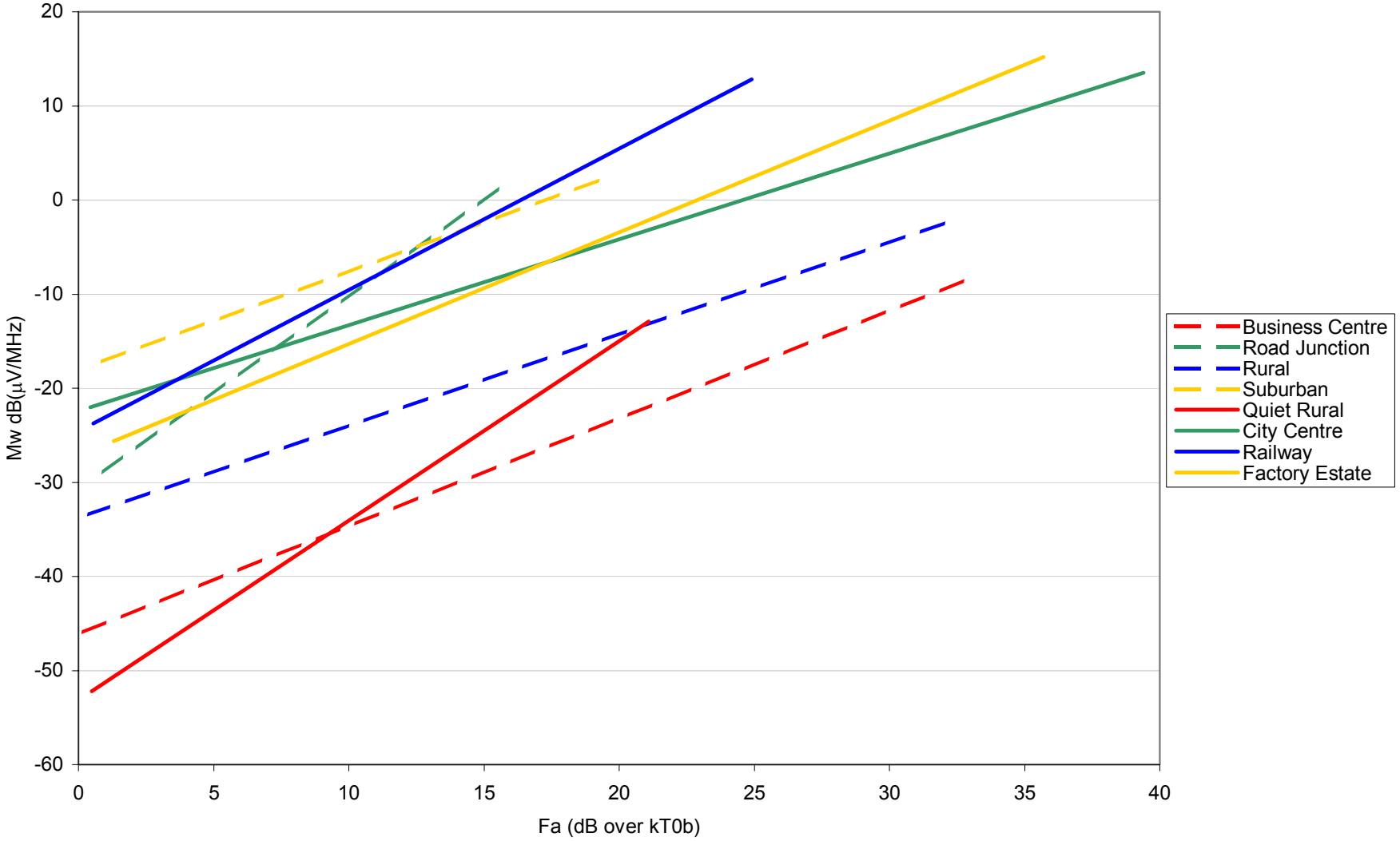

Figure 34 Mw versus Fa

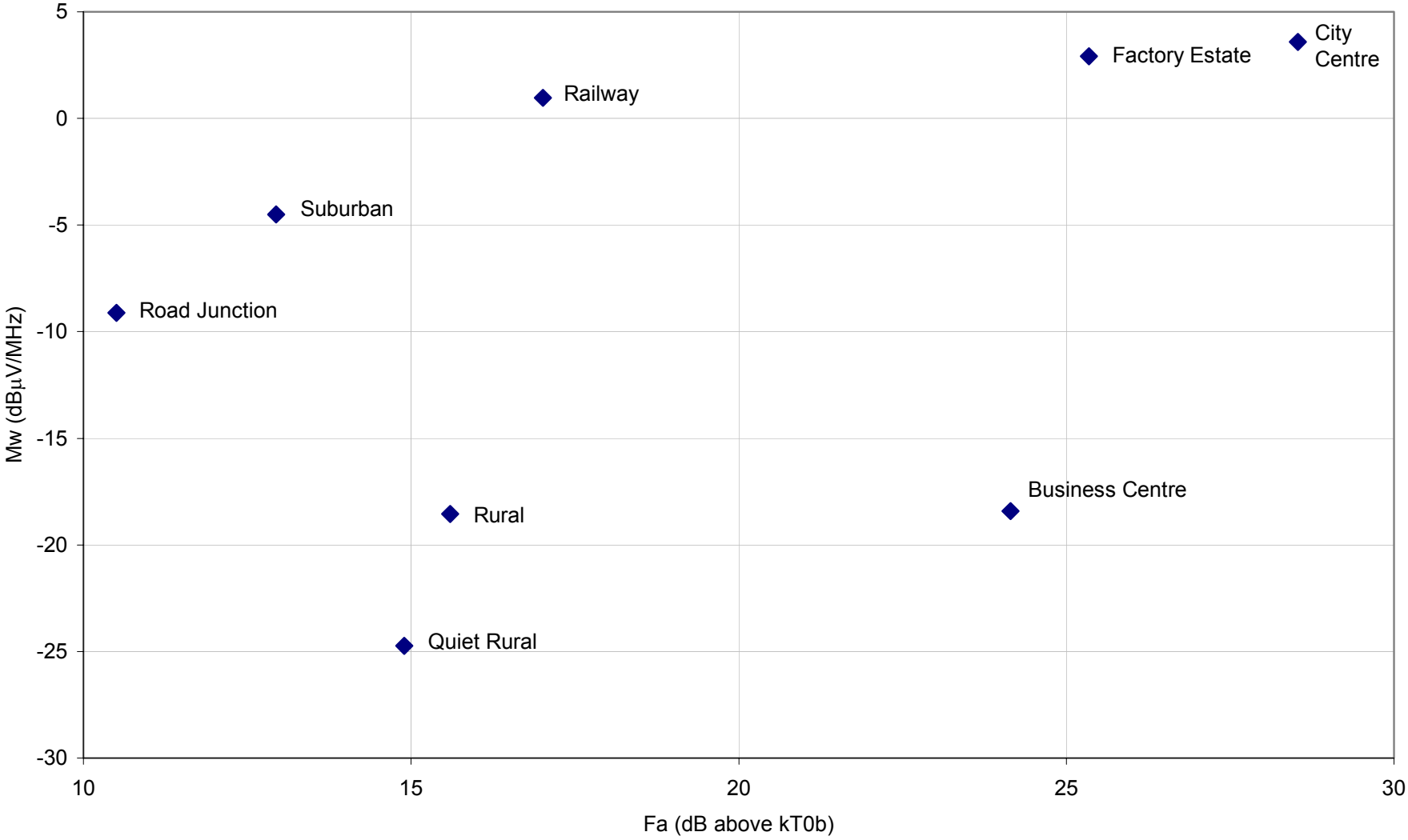

Figure 35 Mw versus Fa at 200 MHz

6 CONCLUSIONS

The Noise Measurement Facility has been successfully built and tested. It has been deployed at eight different sites and shown capable of making reliable measurements of both WGN and IN using measurement bandwidths of up to 10 MHz and across the VHF and UHF bands.

The following conclusions have been drawn:

1. Whilst producing useful results, the eight one-day tests were insufficient to build up a statistically significant set of measurements. The equipment can however be readily deployed for further testing now that it has been built and proven.

2. The definition of F_a in [P.372] needs clarification. In earlier reports it had been interpreted as the median of the distribution. It is now believed that the definition is intended to imply that F_a is to be calculated as the mean of the distribution and that the plots given in the recommendation show the medians of these means.

3. A data analysis method has been devised to circumvent the inherent problem of in-band coherent signals contaminating the F_a estimate, thus enabling the WGN level to be measured using a wideband receiver.

4. The mean values of F_a observed during this study appear significantly higher than the median values given in [P.372]. The best explanation available for this is that the number of electronic and electrical devices has grown dramatically in the UK over the past few decades. Whilst EMC legislation has suppressed the IN emissions from automotive sources, there is a general background of WGN that is possibly caused by the incoherent summation of the radiation from hundreds of pieces of equipment. If so, then this is an important finding that should be verified by further tests.

5. A simplified IN model has been applied successfully to the recorded data. This model assumes class B noise with a Weibull distribution and impulses that are Poisson distributed in time. In the majority of cases it is possible to automatically extract the Weibull parameters such that there is a good correlation between the measured data and simulation results using the same parameters.

6. Our modelling of the class B IN has used a different line fit to the APD graph than that used by the NTIA. By using the point of steepest gradient, we believe that this gives a better estimate of the noise power statistics.

7. The Poisson time distribution models the overall average impulse rate satisfactorily, but does not model the burstiness of the impulses seen in the raw data.

8. Given the assumptions made in the class B IN model, an empirical relationship has been observed that suggests that environments can be compared using just the mean IN voltage density, M_w. This parameter can be measured reliably from the APD graph and scales linearly with bandwidth when presented in units of dB(μV/MHz).

9. Analysis of the APD graphs suggests that a minimum bandwidth of 1 MHz, and preferably 2 MHz, should be used for future surveys in order to avoid overlapping impulses. If the pulse duration is of particular interest, then it is advisable to keep the bandwidth to 5 MHz or below, so that Pulse Duration Distributions (PDD) are not adversely affected by time quantisation. For normal survey work however, using a bandwidth of 10 MHz will minimise the likelihood of pulse collisions and therefore produce the best possible IN statistics.

10. No significant variation with polarisation has been found in the case of WGN. In the case of IN however, there may be some difference between the polarisations. Further work is required to investigate this phenomenon.

7 FURTHER WORK

The NMF has been built and successfully deployed at a number of sites. The following suggestions are made for its future use and development.

1. Further monitoring, both at the sites visited so far and at new sites, is necessary to build up a significant body of statistical data. The analyses of these data would allow trends to be identified, as well as quantification of the spread of the measured parameters.

2. The high levels of WGN should be verified by further tests. The emphasis of such tests would be on measuring F_a at regular intervals over a prolonged period in order to measure its variation over time. It is particularly important to perform extended testing that can establish the median values of F_a for comparison with the [P.372] values.

3. Further surveys should use different antennas to validate the measurements made in this study. Ideally a few spot frequencies should be chosen and a set of omnidirectional antennas used. This approach would have been unwieldy for this study, but is advisable for calibration purposes in future work.

4. Characterisation of the RA's van in a chamber is highly recommended. A completely quiet environment was not available during this study, but it was found that such a facility would be essential to properly characterise the effects of the van power supplies on the measurements.

5. There is some evidence from the data recorded during this study that the level of IN varies with polarisation. The NMF could be used to specifically investigate this phenomenon.

6. The use of the Poisson distribution for the timing of impulses in the NTIA model has the advantage that it is analytically tractable and can readily be made to fit the large-scale characteristics of the measured data. It does not however model the burstiness of impulses that are seen in practice. A more convincing model would include this characteristic as well as matching the overall impulse rate used by the Poisson distribution. The existing digitised IF data could be used to investigate this further.

7. The extraction of the Weibull distribution parameters for the IN model could be performed in near real-time and incorporated in bench and portable analysis equipment. The Rohde & Schwarz FSU range of spectrum analysers already incorporate histogramming functions ('APD' and 'CCDF') which could form the basis for such functionality. Future work could include working with the ITU to adopt a standard measure of the IN using the class B model. This would encourage the test equipment manufacturers to build in the appropriate functions. Once available in near real-time, the measurement of IN levels would be much simplified.

8. The definition of F_a applies to a reference point that is the output of a lossless antenna. It is recommended that a similar reference point be used for the IN mean and standard deviation, rather than the output of the receiver, as used in this report. Agreement on a reference point is a matter for discussion within the ITU.

9. There appears to be an empirical link between the Weibull distribution parameters, which was unexpected. Graphs of S_w versus M_w (e.g. Figure 31) show a strong correlation when all the tests at one site are plotted on the same axes. As yet there is no physical explanation for this phenomenon. Further research would be needed to confirm that such a relationship exists.

10. The survey data from the Railway site has not been analysed to determine the noise levels at the 'point of closest approach'. Such an analysis may prove beneficial in that it could produce a general method for estimating the levels of noise due to individual, moving trains.

11. The existing NMF does not have RF preselection filters and there is therefore some concern that strong out-of-band signals could affect the results. This issue should be investigated in the laboratory. Ideally, one would wish to work without additional filters, as it is important to avoid introducing extra loss and noise, but it is recognised that a working method that incorporates their use may have to be developed.

12. The simplified IN model used in this study has treated class A noise as class B. The Middleton noise model includes a very thorough characterisation of the IN. Whilst not, at the present time, suitable for use in survey work, it is suggested that MATLAB scripts be developed to extract the Middleton model parameters from data collected on the NMF. This would lead to useful insights with respect to the relative levels of class A, B and C impulsive noise.

8 ABBREVIATIONS

ACR	Average Crossing Rate
APD	Amplitude Probability Distribution
CCDF	Complementary Cumulative Distribution Function
CDF	Cumulative Distribution Function
DERA	Defence Evaluation and Research Agency (now Qinetiq)
EMC	Electromagnetic Compatibility
IF	Intermediate Frequency
IN	Impulsive Noise
ITU	International Telecommunications Union
MMN	Man-Made Noise
NAD	Noise Amplitude Distribution
NMF	Noise Measurement Facility
NTIA	National Telecommunications and Information Administration
PD	Pulse Duration (= PW)
PDD	Pulse Duration Distribution
PDF	Probability Distribution Function
PDW	Pulse Descriptor Word
PID	Pulse Interval Distribution
PSD	Power Spectral Density
PW	Pulse Width (= PD)
RA	Radiocommunications Agency
RF	Radio Frequency
TOA	Time Of Arrival
UHF	Ultra High Frequency
VHF	Very High Frequency
WGN	White Gaussian Noise

9 DEFINITIONS

α	'Exponent' parameter for the IN Weibull distribution at the output of the receiver
Δt	Simulation time increment
γ	Mean rate of impulses that exceed a given threshold (impulses/s)
Γ	Standard function that interpolates the factorial function
a	Weibull distribution parameter
A(x)	Amplitude probability distribution of x
$A_g()$	WGN amplitude probability distribution
$A_w()$	Weibull amplitude probability distribution
b	Weibull distribution parameter
b	3dB Bandwidth (= Noise Equivalent Bandwidth unless otherwise stated)
f	External noise factor, see ITU-R P.372-7 [P.372]
f_a	External Noise Figure, as defined in [P.372] and represents the mean WGN power level at the output of the antenna
F_s	Sampling rate
m_w, M_w	Mean IN power level at the output of the receiver. This can be usefully expressed in terms of a voltage density in dB(μV/MHz)
$p_g()$	WGN probability density function
$p_w()$	Weibull probability density function
$P(x)$	Probability of x
s_w, S_w	Standard deviation of the IN noise at the output of the receiver
T	Mean pulse duration
v	Voltage
w, W	Power
w_{0g}, W_{0g}	Mean WGN power level at the output of the receiver
w_{0w}, W_{0w}	Power level of the IN Weibull distribution at the output of the receiver at the 37% exceedence level

10 REFERENCES

[Achatz98] Achatz, R.J., Lo, Y., Papazian, P.B., Dalke, R.A. and Hufford, G.A. *Man-Made Noise in the 136 to 138-MHz VHF Meteorological Satellite Band*. NTIA Report 98-355, 1998.
(Available from www.its.bldrdoc.gov/pub)

[Achatz01] Achatz, R.A. and Dalke, R.A. *Man-Made Noise Power Measurements at VHF and UHF Frequencies*. NTIA Report 02-390, 2001.
(Available from www.its.bldrdoc.gov/pub)

[Barton97] Barton, D.K. *Modern Radar System Analysis.* London: Artech House, 1997.
(ISBN 0-89006-170-X, MASS reference MC0250)

[Biddulph88] Biddulph, D. *Radio Communication Handbook, 6th ed*. Potters Bar: Radio Society of Great Britain, 1998.
(ISBN 1-872309024-0, MASS reference MC04739)

[Blake86] Blake, L.V. *Radar Range-Performance Analysis*. London: Artech House, 1986.
(ISBN 0-89006-224-2, MASS reference MC0122)

[Blanchard00] Blanchard, L.S. and Whitehead, D. *A study to assess the possible effects of radio based services of electromagnetic emissions from the proposed increase of electrically powered public and private transport*. Transport Research Laboratory report PR/SE/186/00, 2000.

[CCIR 258-5] CCIR Report 258-5. *Man-made radio noise*. Reports of the CCIR annex to Vol 6, ITU, Geneva, 1990.
(Available from IEE Library, London)

[CCIR 322-3] CCIR Report 322-3. *Characteristics and applications of atmospheric radio noise data*. ITU, Geneva, 1986.
(Available from IEE Library, London)

[Clark62] Clarke, C. *Atmospheric radio-noise studies based on amplitude-probability measurements at Slough, England, during the international geophysical year.* Institution of Electrical Engineers, Paper No. 3908E, 1962.
(Available from IEE Library, London)

[Davenport87] Davenport Jr., W.B. and Root, W.L. *An Introduction to the Theory of Random Signals and Noise*. New York: IEEE Press, 1987.
(ISBN 0-87942-235-1, Available on loan from IEE Library, London)

[Evans99] Evans, B.G. *Satellite Communication Systems*. Stevenage: Institution of Electrical Engineers, 1999.
(ISBN 0-85296-899-X)

[FSU3 Manual] *Spectrum Analyzer Operating Manual*, Rohde & Schwarz, 1129.9055.12-02-.

[Hagn] Hagn, G.H. *Man-Made Radio Noise and Interference*. proc. AGARD Conf. No. 420, Lisbon, Portugal, Oct. 26 – 30, 1987, pp. 5-1 to 5-15.

[Hall91] Hall, M.P.M, Barclay, L.W. and Hewitt, M.T. *Radiowave Propagation*. Stevenage: Institution of Electrical Engineers, 1991.
(ISBN 0-85296-819-1, MASS reference MC0251)

[Hall96] Hall, M.P.M, Barclay, L.W. and Hewitt, M.T. *Propagation of Radiowaves*. Stevenage: Institution of Electrical Engineers, 1996.
(ISBN 0-85296-819-1)

[Horowitz82] Horowitz and Hill. *The Art of Electronics*, Cambridge: Cambridge University Press, 1982.
(ISBN 0-521-29837-7)

[Hovanessian88] Hovanessian, S.A. *Introduction To Sensor Systems*. Norwood: Artech House, 1988.
(ISBN 0-89006-271-4, MASS reference MC0147)

[Jeruchim92] Jeruchim, M.C, Balaban, P and Shanmugan, K.S. *Simulation of Communication Systems*. New York: Plenum Press, 1992.
(ISBN 0-306-43989-1, Available on loan from IEE Library, London)

[Kennedy81] Kennedy, G. *Electronic Communication Systems*, 2nd ed. London: McGraw-Hill, 1981.
(ISBN 0-07-034052-8)

[Krauss80] Krauss, H.L., Bostian, C.W. and Raab, F.H. *Solid State Radio Engineering*. New York: John Wiley & Sons, 1980.
(ISBN 0-471-03018-X)

[Lathi83] Lathi, B.P. *Modern Digital and Analog Communications Systems*. New York: CBS College Publishing, 1983.
(ISBN 4-8337-0156-1)

[Lauber77] Lauber, W.R. and Bertrand, J.M. *Preliminary urban VHF/UHF radio noise intensity measurements in Ottawa, Canada*. Proc. 2nd symposium and technical exhibition on EMC. IEEE cat. no. 77CH1224-5EMC, pp. 357 - 362. 1977.
(Available from IEE Library, London)

[Lauber84] Lauber, W.R. and Bertrand, J.M. *Man-made noise level measurements of the UHF radio environment*. In: Proc. of the IEEE National Symposium on EMC, San Antonio, TX, 1984.
(Available from IEE Library, London)

[Lynn82] Lynn, P.A. *An Introduction to the Analysis and Processing of Signals*. London: MacMillan Publishers Ltd., 1982.
(ISBN 0-333-34030-2)

[Maslin87] Maslin, N. *HF Communications*. London: Pitman Publishing, 1987.
(ISBN 0-273-02675-5, MASS reference MC0438)

[Middleton73] Middleton, D. *Man-made noise in urban environments and transportation systems: Models and Measurements.* In: IEEE Transactions on vehicular technology, Vol. VT-22, No. 4, pp. 148 - 157. 1973

[Middleton75] Middleton, D. *Statistical-physical models of man-made and natural radio-noise envrironments - Part I: First-order probability models of the instantaneous amplitude*. Office of Telecommunications Report OT 74-36, April 1975.

[Middleton76] Middleton, D. *Statistical-physical models of man-made and natural radio-noise envrironments - Part II: First-order probability models of the envelope and phase*. Office of Telecommunications Report OT 76-86, April 1976.

[Middleton78a] Middleton, D. *Statistical-physical models of man-made and natural radio-noise envrironments - Part III: First-order probability models of the instantaneous amplitude of Class B interference.* NTIA Contractor Report 78-1, June 1978.

[Middleton78b] Middleton, D. *Statistical-physical models of man-made and natural radio-noise envrironments - Part IV: Determination of the first-order parameters of Class A and Class B interference*. NTIA Contractor Report 78-2, September 1978.

[Middleton96] Middleton, D. *An Introduction to Statistical Communication Theory*. New York: IEEE Press, 1996.
(ISBN 0-7803-1178-7, Available on loan from IEE Library, London)

[MiddletonJ01] Middleton, J. *The calibration of VHF/UHF field strength measuring equipment*. BBC R&D White Paper WHP001, 2001.

[Modestino81a] Modestino, J. W. and Sankur, B. *Analysis and modeling of impulsive noise*. Arch. Elek. Ubertragung, Vol. 35, pp. 481 - 488. 1981.
(Available from IEE Library, London)

[Modestino81b] Modestino, J. W. and Sankur, B. *Performance of receivers in impulsive noise.* Arch. Elek. Ubertragung, Vol. 36, pp. 111 - 118. 1981.

[Modestino84] Modestino, J. W. and Matis, K.R. *Interactive simulation of digital communication systems*. In: IEEE Journal On Selected Areas In Communications, Vol. SAC-2, No. 1. 1984.
(Available from IEE Library, London)

[Morrison92] Morrison, R. *Noise and Other Interfering Signals*. USA. John Wiley & Sons, 1992.
(ISBN 0-471-54288-1, Available on loan from IEE Library, London)

[Murthy95] Murthy, S.N. and Krishnamraju, G. *Interference to low earth orbit satellite (LEOS) services in VHF band from ground based emissions*. IETE Technical Review, Vol. 12, Nos. 5 & 6, pp. 325 - 329. 1995.
(Available from IEE Library, London)

[Northey00] Northey, B.J. and Whitham, P.S. *A comparison of DSTO and DERA HF background noise measuring systems with the International Radio Consultative Committee (CCIR) model data*, Defence Science and Technology Organisation, Australia. DSTO publication DSTO-TR-0855, 2000.
(Available from www.dsto.defence.gov.au/corporate/reports)

[Ohta99] Ohta, M., Mitani, Y. and Ogawa, H. *Multi-dimensional generalisation in space and time domains for Middleton's study in stochastic evaluation of correlative many EM noise processes.* Progress in Electromagnetics Research, PIER 24, 97-118. 1999.

[Ohta01] Ohta, M. and Ogawa, H. *A trial on hierarchical extraction of higher order correlation between electromagnetic and sound waves around a VDT environment – Practical use of background noise and probability prediction*. Progress in Electromagnetics Research, PIER 34, 285-298. 2001.

[Okunev97] Okunev, Y. *Phase and Phase-Difference Modulation in Digital Communications*. London: Artech House, 1997.
(ISBN 0-89006-937-9, MASS reference 0450)

[Oshita82] Oshita, S. and Feher, K. *Performance of coherent PSK and DPSK systems in an impulsive and gaussian noise environment.* In: IEEE Transactions on Communications, Vol. COM-30, No. 12, pp. 2540 - 2546. 1982.

[P.372] *Radio Noise*. ITU-R Recommendation P.372-7, Geneva, 2001.

[Pace00] Pace, P. *Advanced Techniques for Digital Receivers*. Boston: Artech House, 2000.
(ISBN 1-58053-053-2, MASS reference MC0480)

[Parsons79] Parsons, J.D. and Sheikh, A.U.H. *The characterisation of impulse noise and considerations for a noise-measuring receiver*. In: The Radio and Electronic Engineer, Vol. 49, No. 9, 1979. pp. 467 - 476.
(Available from IEE Library, London)

[Parsons83] Parsons, J.D. and Sheikh, A.U.H. *Statistical characterization of v.h.f man-made radio noise*. The Radio and Electronic Engineer, Vol. 53, No.3, pp. 99 - 106. March 1983.
(Available from IEE Library, London)

[Parsons89] Parsons, D. and Gardiner, J.G. *Mobile Communications Systems*. London: Blackie and Son Ltd., 1989.
(ISBN 0-216-92261-5, Available on loan from IEE Library, London)

[Parsons92] Parsons, D. *The Mobile Radio Propagation Channel*. London: Pentech Press Ltd., 1992.
(ISBN 0-7273-1316-9, Available on loan from IEE Library, London)

[PFAT] United Kingdom Table of Radio Frequency Allocations, 9kHz - 105 GHz.
(Available from www.radio.gov.uk)

[Rice45] Rice, S.O., *Mathematical Analysis of Random Noise II*, Bell System Tech. J., 24: 46, 1945.

[Riemann] Riemann, A.I. and Evans, N.E. *Man-made impulsive noise measured at 450 MHz in a hospital environment*. University of Ulster, N. Ireland.

[Sheikh83] Sheikh, A.U.H. and Parsons, J.D. *The frequency dependence of urban man-made noise*. The Radio and Electronic Engineer, Vol. 53, No.3, pp. 92 - 98. March 1983.
(Available from IEE Library, London)

[Schleher86] Curtis Schleher, D. *Introduction to Electronic Warfare.* London: Artech House, 1986.
(ISBN 0-89006-142-4, MASS reference MC0502)

[Shukla01] Shukla, A. *Feasibility Study Into the Measurement of Man-Made Noise.* DERA Report DERA/KIS/COM/CR010470, 2001.
(Available from www.radio.gov.uk)

[Skolnik 70] Skolnik, M.I. *Radar Handbook*. New York: McGraw-Hill, 1970.
(ISBN 07-057908-3., MASS reference MC0293)

[Skomal85] Skomal, E.N. and Smith Jr., A.A. *Measuring the radio frequency environment*. New York: Van Nostrand Reinhold Company Ltd., 1985. (ISBN 0-442-28184-6, Available on loan from IEE Library, London)

[Spaulding62] Spaulding, A.D, Roubique, C.J. and Crichlow, W.Q. *Conversion of the amplitude-probability distribution function for atmospheric radio noise from one bandwidth to another*. Journal of Research of the National Bureau of Standards - D. Radio Propagation, Vol. 66D, No. 6, pp. 713 - 720. 1962.
(Available from IEE Library, London)

[Turkmani86] Turkmani, A.M.D and Parsons, J.D. *A wide band, high dynamic range receiving system for measuring the parameters of impulsive noise.* 4th International Conference on Radio Receivers and Associated Systems, Bangor, IERE Conf. Pub. No. 68, 1986.
(Available from IEE Library, London)

[Weibull51] Weibull W., *A statistical distribution function of wide applicability*, J.Appl.Mech.,18, pp.293-297, 1951.

[Winder98] Winder, Steve. *Telecommunications Engineer's Pocket Book*, 2nd ed. Oxford: Butterworth-Heinemann, 1998.
(ISBN 0-7506-39369)

[Withers99] Withers, D. *Radio Spectrum Management*, 2nd ed. Stevenage: Institution of Electrical Engineers, 1999.
(ISBN 0-85296-770-5, Available on loan from IEE Library, London)

[VanderZiel55] Van der Ziel, A. *Noise*. New York, Prentice-Hall, 1955.
(Available on loan from IEE Library, London)

[Ziemer67] Ziemer, R.E. *Error probabilities due to additive combinations of gaussian and impulsive noise*. Avionics Laboratory, Wright-Patterson AFB, Dayton, Ohio, IEEE Transactions on Communications Technology, 15-3, pp. 471 - 474. 1967.

APPENDIX A: EXAMPLE APD AND NAD GRAPHS

This section contains a selection of representative APD and NAD graphs in a series of frequency bands. NAD graphs are only available in those cases where a significant amount of impulsive noise was observed.

APDs have been drawn assuming a reference temperature, T_0, of 290K. The following colour scheme is used on these graphs:

Red	ADC limit (+1v)
Magenta	APD of a single recording (30s duration)
Black	Total APD of all the recordings in a batch (typically 5 or 10)
Blue	APD of the data recorded in the chamber at RA's Whyteleafe site
Green	APD of the data recorded when the input to the analyser was terminated with a 50Ω load.

Only one line is plotted on the NAD. This is the composite of all the PDWs from all the recordings in a batch.

Each graph has text annotation giving the Centre Frequency (CF), Resolution Band Width (RBW), Power Reference Level (PRL), Polarisation, ambient environment temperature, measurement system temperature and the start time of the first recording in the batch.

A.1 40 to 50 MHz

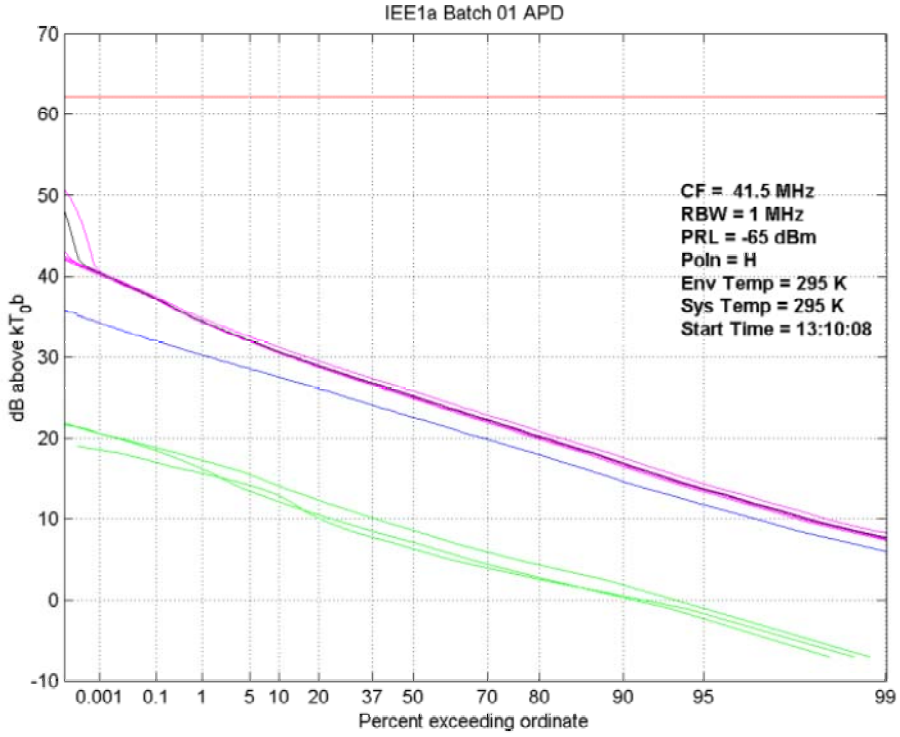

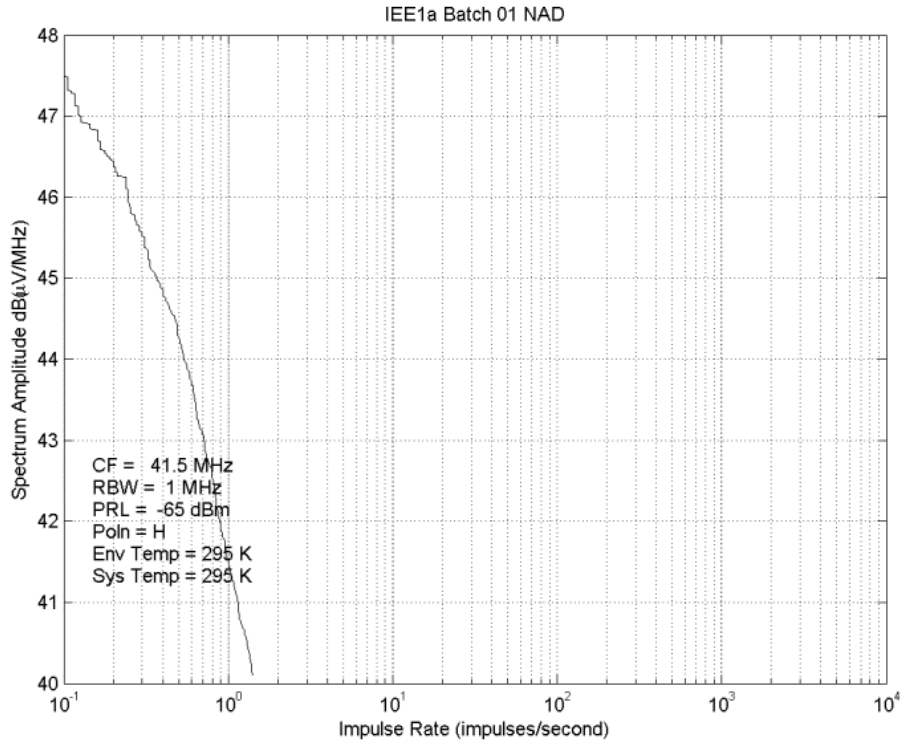

Figure 36 City Centre APD and NAD (40 to 50 MHz band)

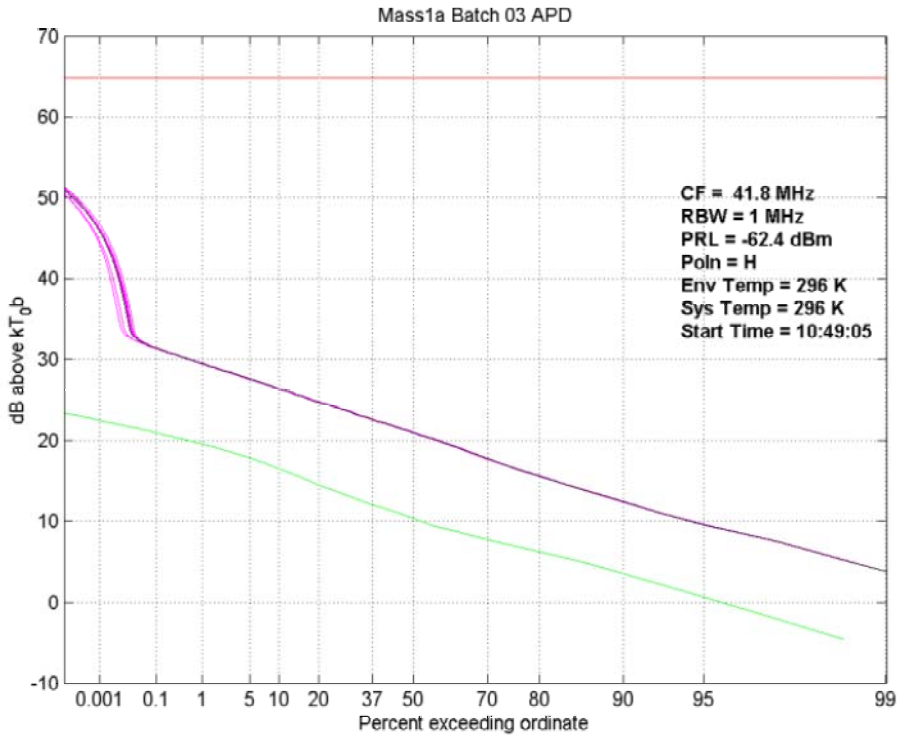

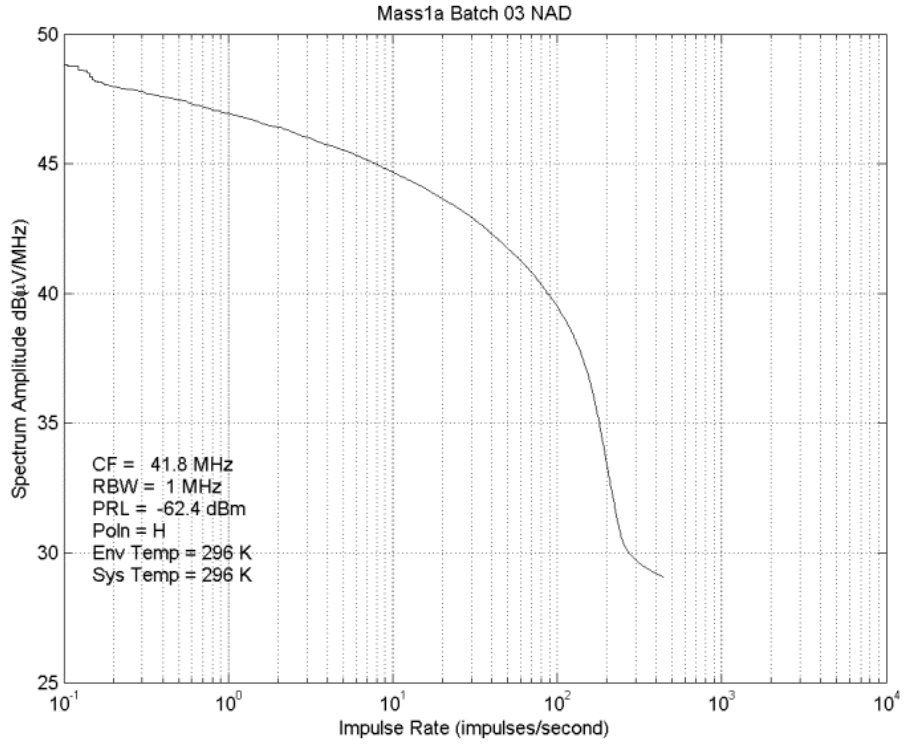

Figure 37 Suburban APD and NAD (40 to 50 MHz band)

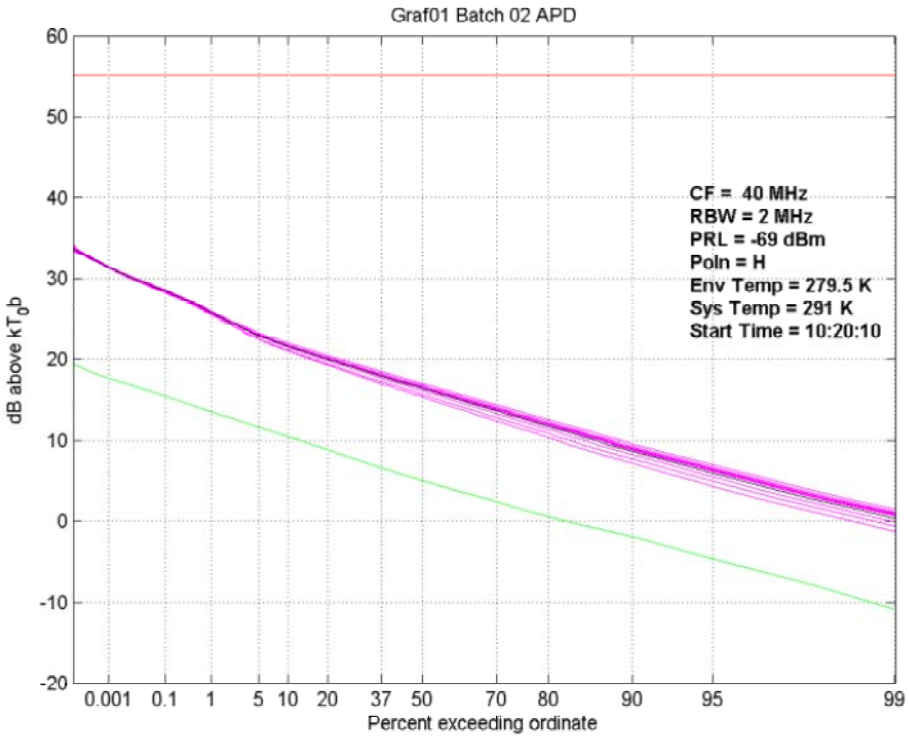

Figure 38 Quiet Rural APD (40 to 50 MHz band)

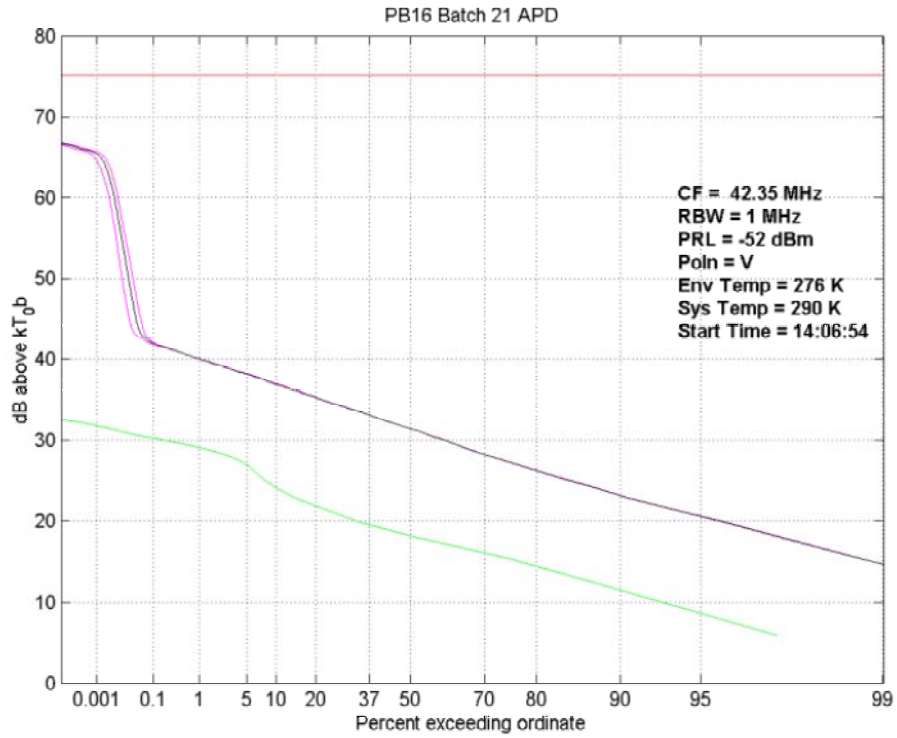

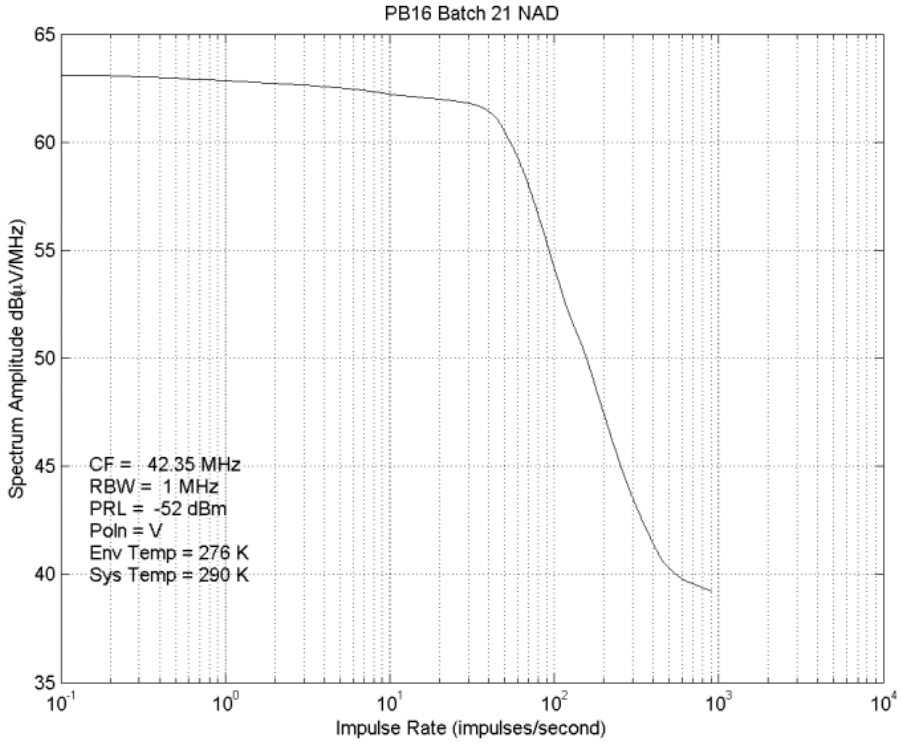

Figure 39 Railway APD and NAD (40 to 50 MHz band)

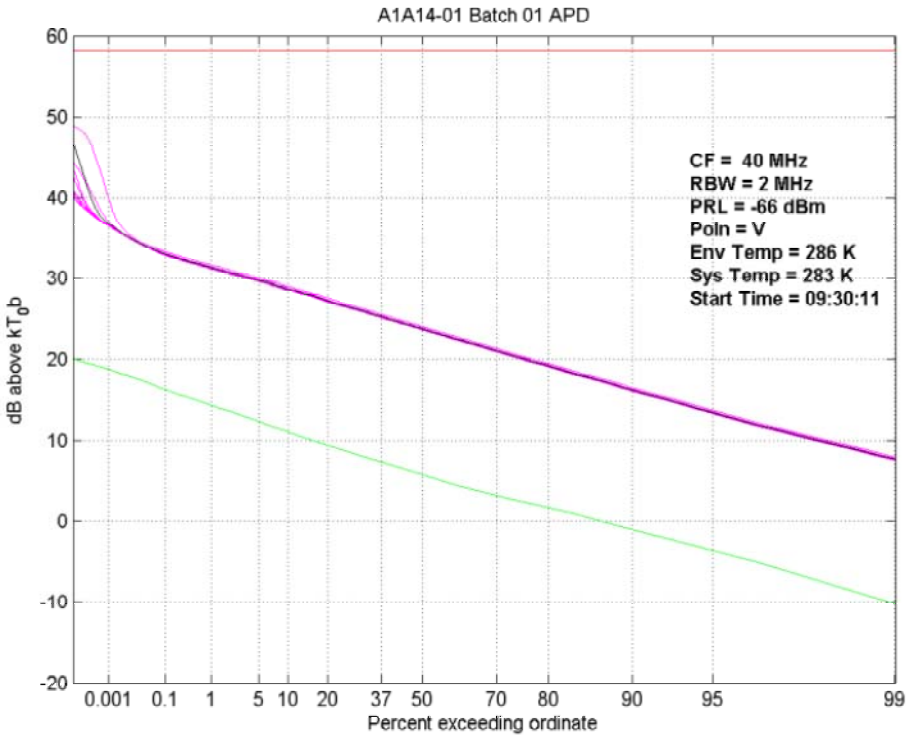

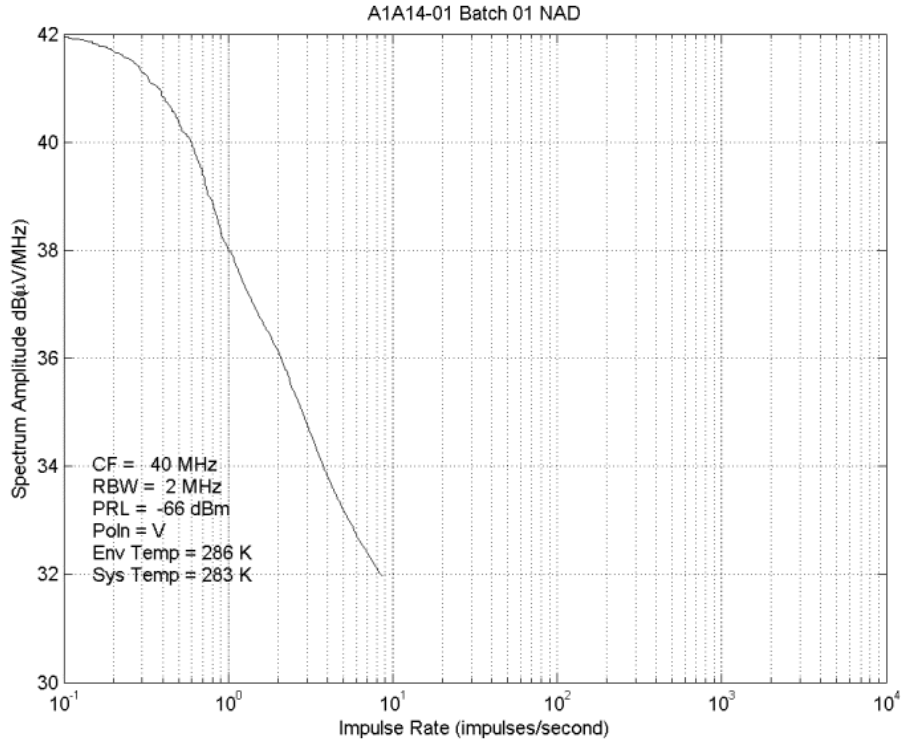

Figure 40 Road Junction APD and NAD (40 to 50 MHz band)

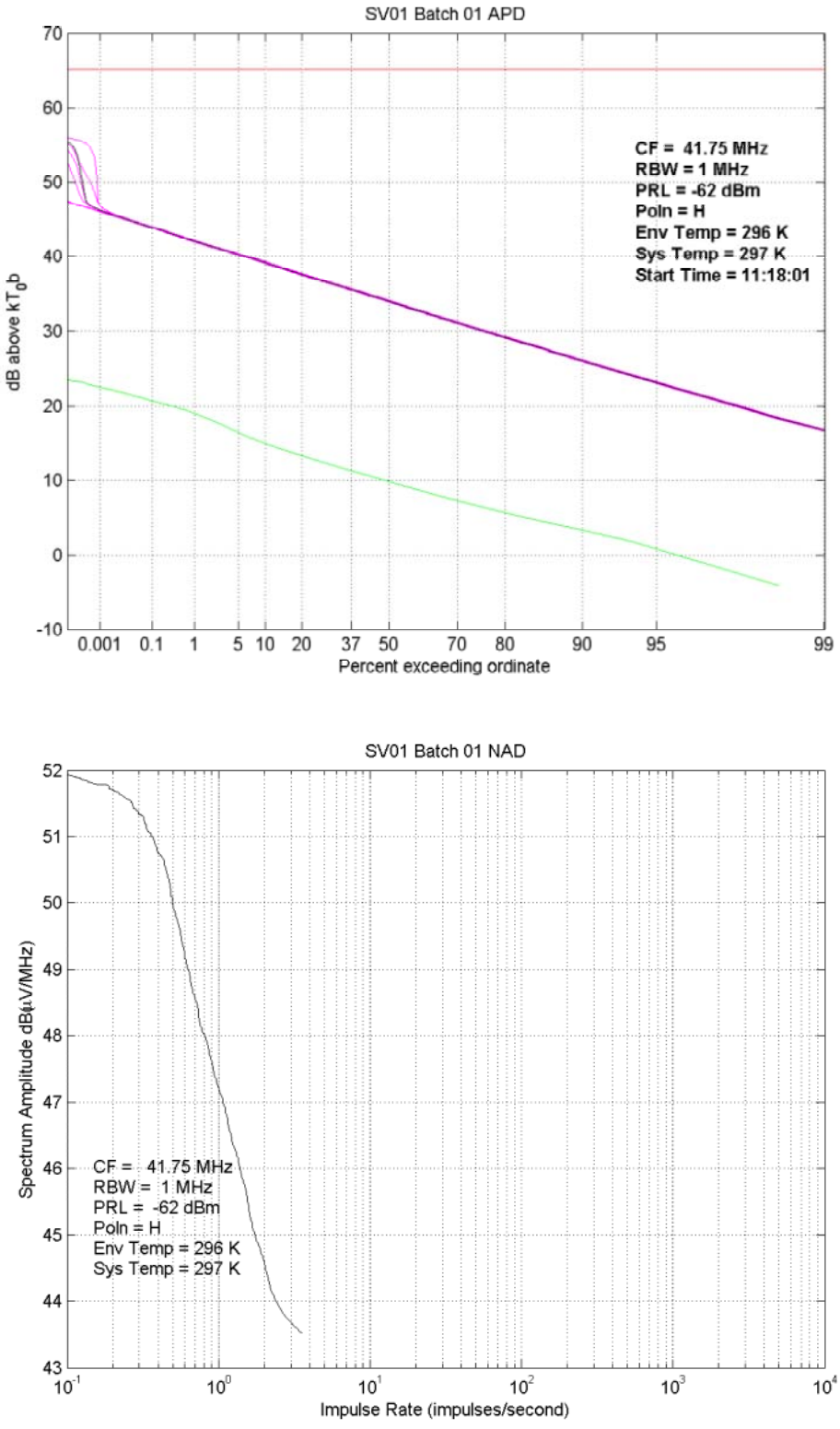

Figure 41 Business Centre APD and NAD (40 to 50 MHz band)

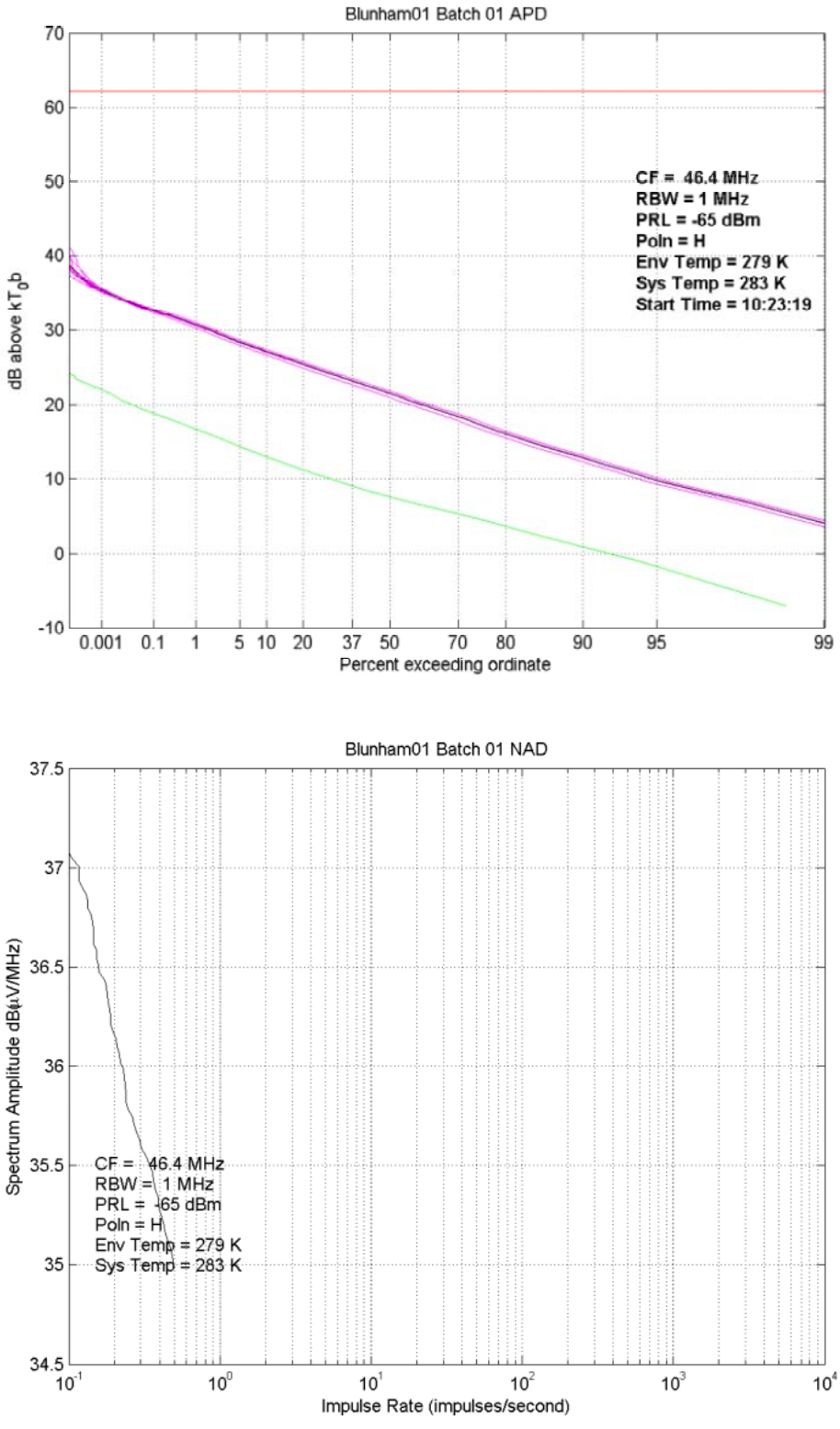

Figure 42 Rural APD and NAD (40 to 50 MHz band)

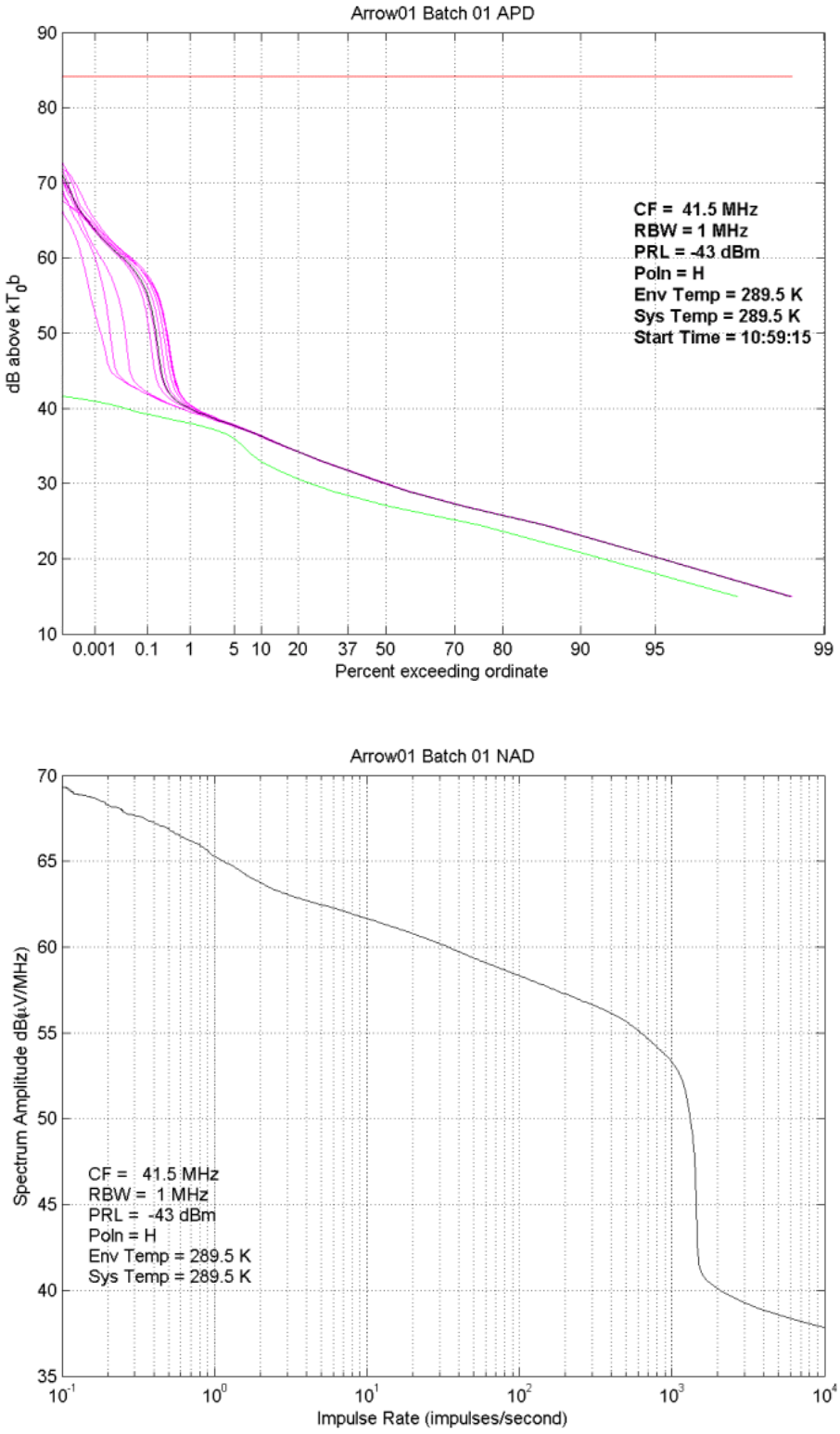

Figure 43 Factory Estate APD and NAD (40 to 50 MHz band)

A.1 130 to 150 MHz

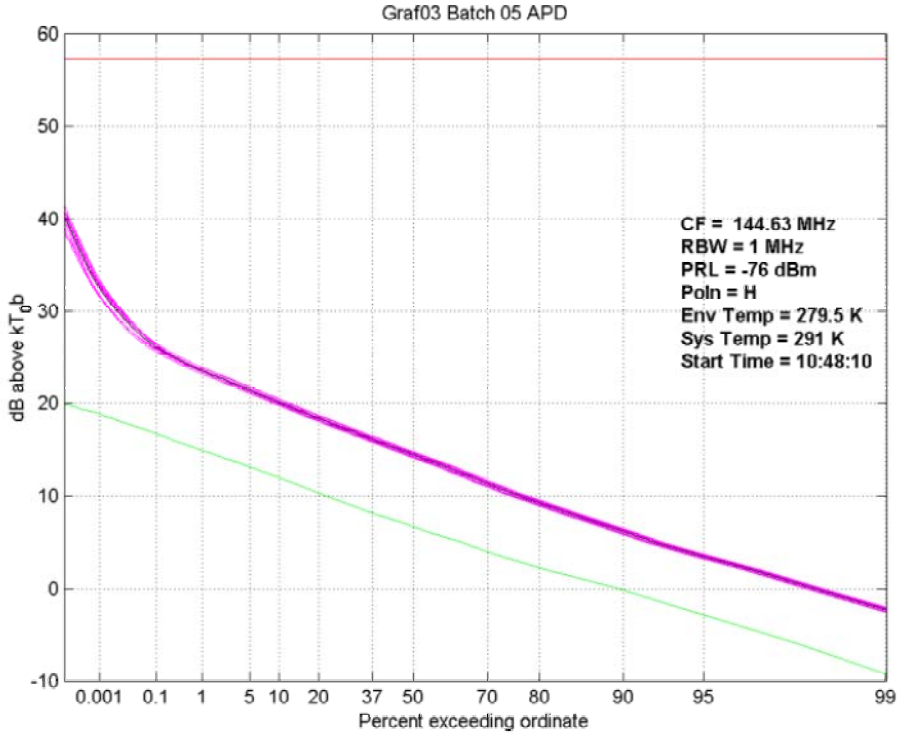

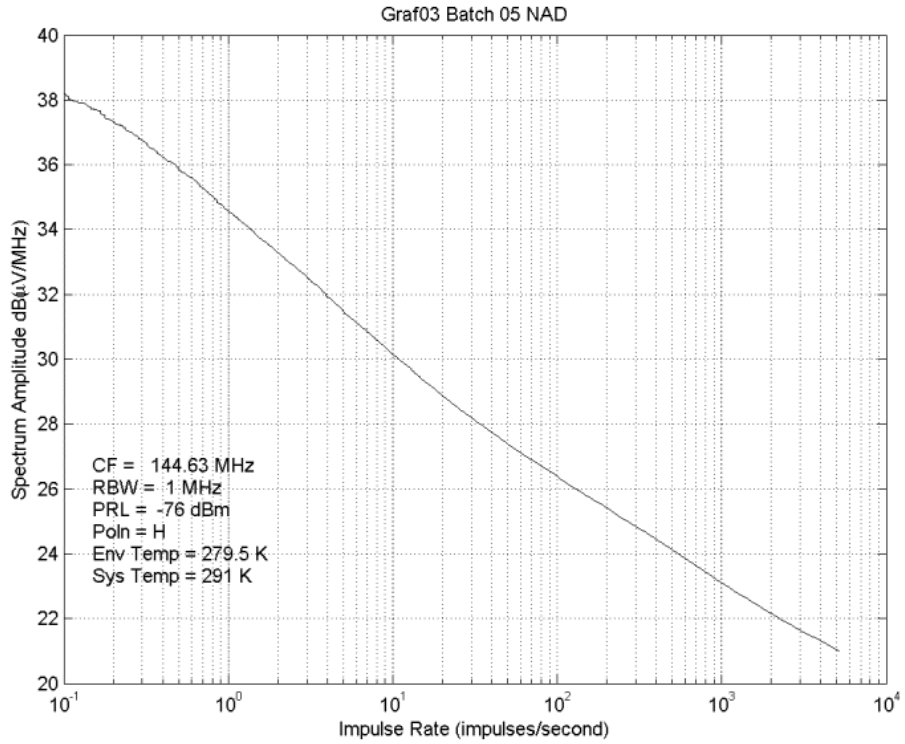

Figure 44 Quiet Rural APD and NAD (130 to 150 MHz band)

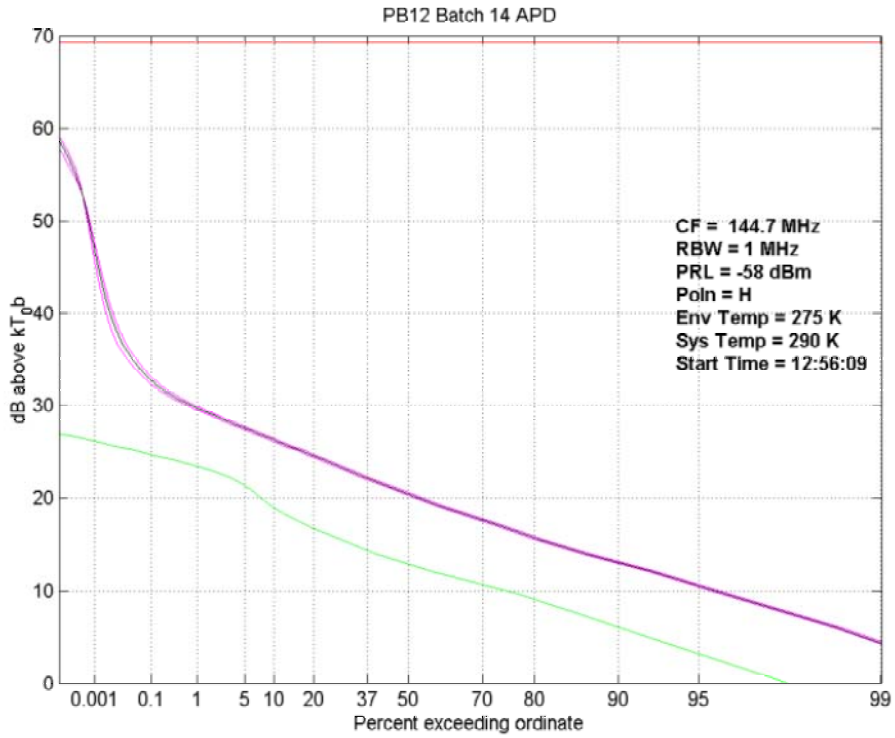

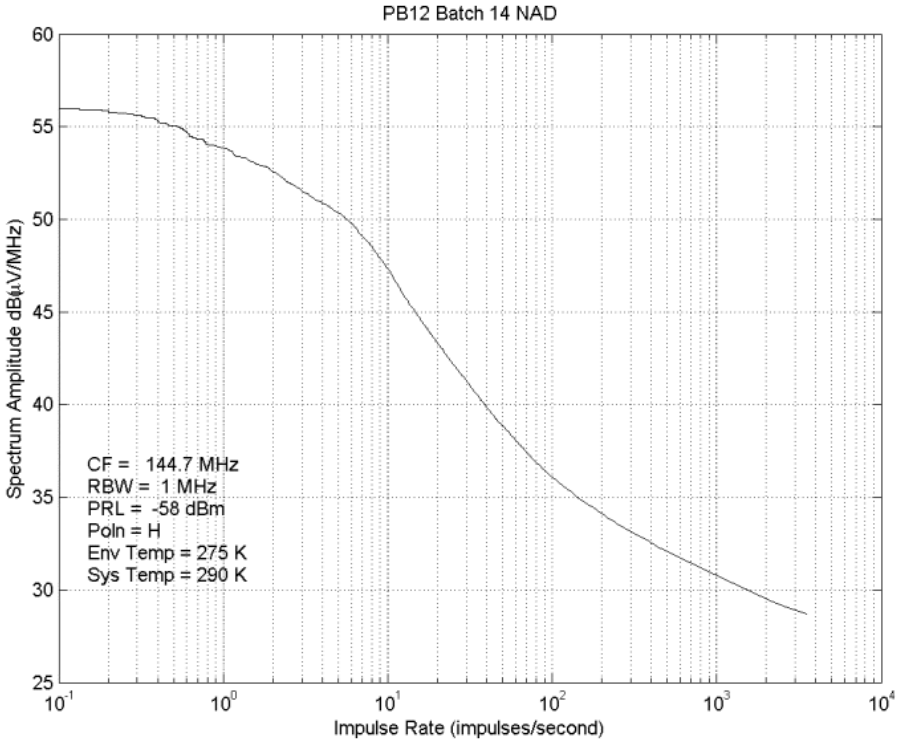

Figure 45 Railway APD and NAD (130 to 150 MHz band)

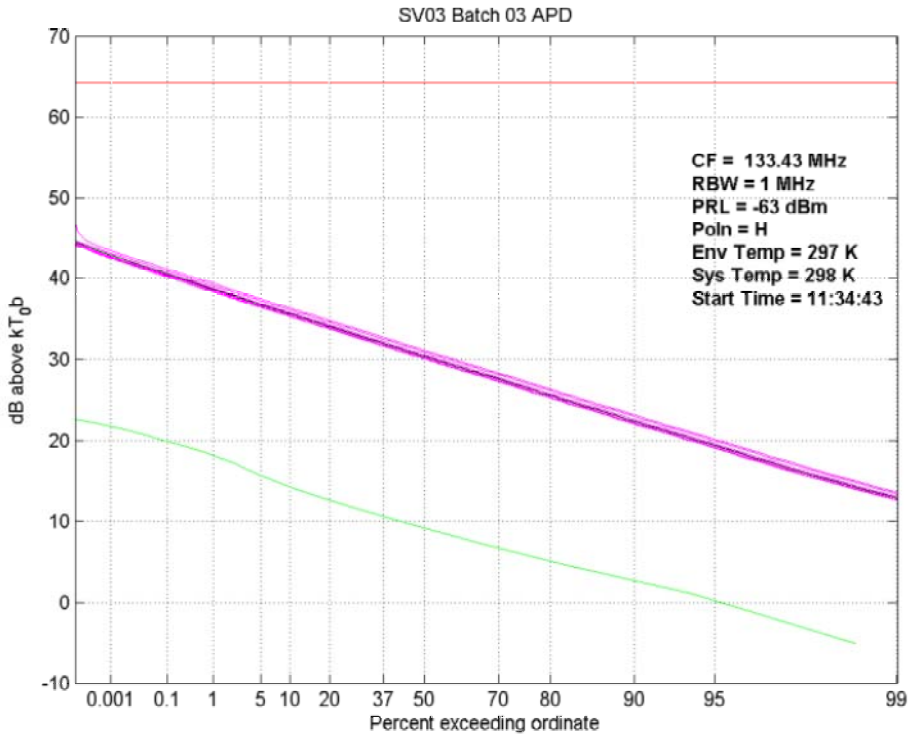

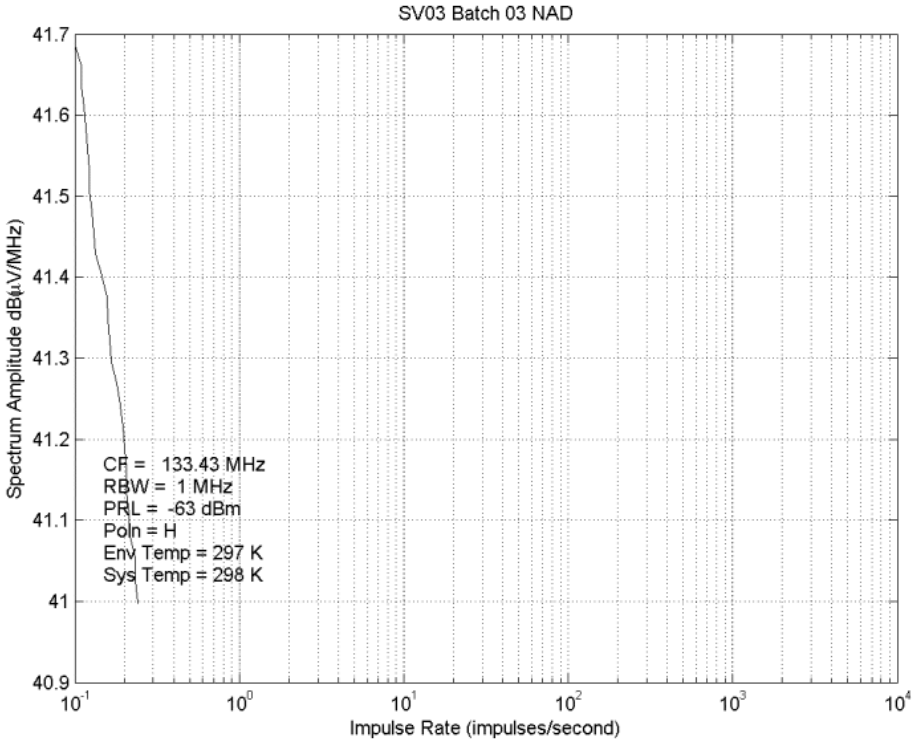

Figure 46 Business Centre APD and NAD (130 to 150 MHz band)

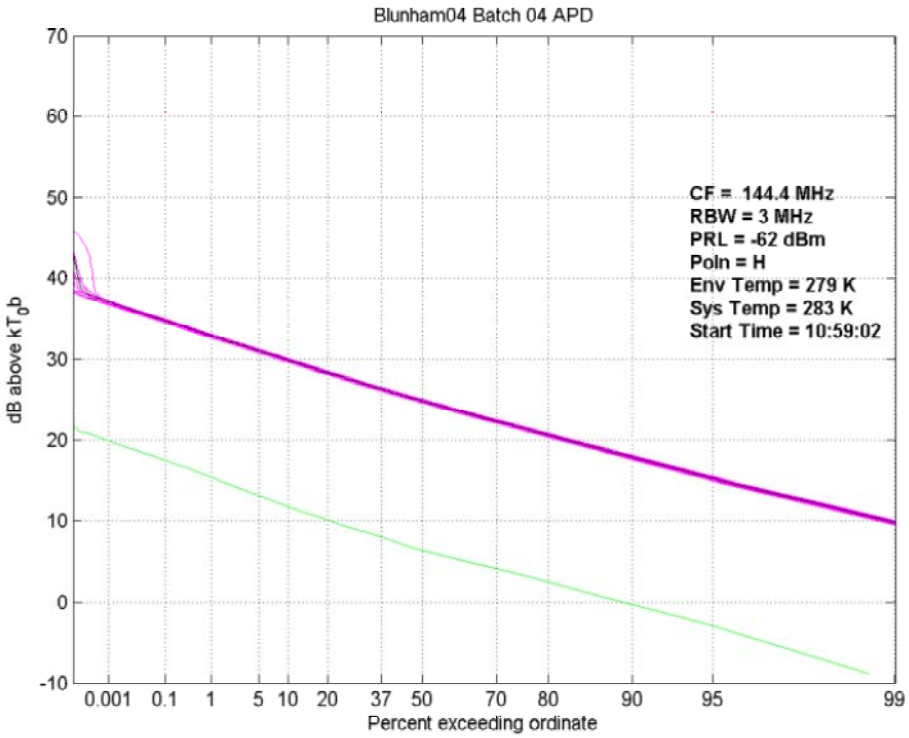

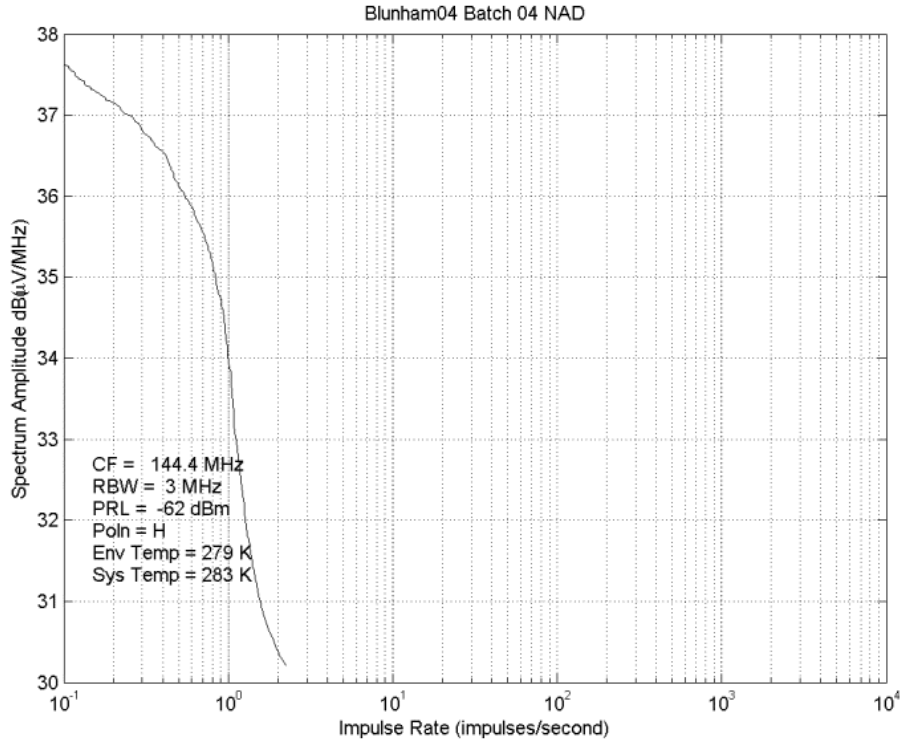

Figure 47 Rural APD and NAD (130 to 150 MHz band)

A.2 240 to 300 MHz

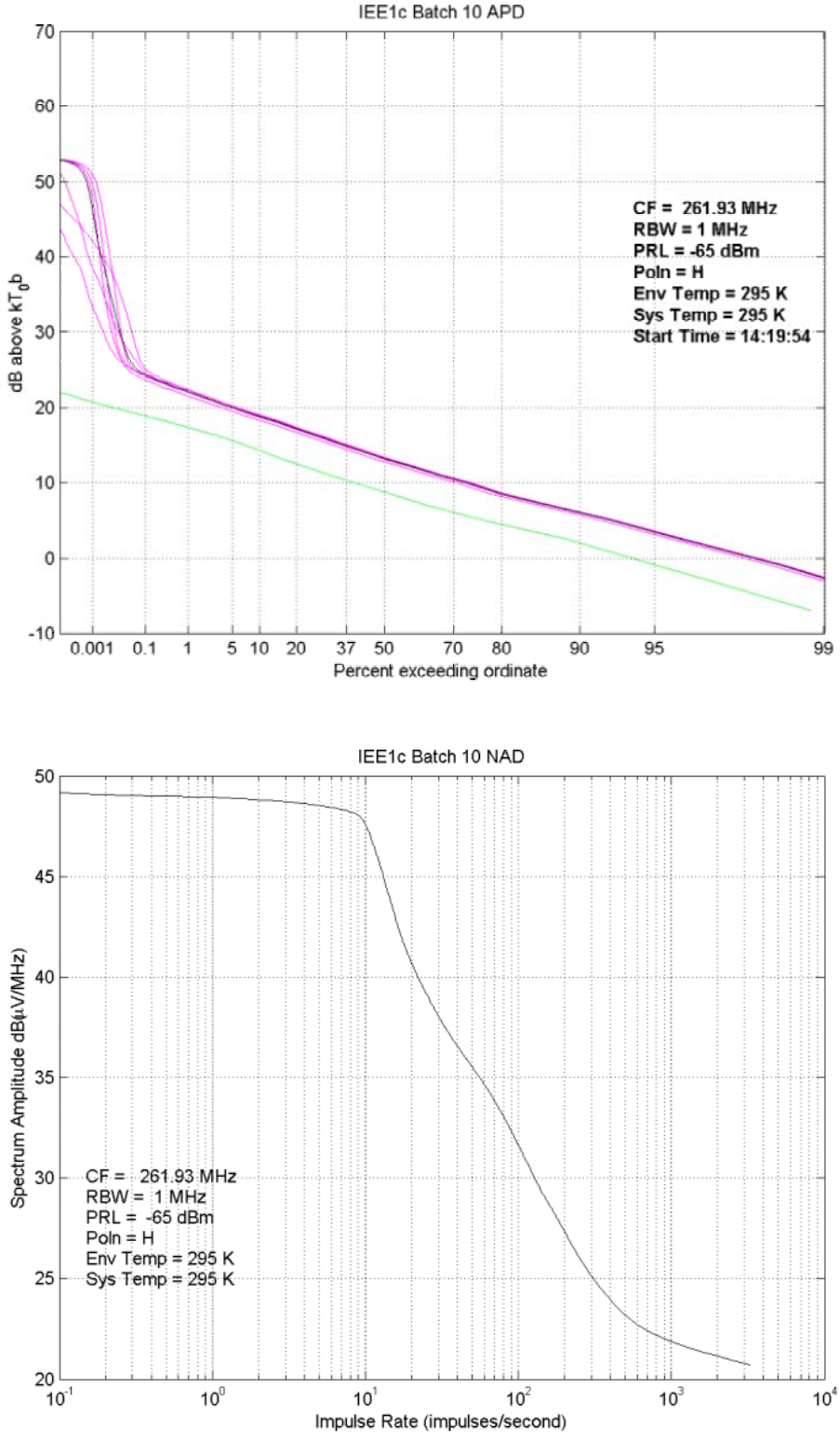

Figure 48 City Centre APD and NAD (240 to 300 MHz band)

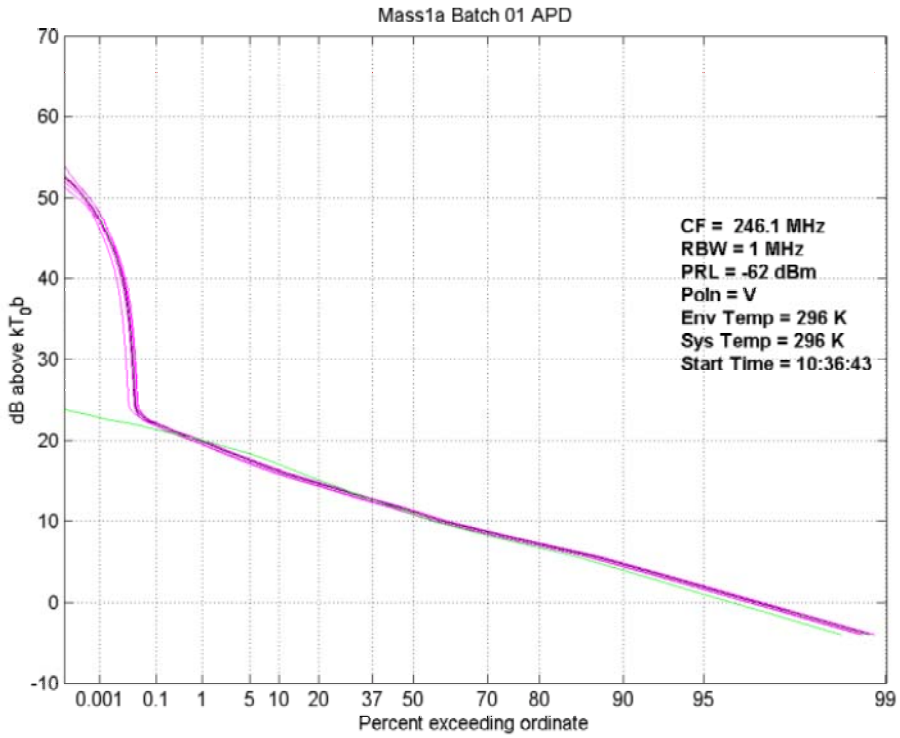

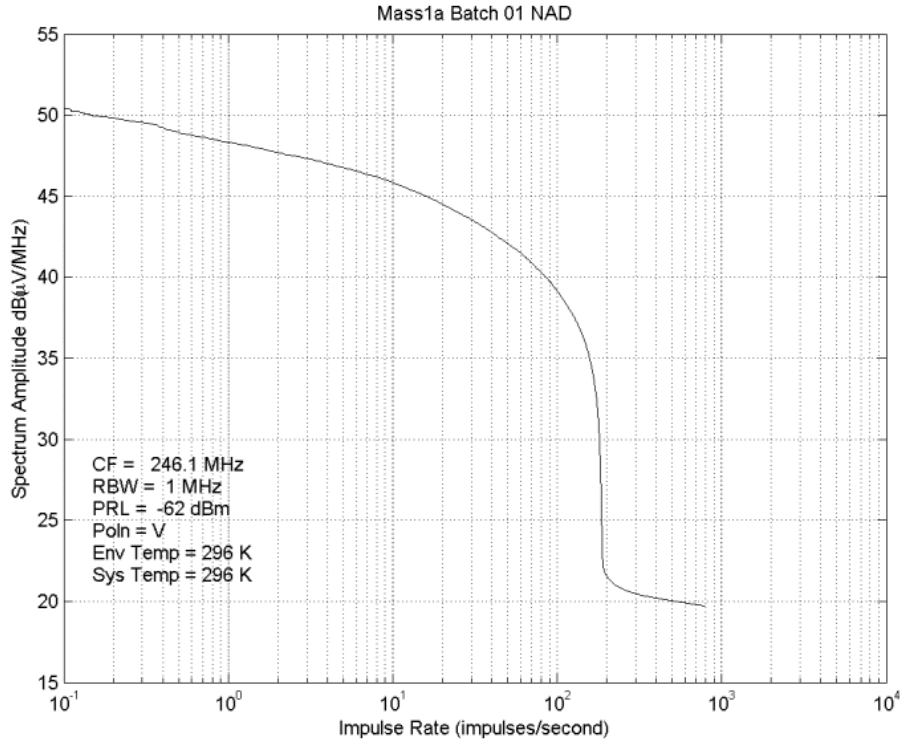

Figure 49 Suburban APD and NAD (240 to 300 MHz band)

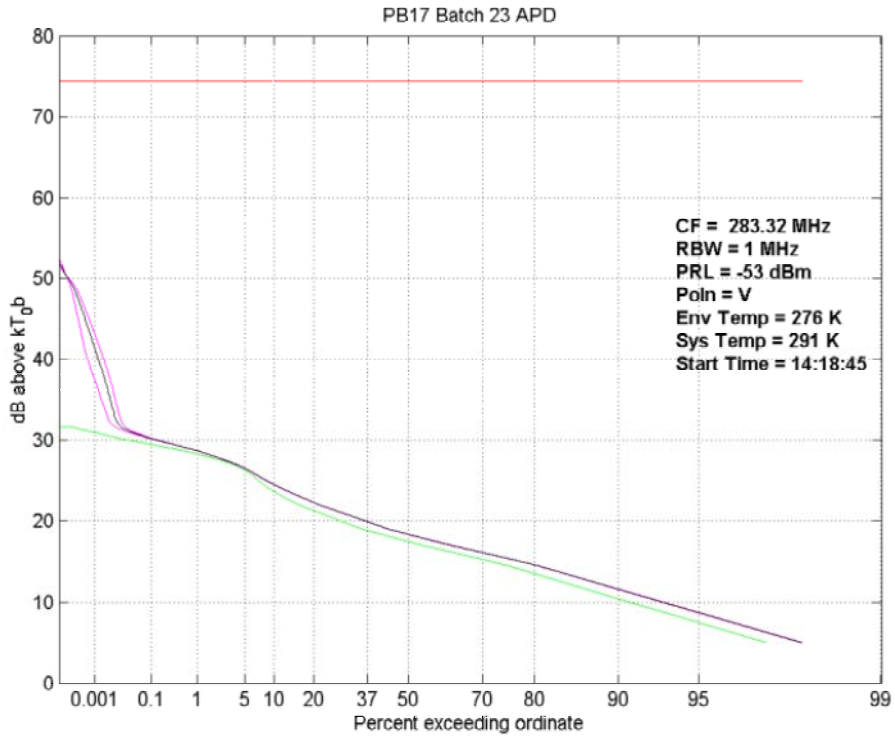

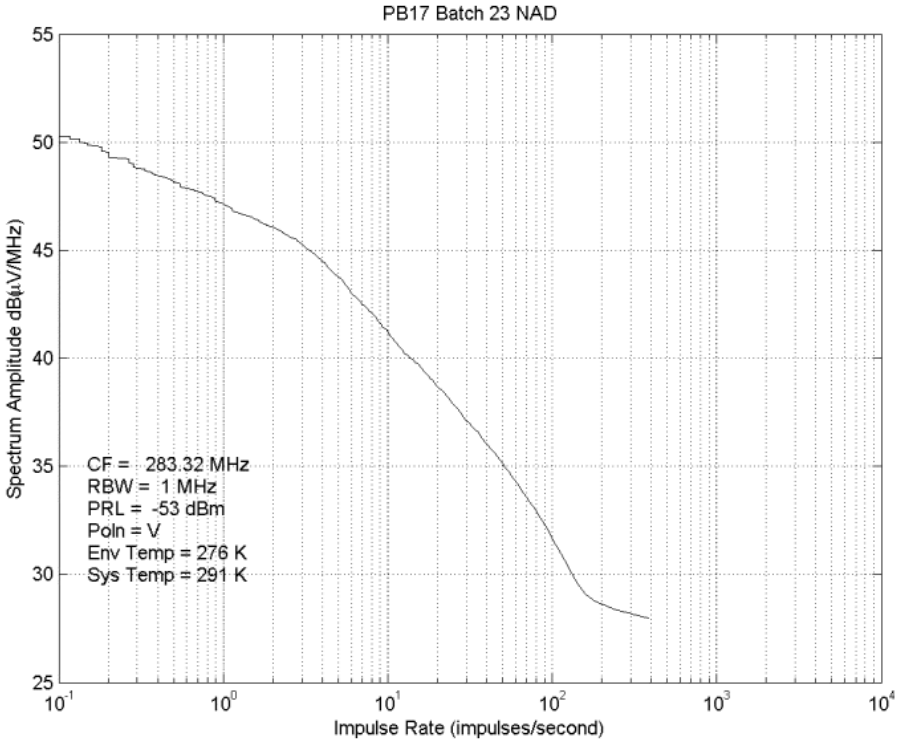

Figure 50 Railway APD and NAD (240 to 300 MHz band)

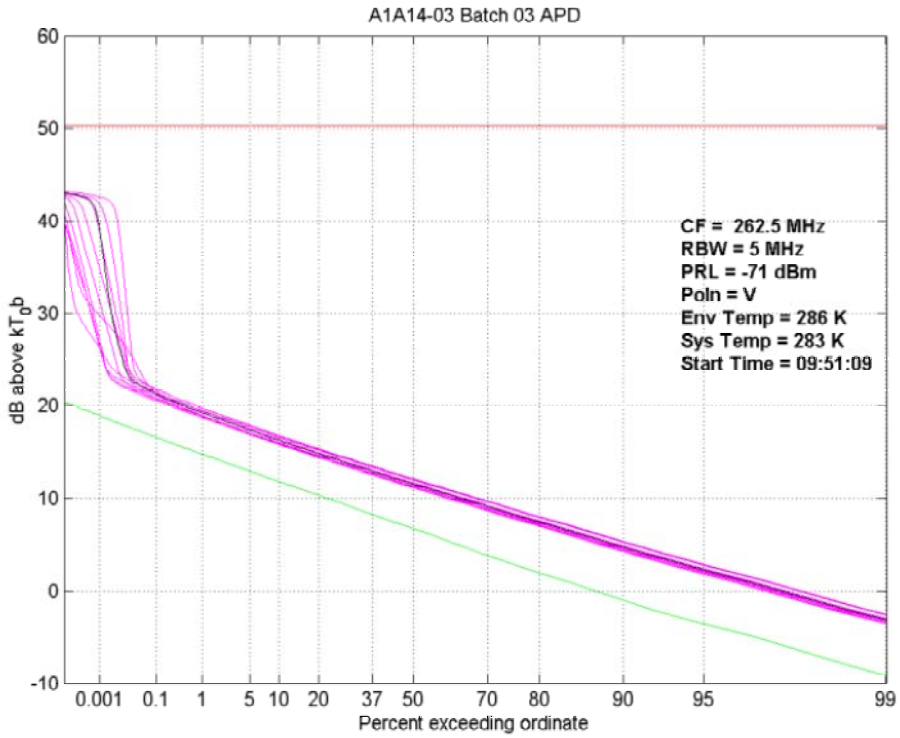

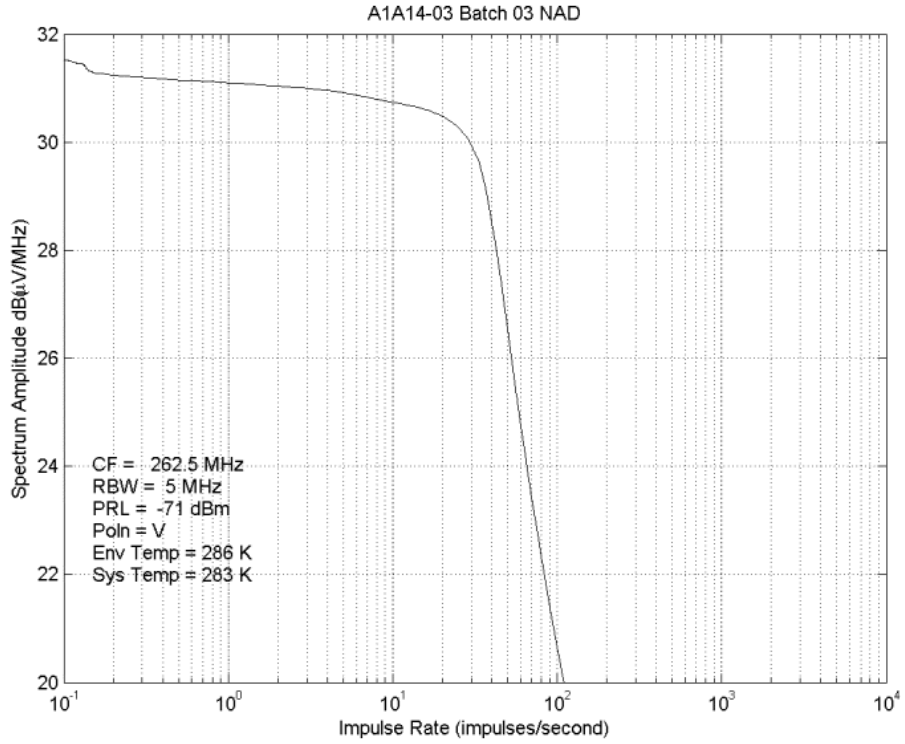

Figure 51 Road Junction APD and NAD (240 to 300 MHz band)

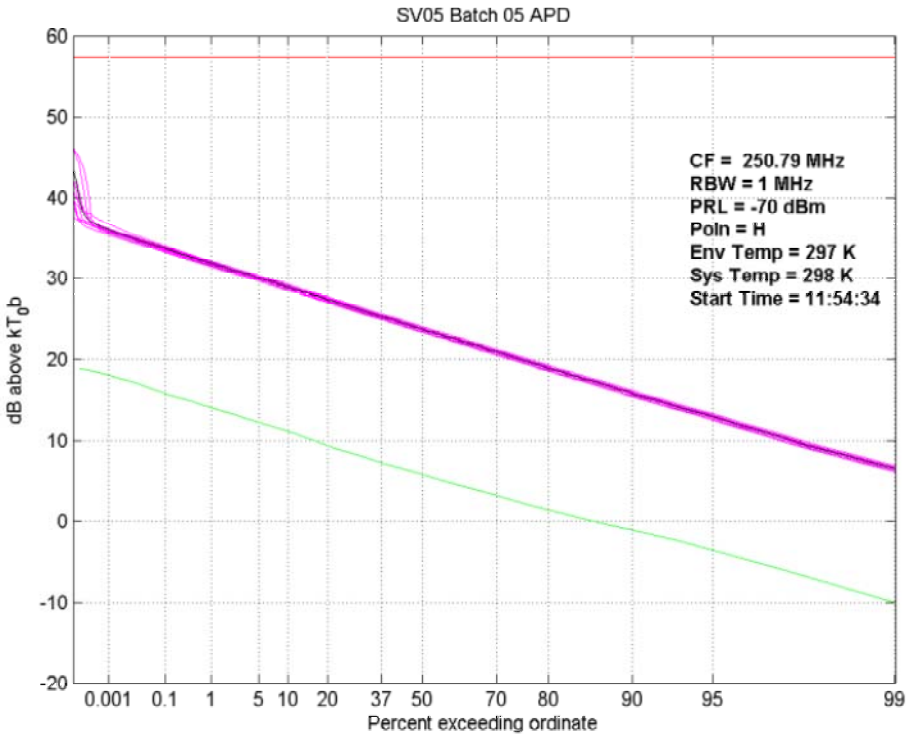

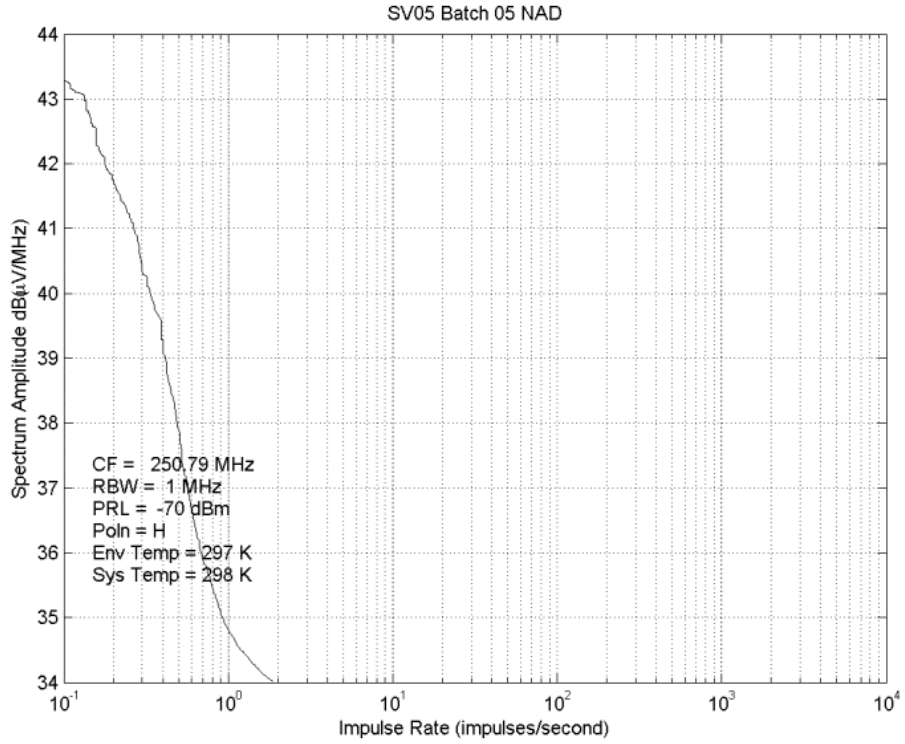

Figure 52 Business Centre APD and NAD (240 to 300 MHz band)

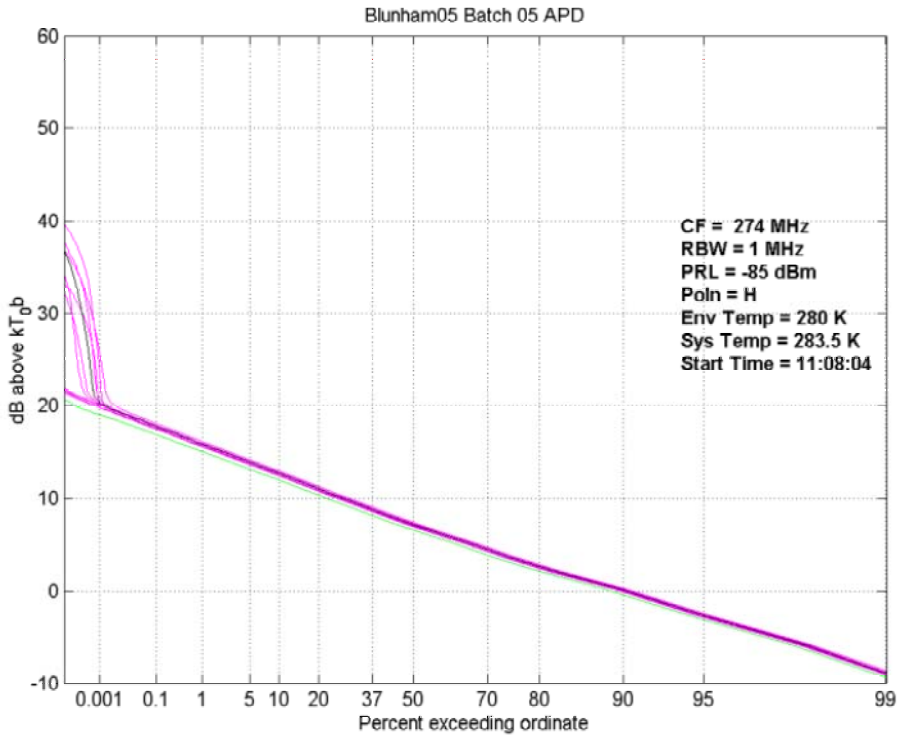

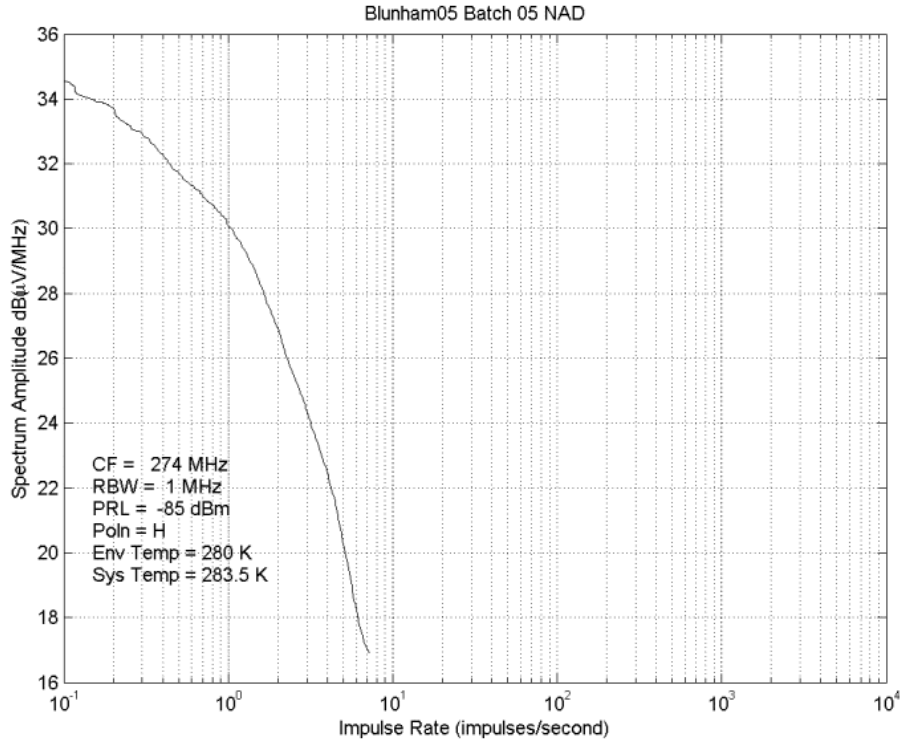

Figure 53 Rural APD and NAD (240 to 300 MHz band)

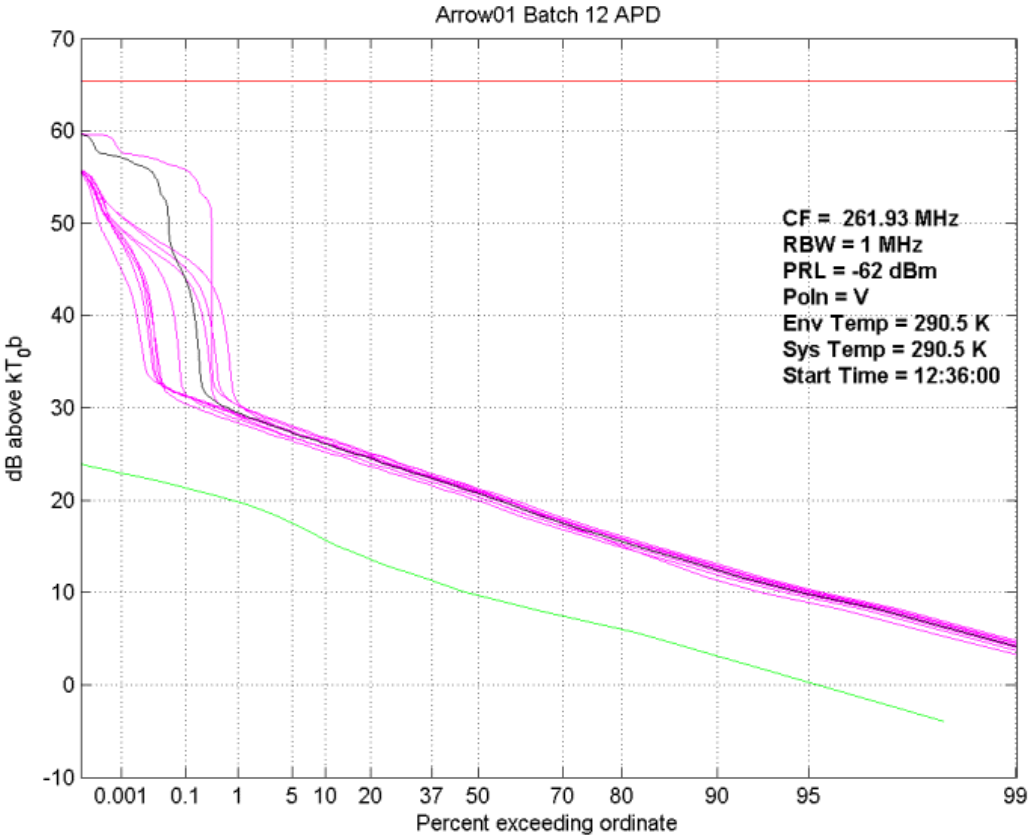

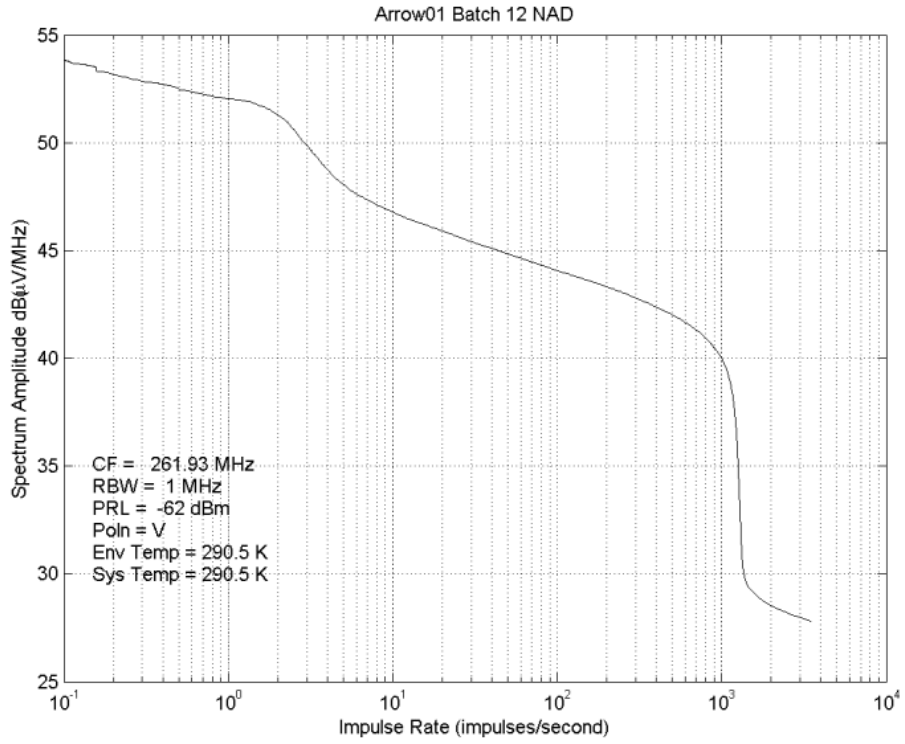

Figure 54 Factory Estate APD and NAD (240 to 300 MHz band)

A.3 300 to 360 MHz

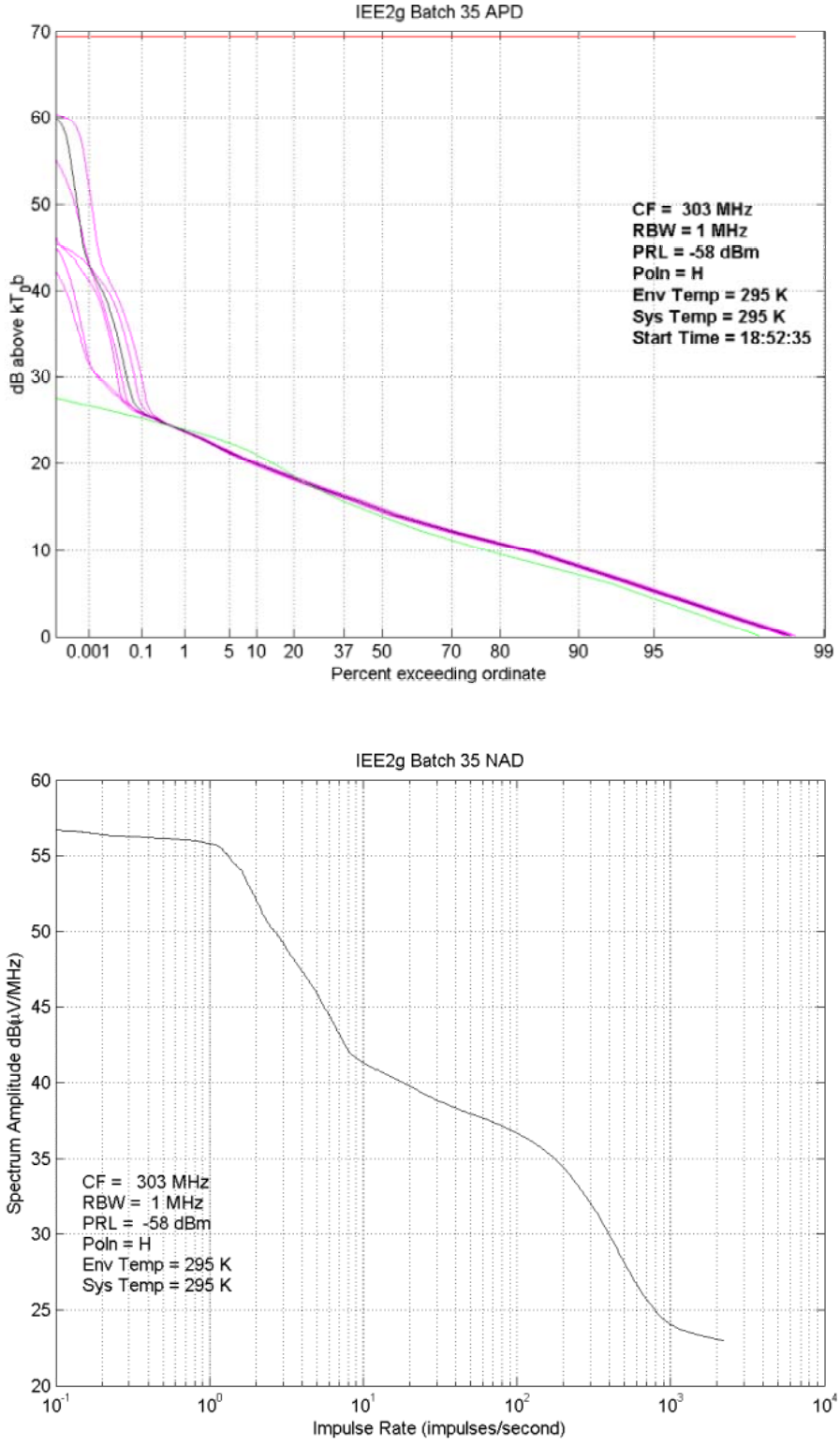

Figure 55 City Centre APD and NAD (300 to 360 MHz band)

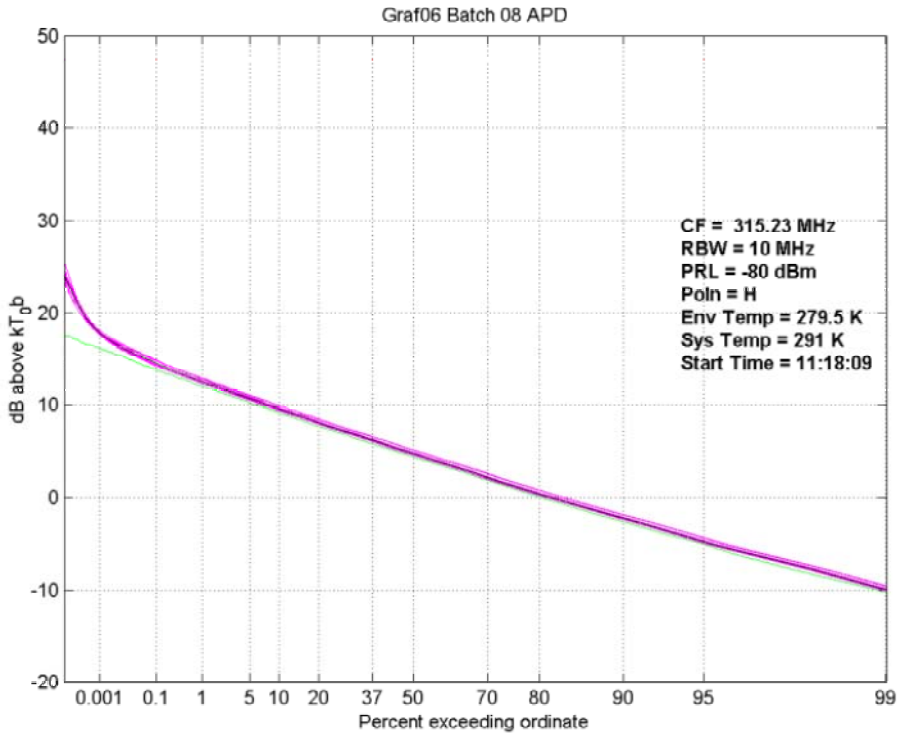

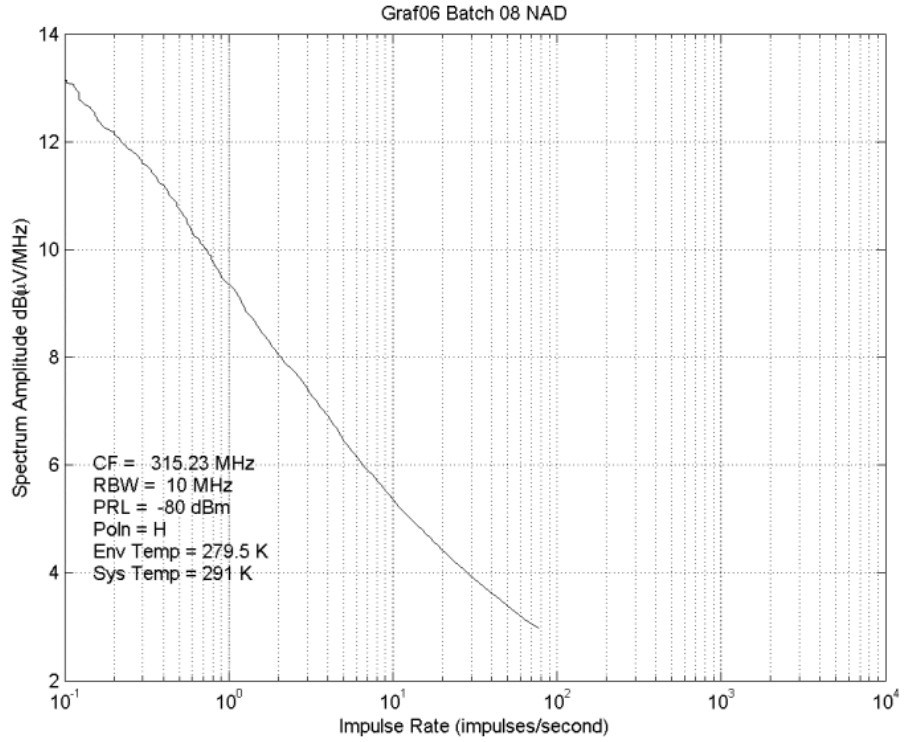

Figure 56 Quiet Rural APD and NAD (300 to 360 MHz band)

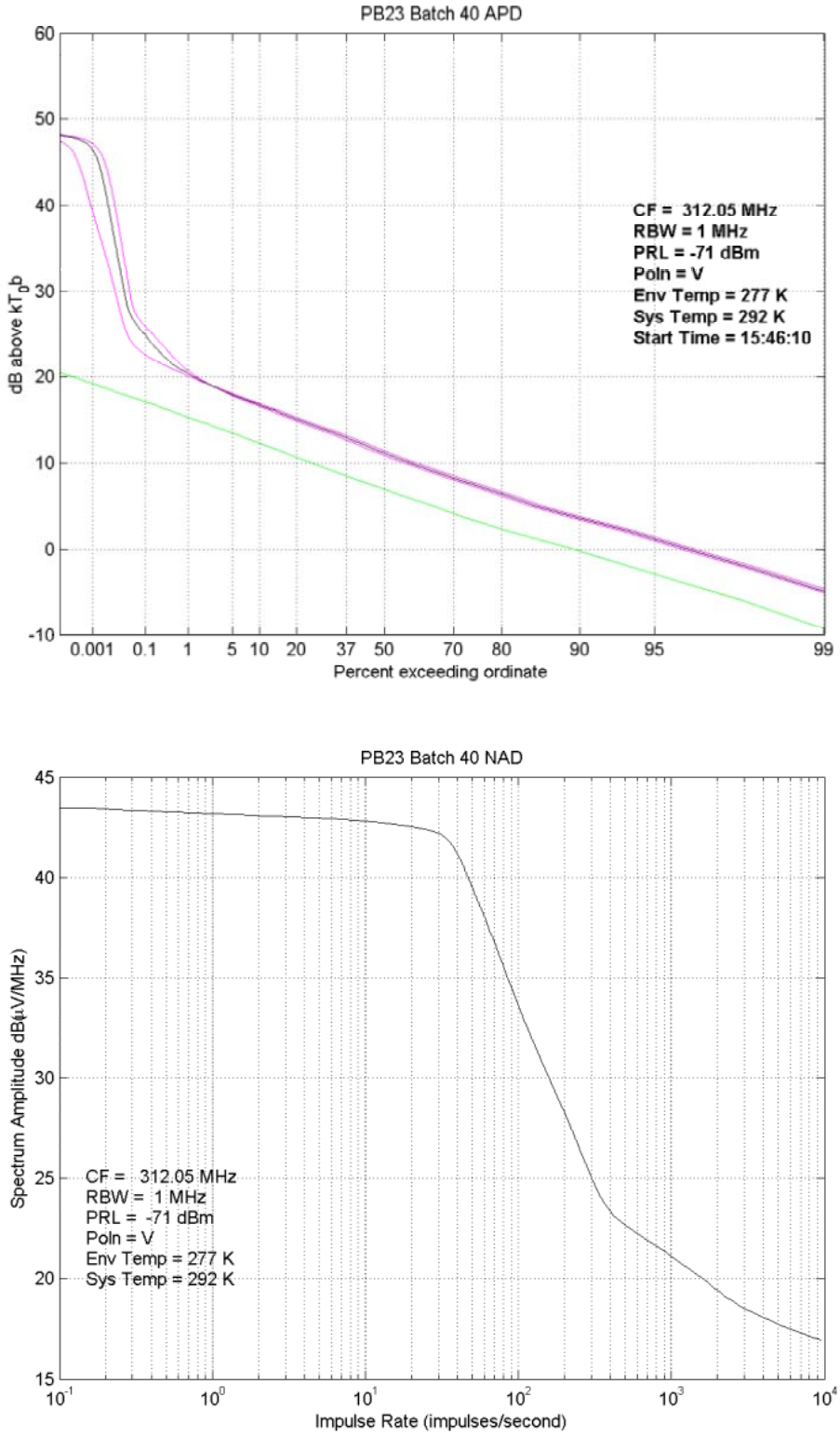

Figure 57 Railway APD and NAD (300 to 360 MHz band)

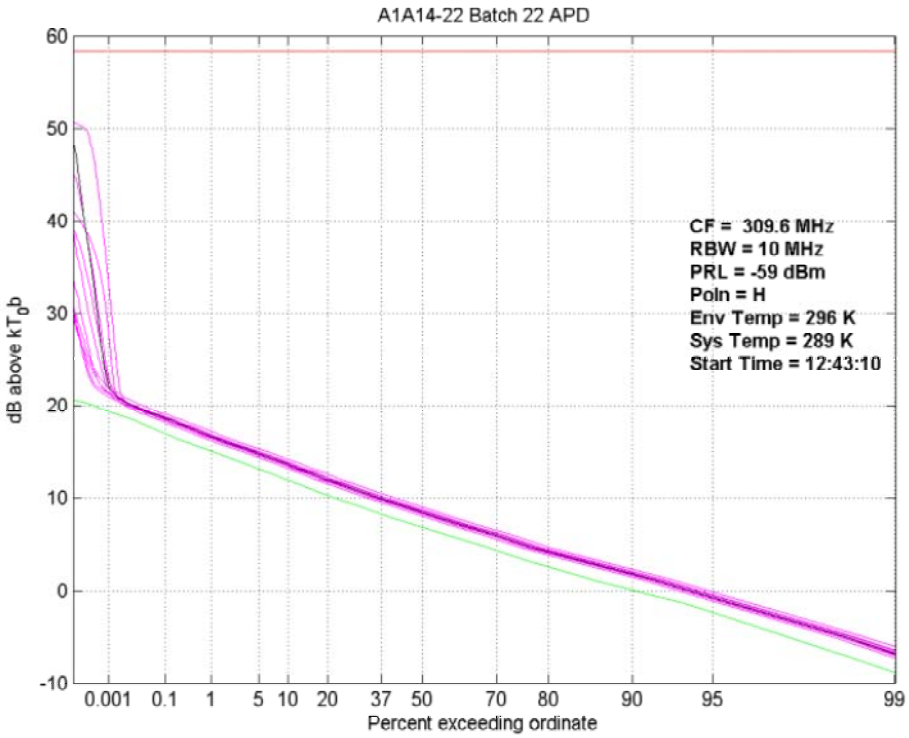

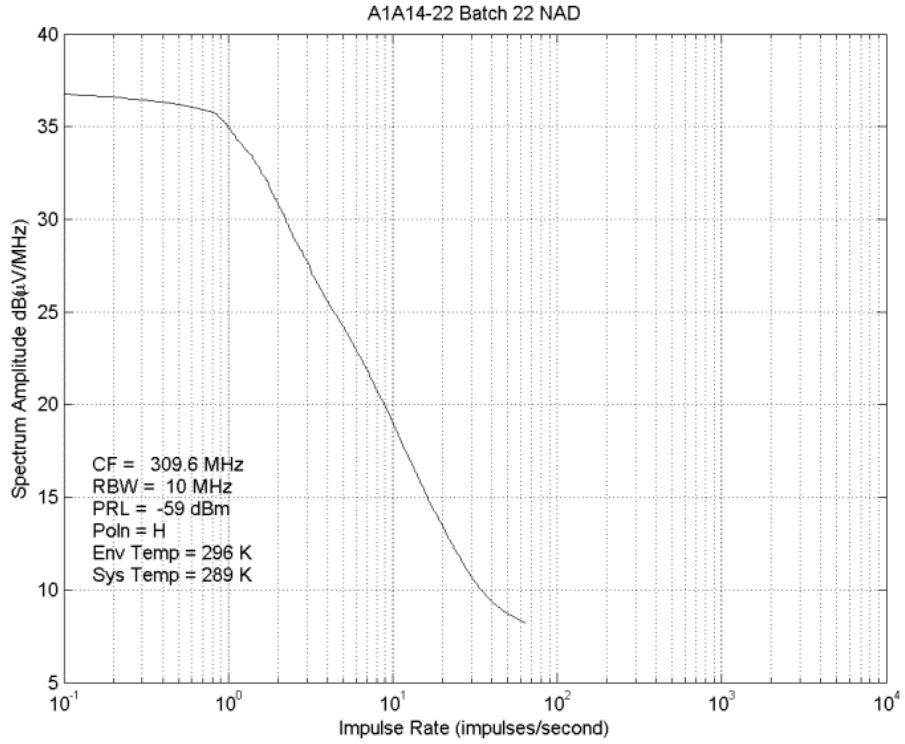

Figure 58 Road Junction APD and NAD (300 to 360 MHz band)

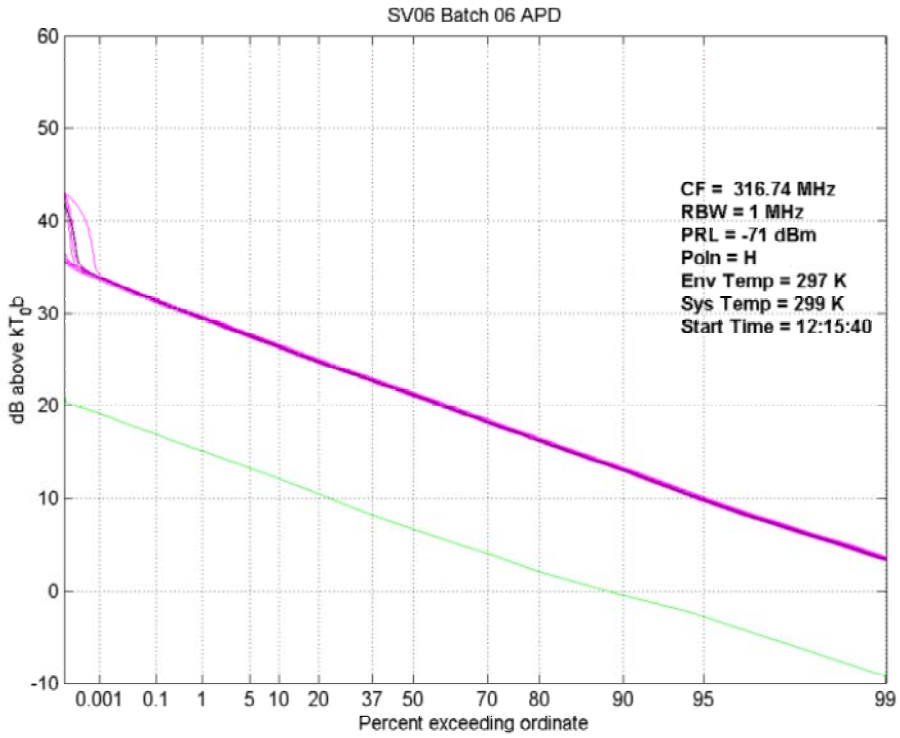

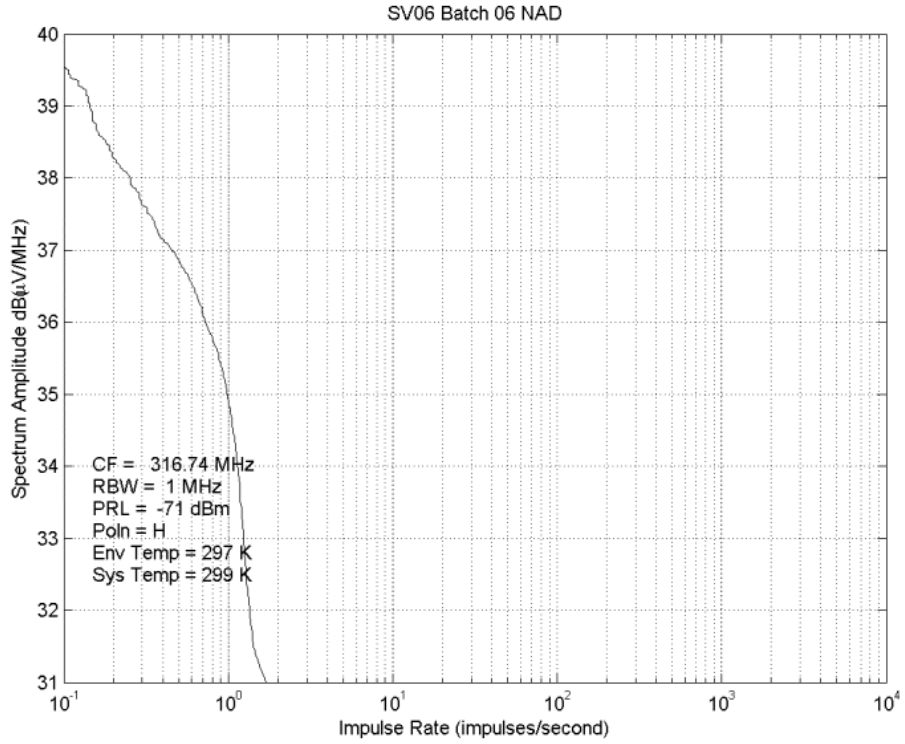

Figure 59 Business Centre APD and NAD (300 to 360 MHz band)

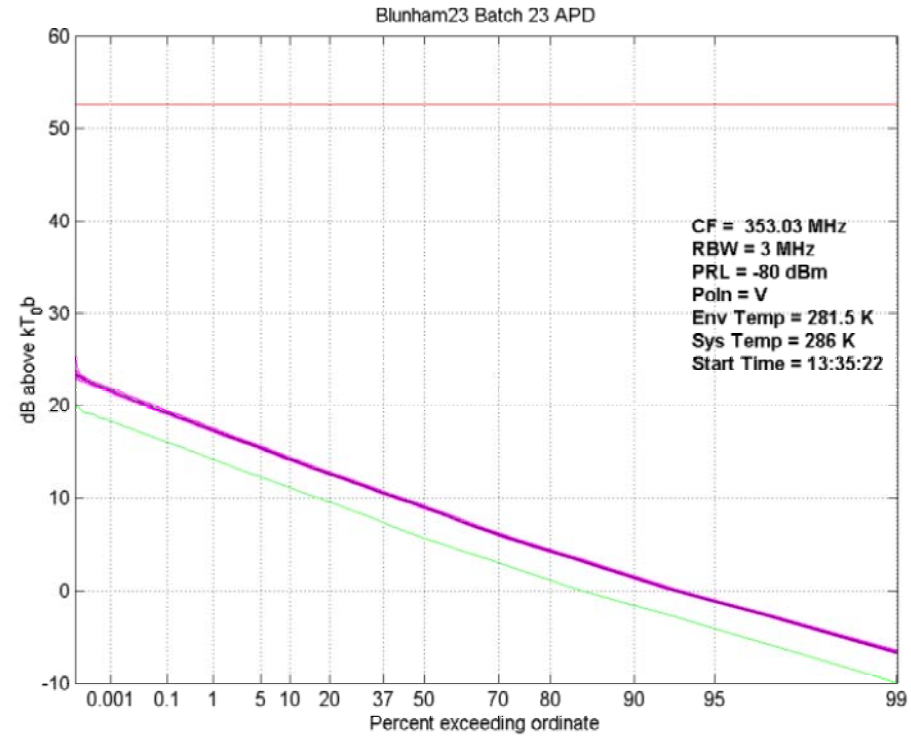

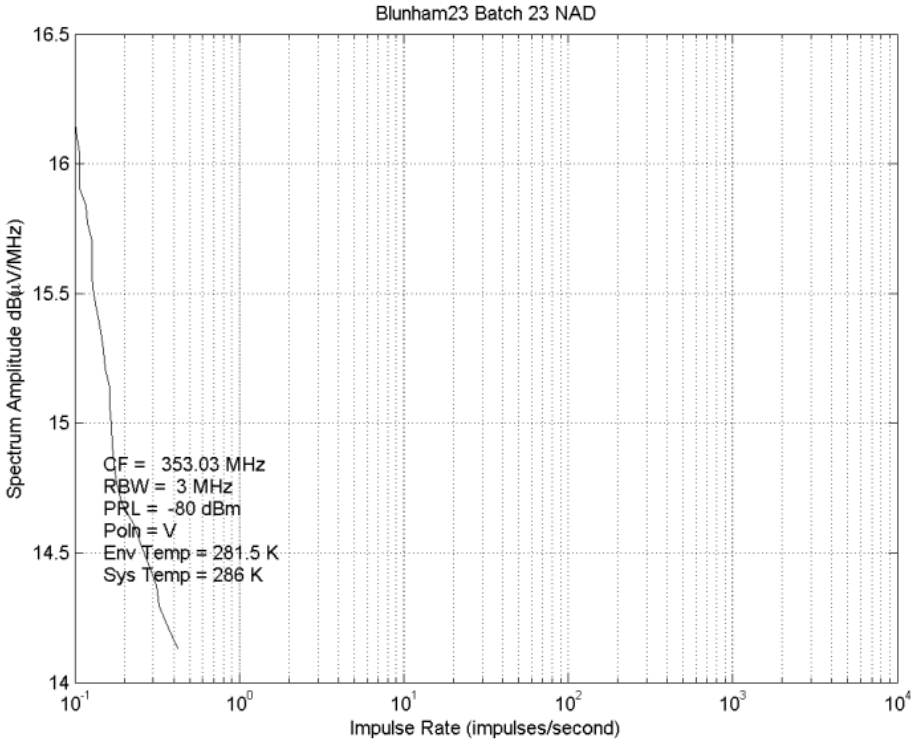

Figure 60 Rural APD and NAD (300 to 360 MHz band)

A.4 440 to 500 MHz

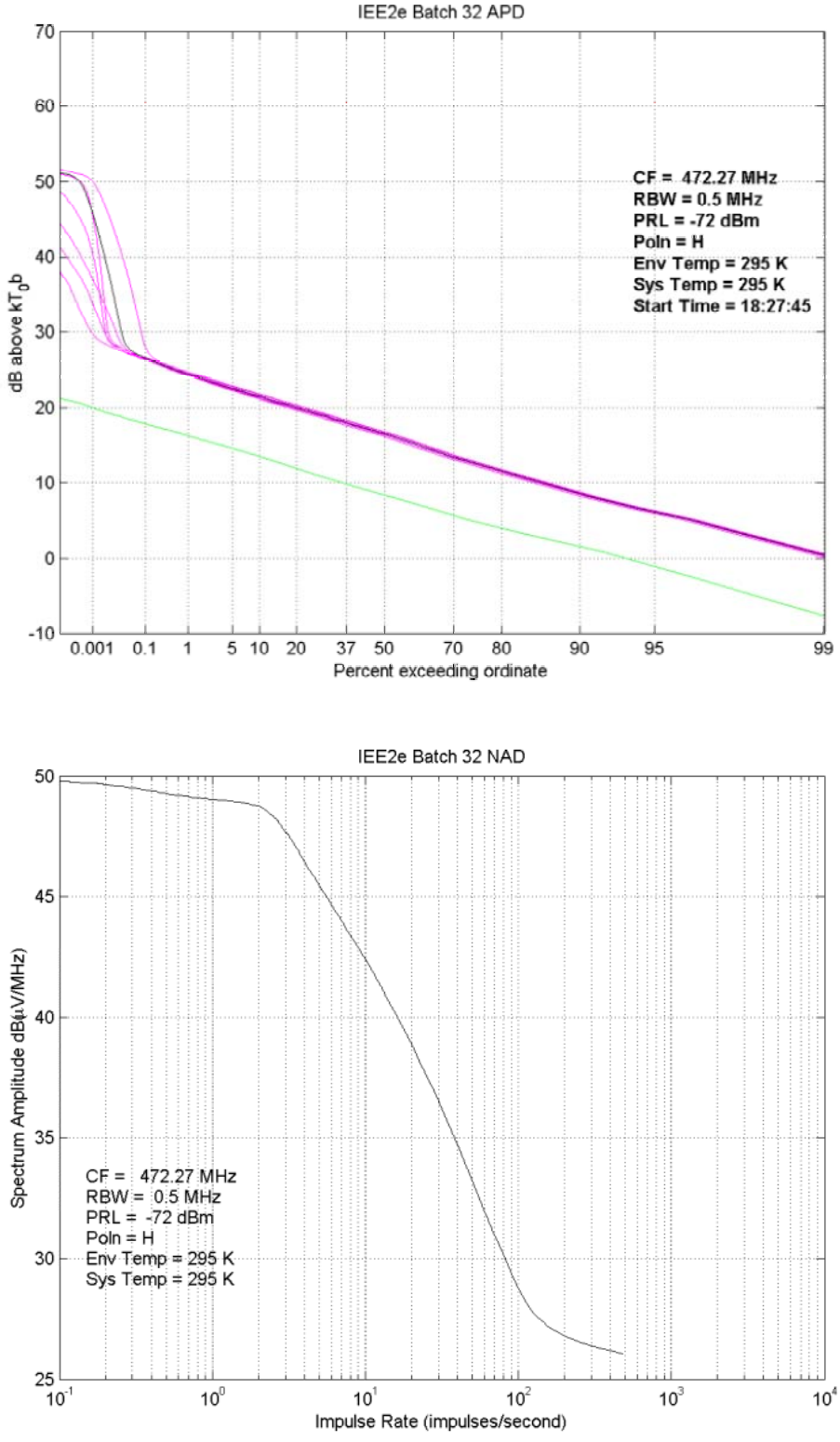

Figure 61 City Centre APD and NAD (440 to 500 MHz band)

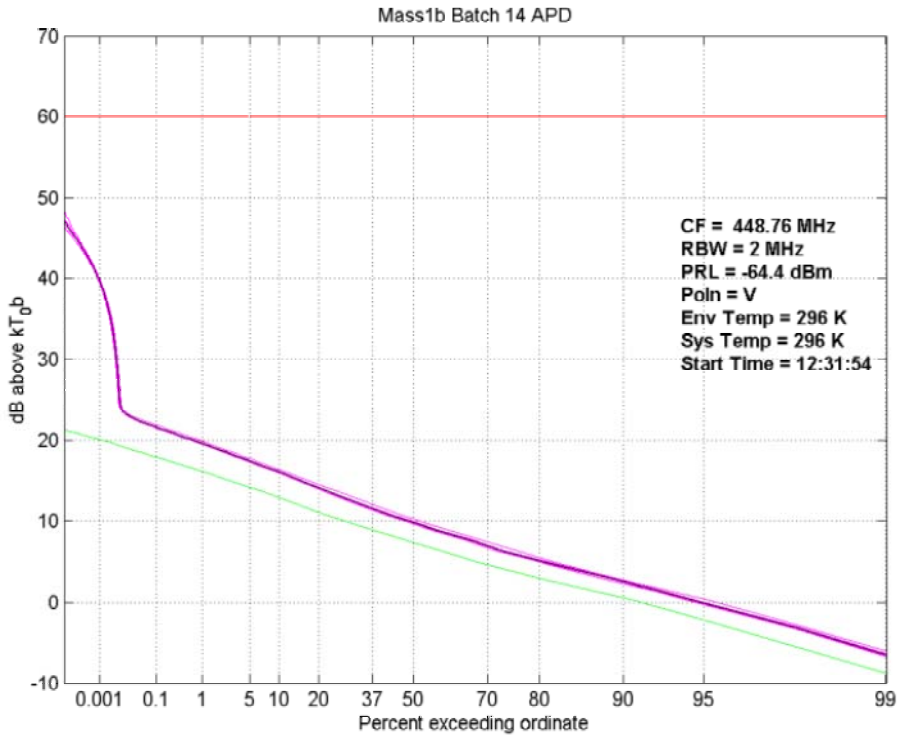

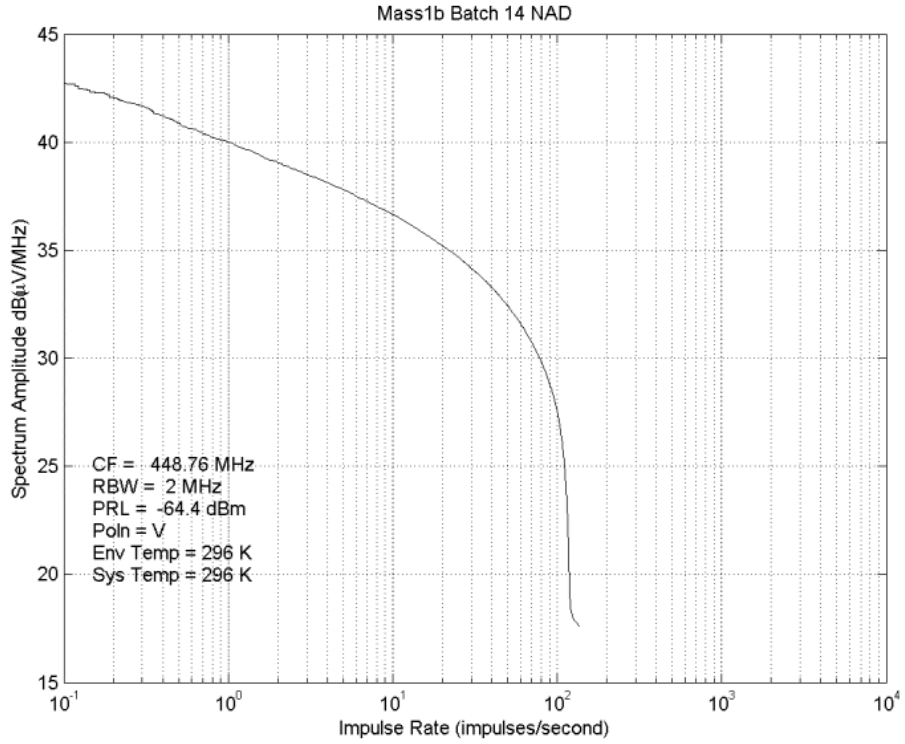

Figure 62 Suburban APD and NAD (440 to 500 MHz band)

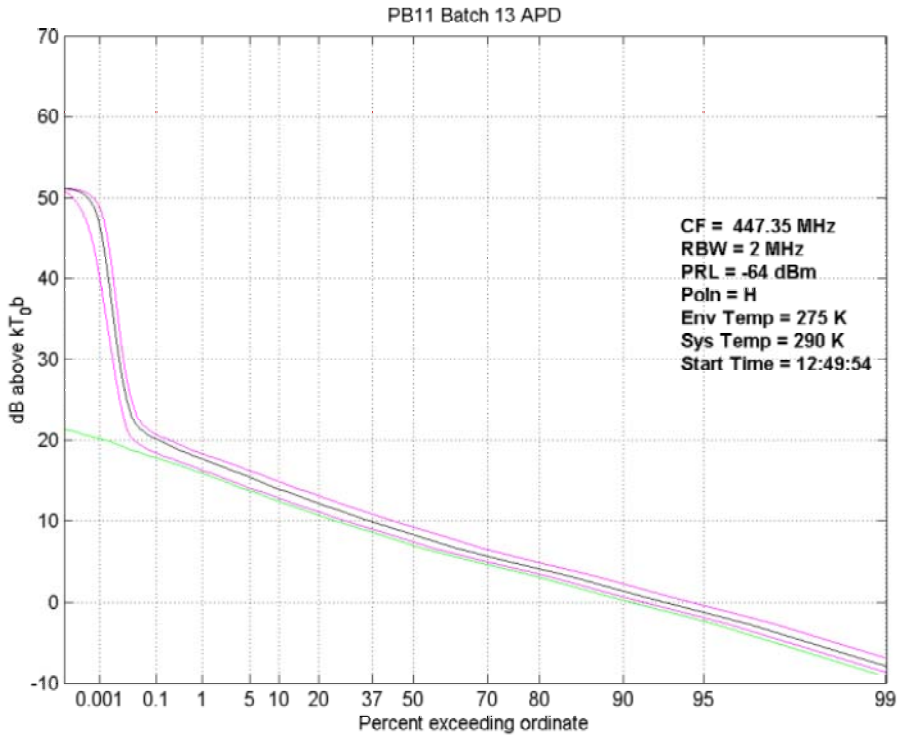

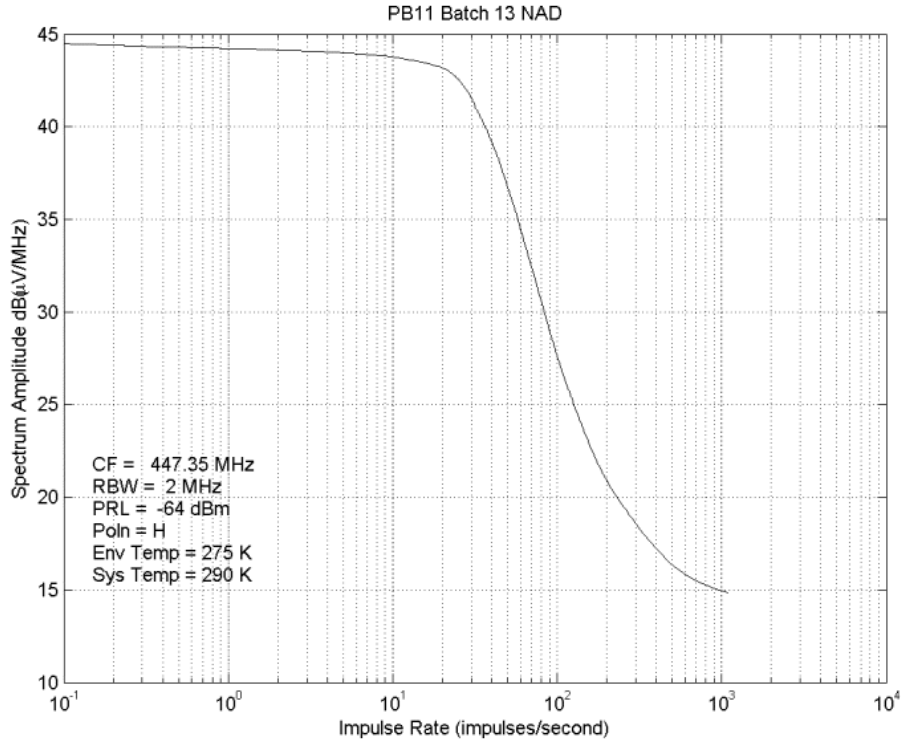

Figure 63 Railway APD and NAD (440 to 500 MHz band)

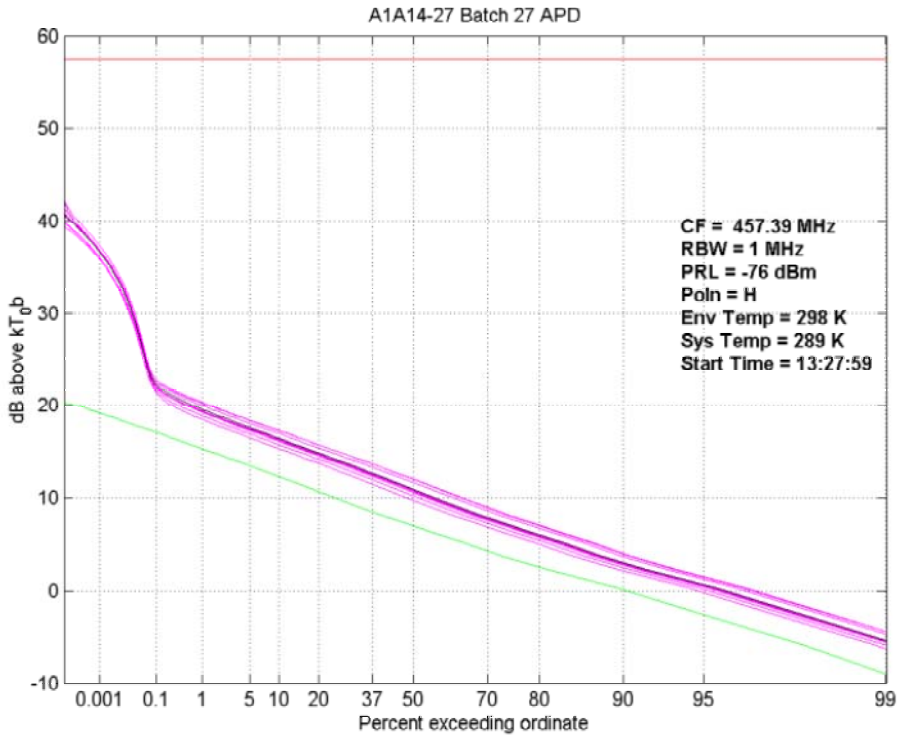

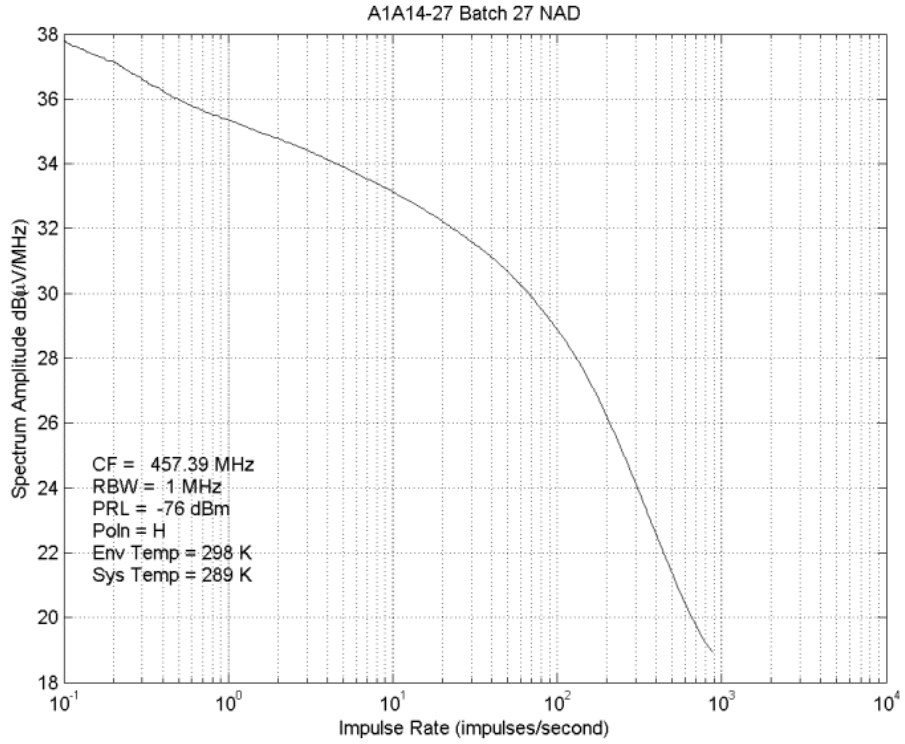

Figure 64 Road Junction APD and NAD (440 to 500 MHz band)

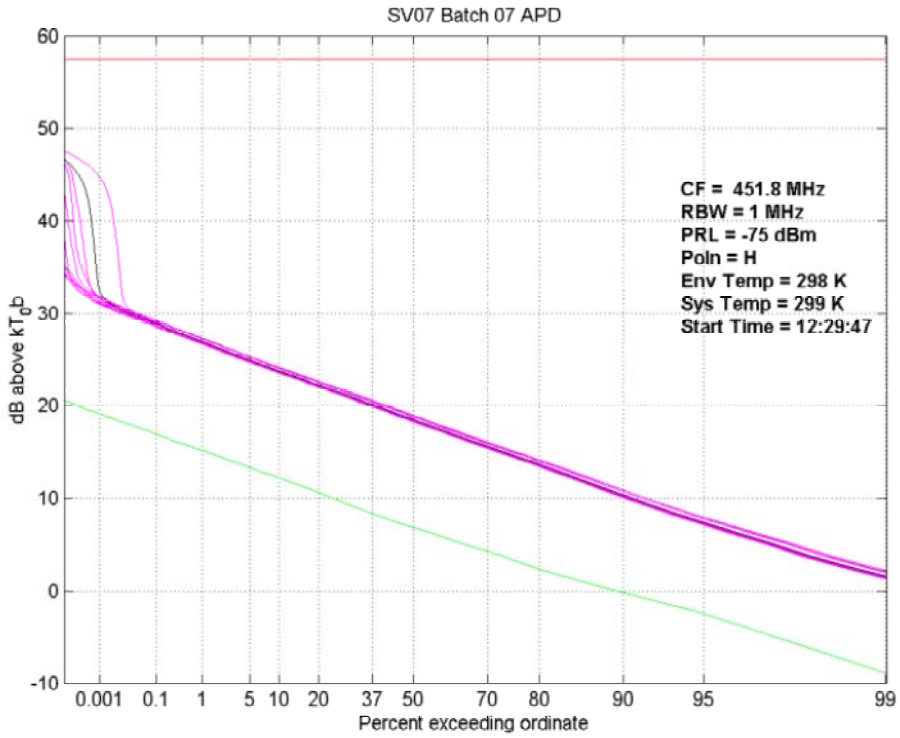

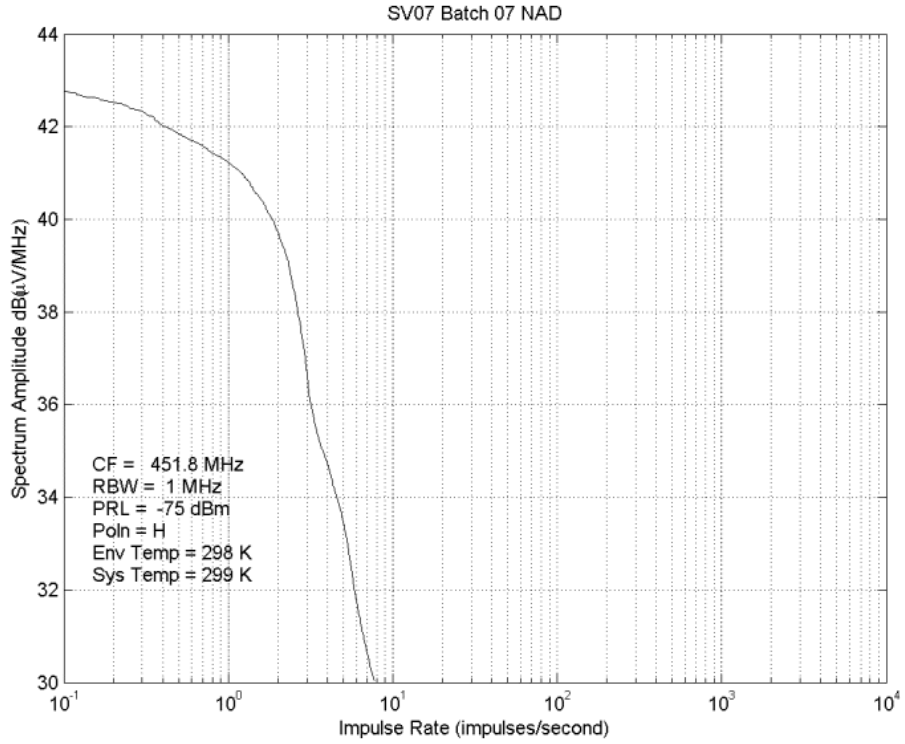

Figure 65 Business Centre APD and NAD (440 to 500 MHz band)

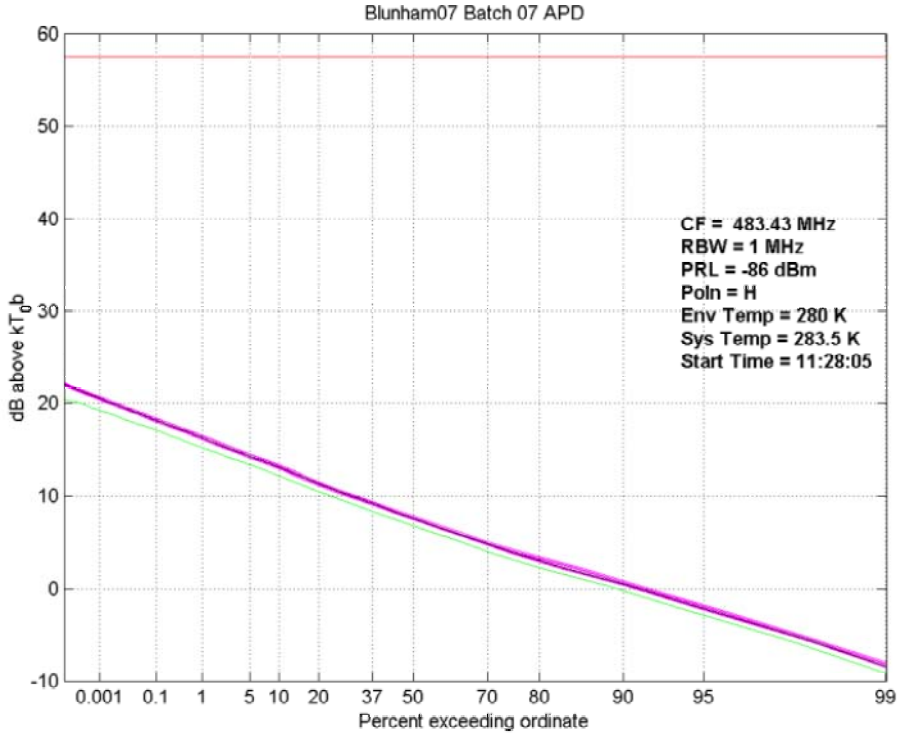

Figure 66 Rural APD (440 to 500 MHz band)

A.5 977 to 1010 MHz

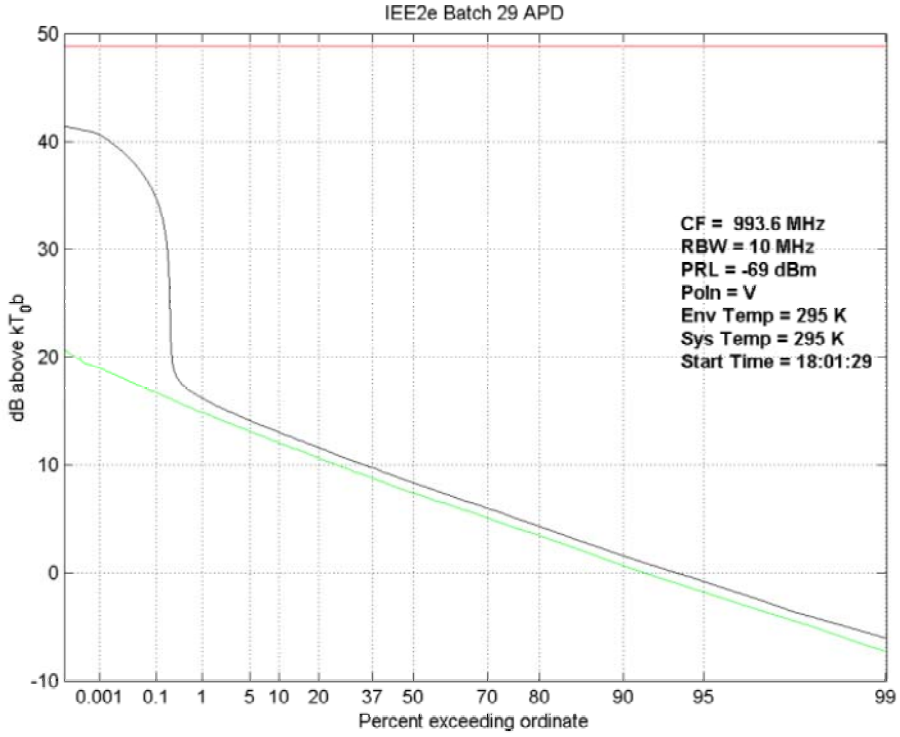

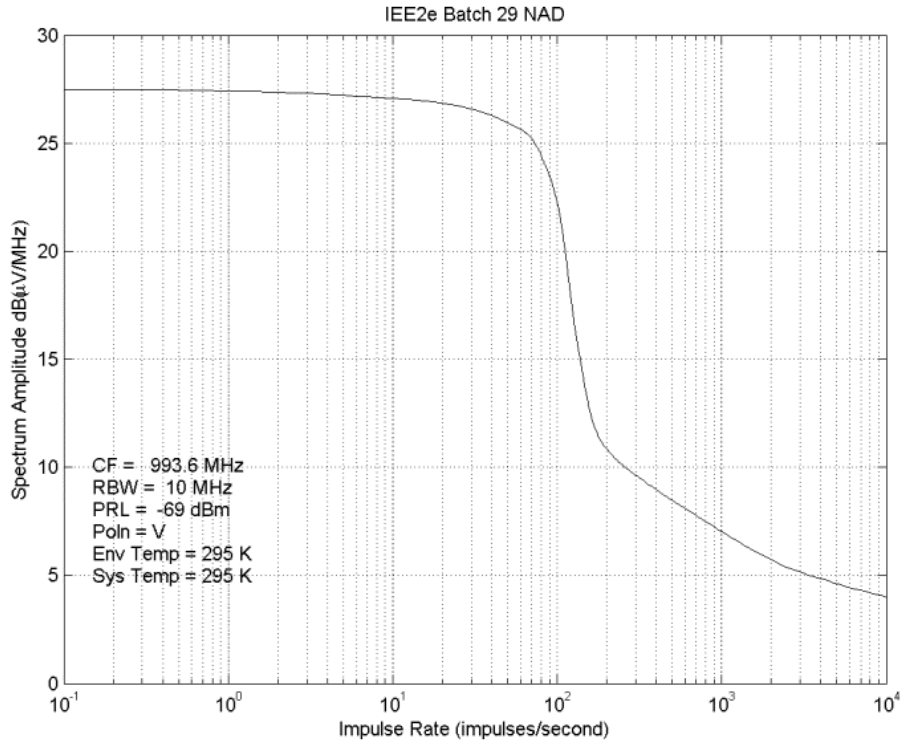

Figure 67 City Centre APD and NAD (977 to 1010 MHz band)

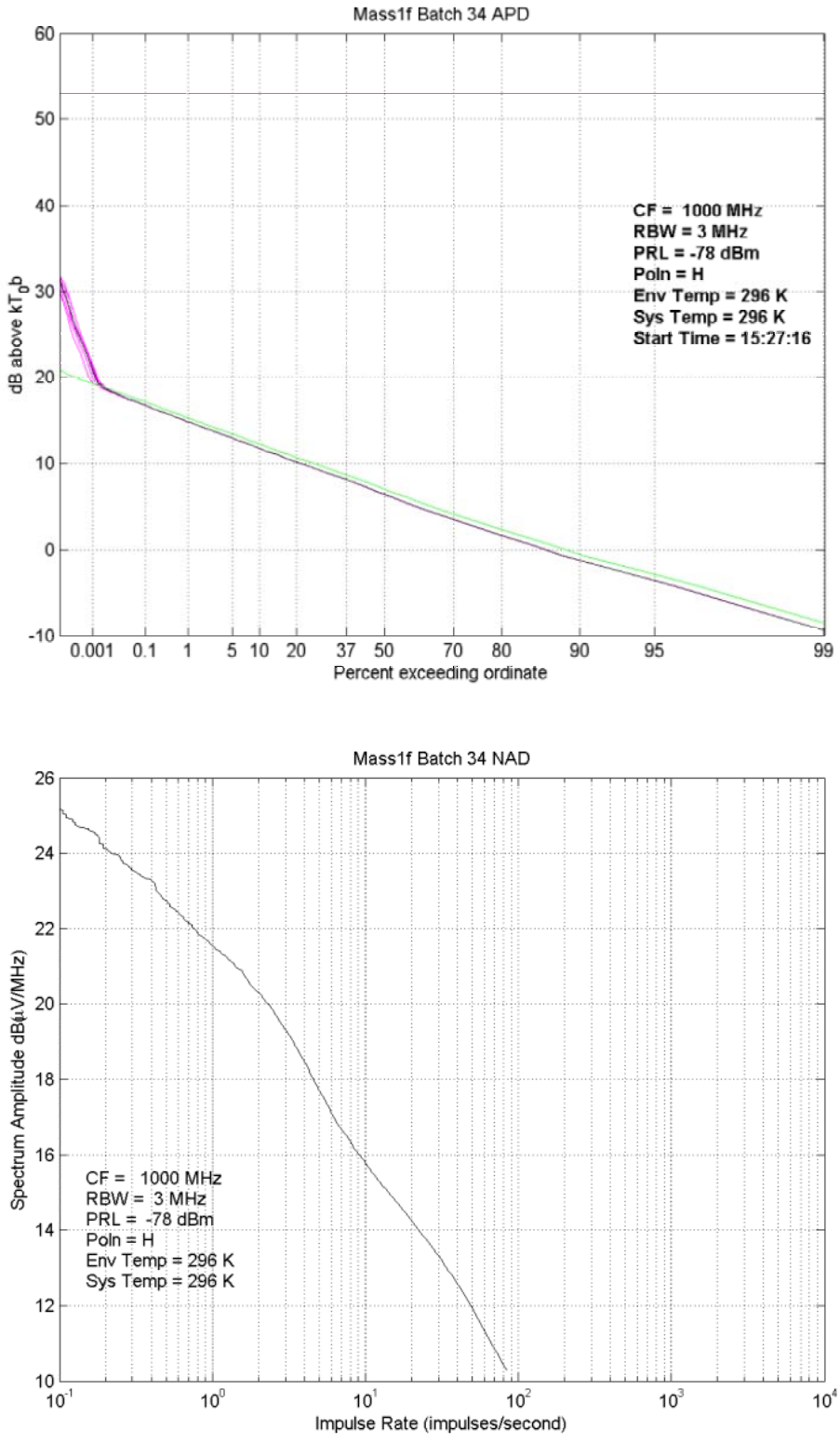

Figure 68 Suburban APD and NAD (977 to 1010 MHz band)

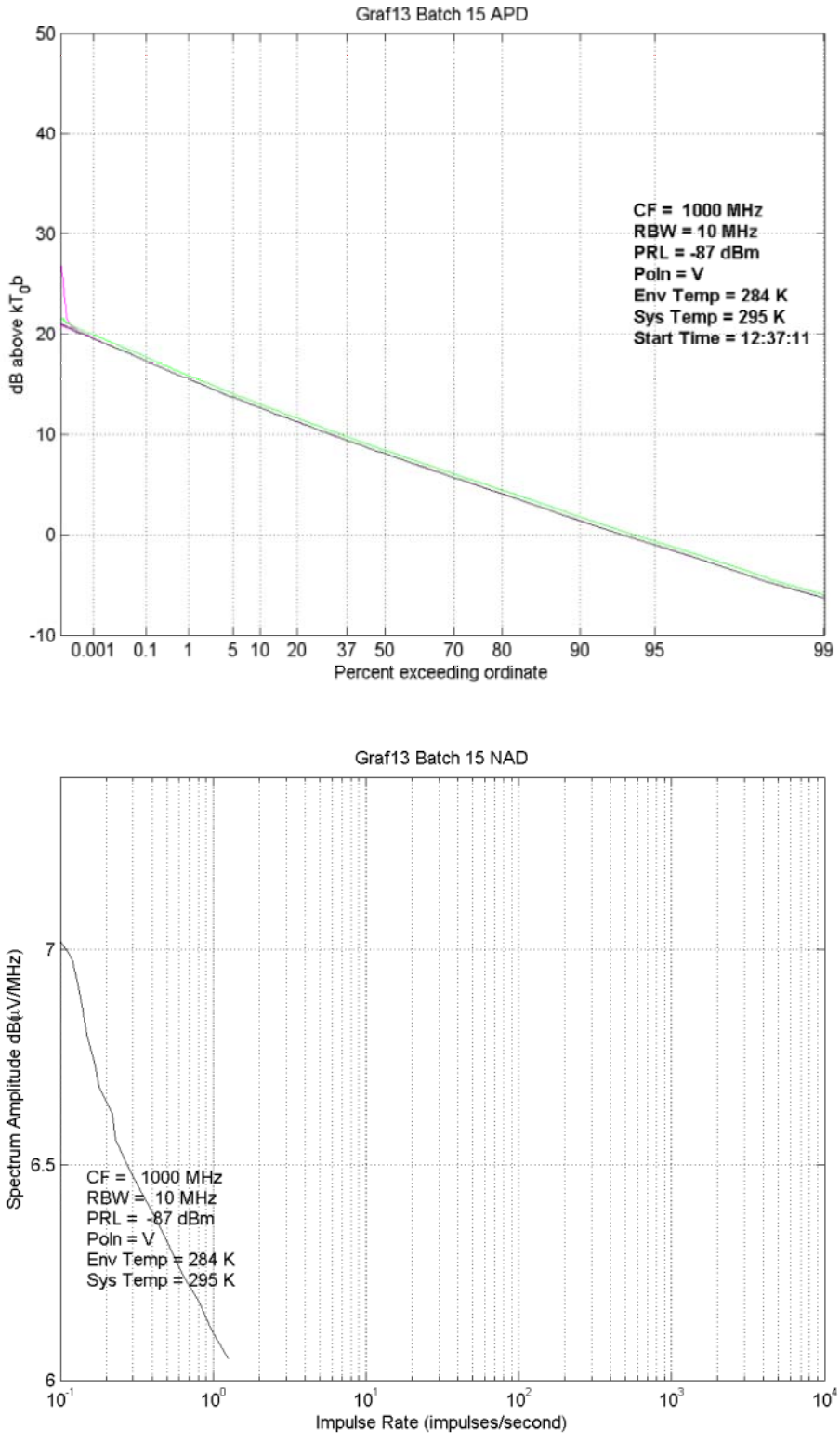

Figure 69 Quiet Rural APD and NAD (977 to 1010 MHz band)

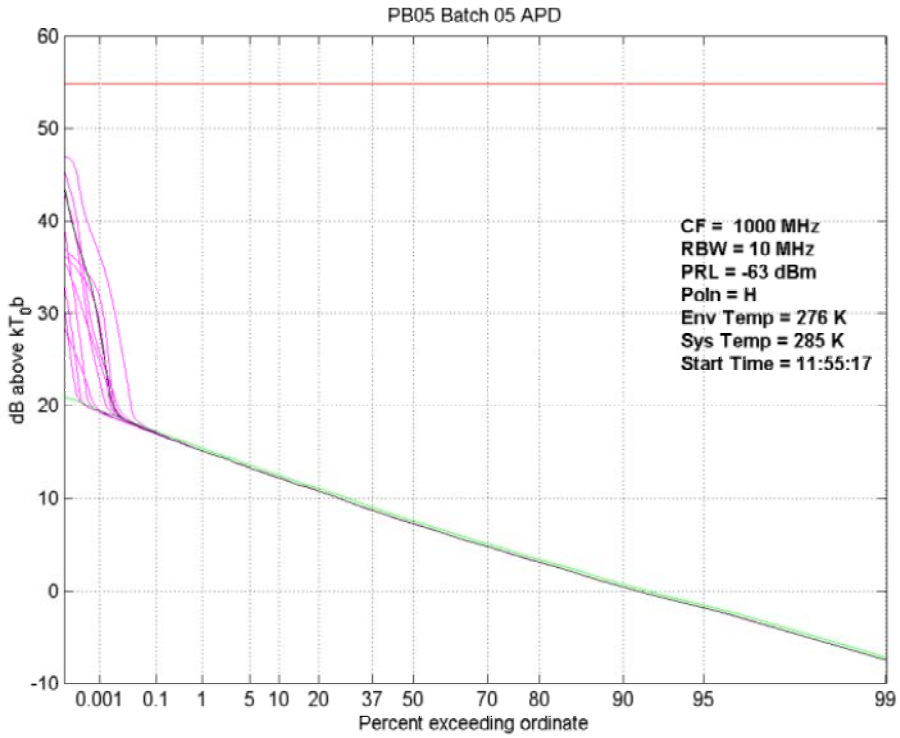

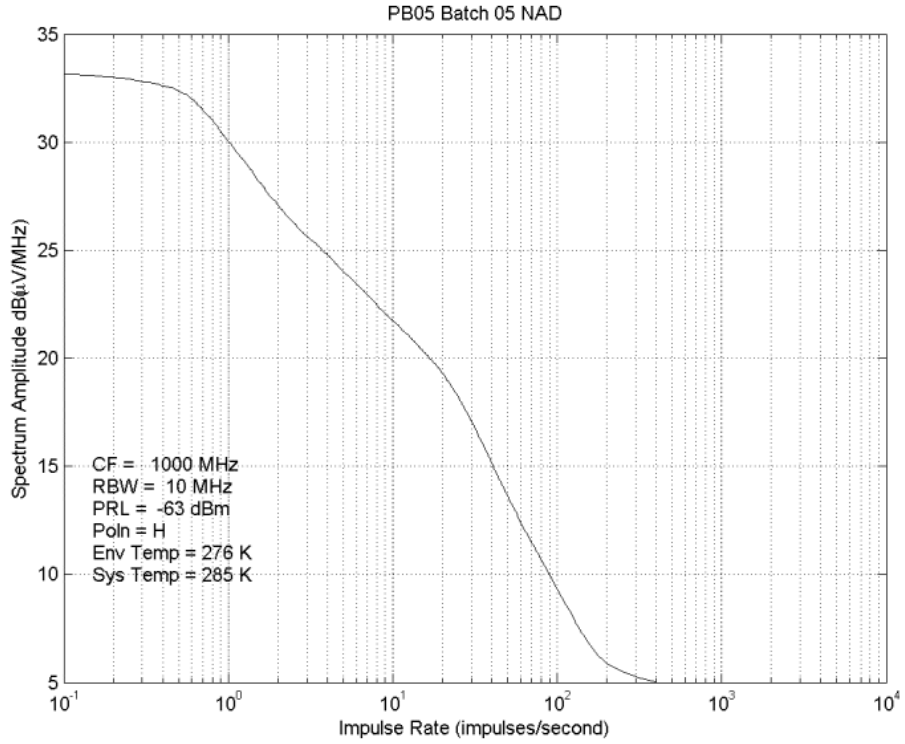

Figure 70 Railway APD and NAD (977 to 1010 MHz band)

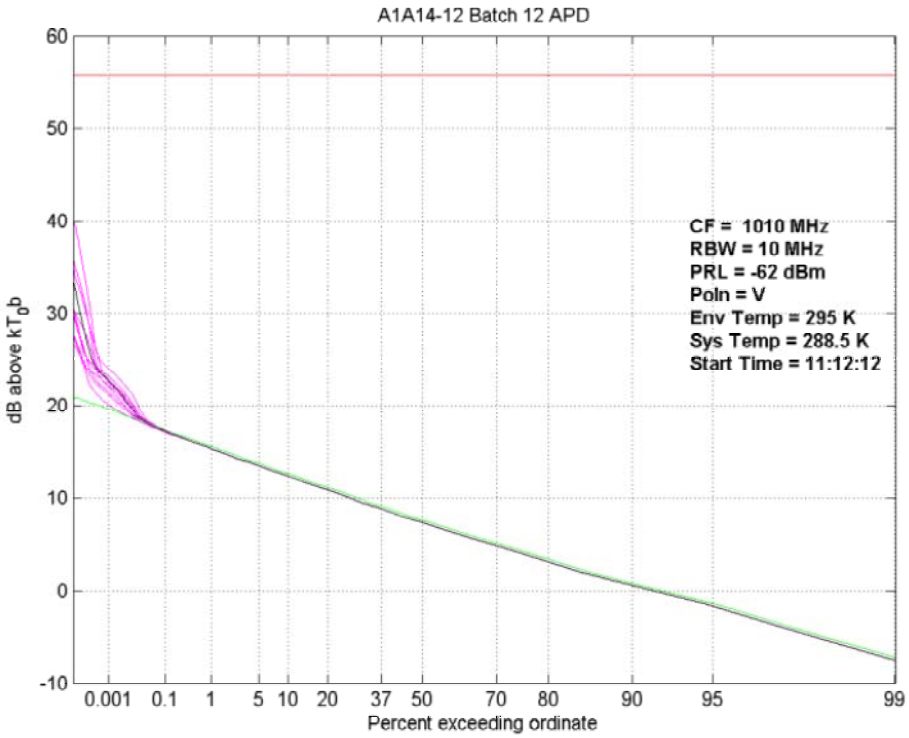

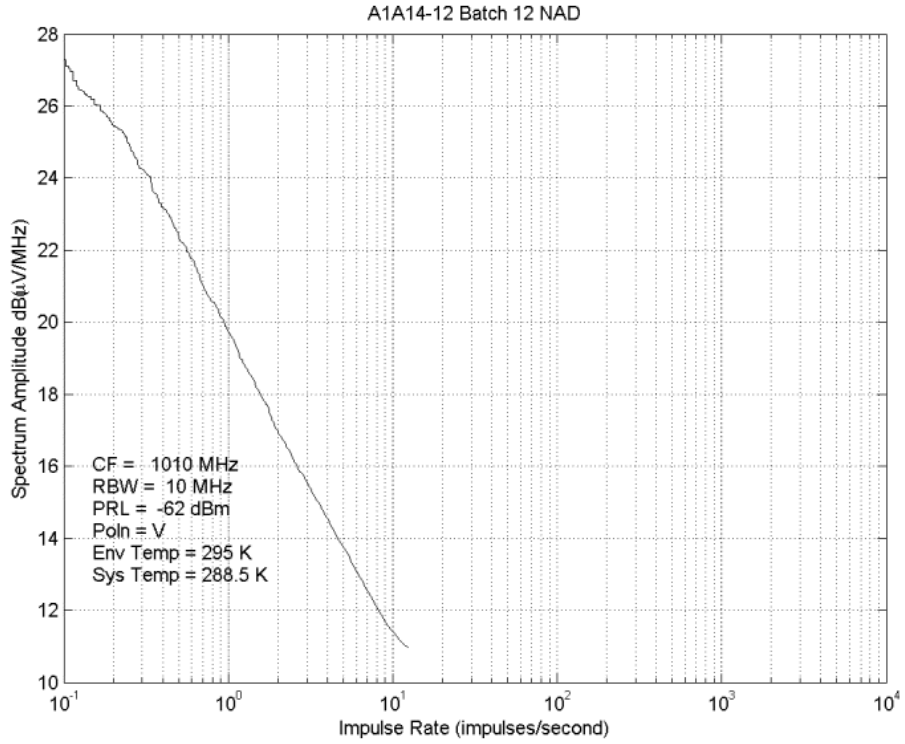

Figure 71 Road Junction APD and NAD (977 to 1010 MHz band)

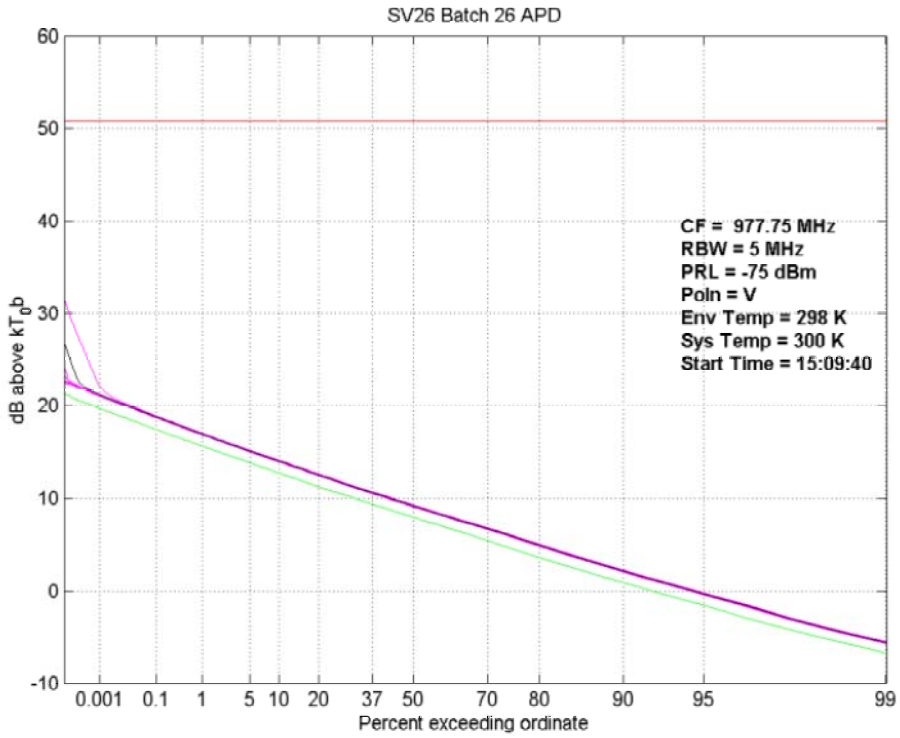

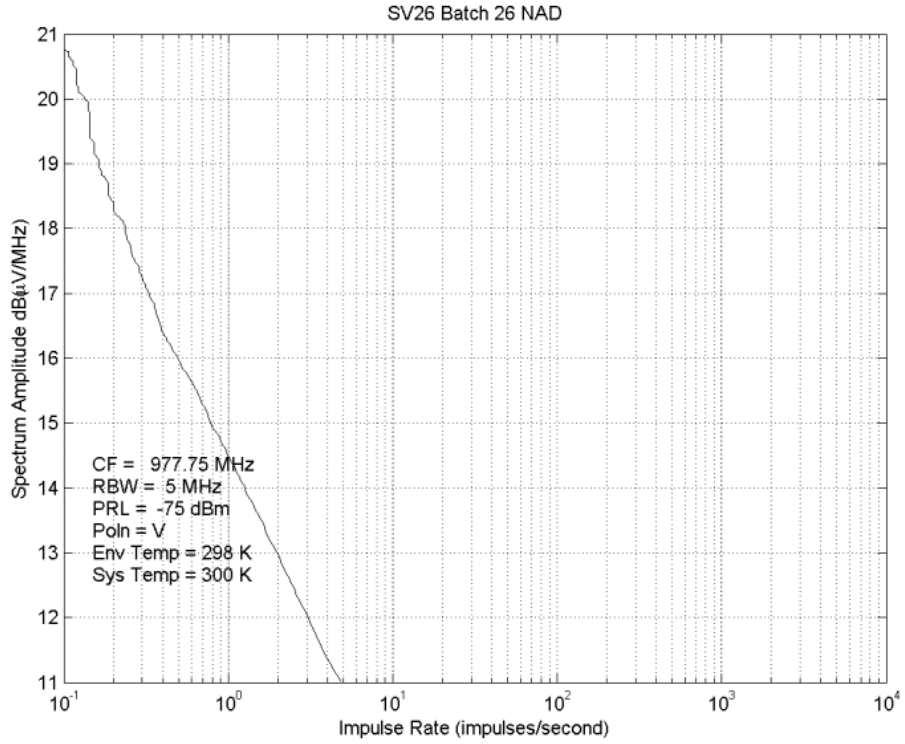

Figure 72 Business Centre APD and NAD (977 to 1010 MHz band)

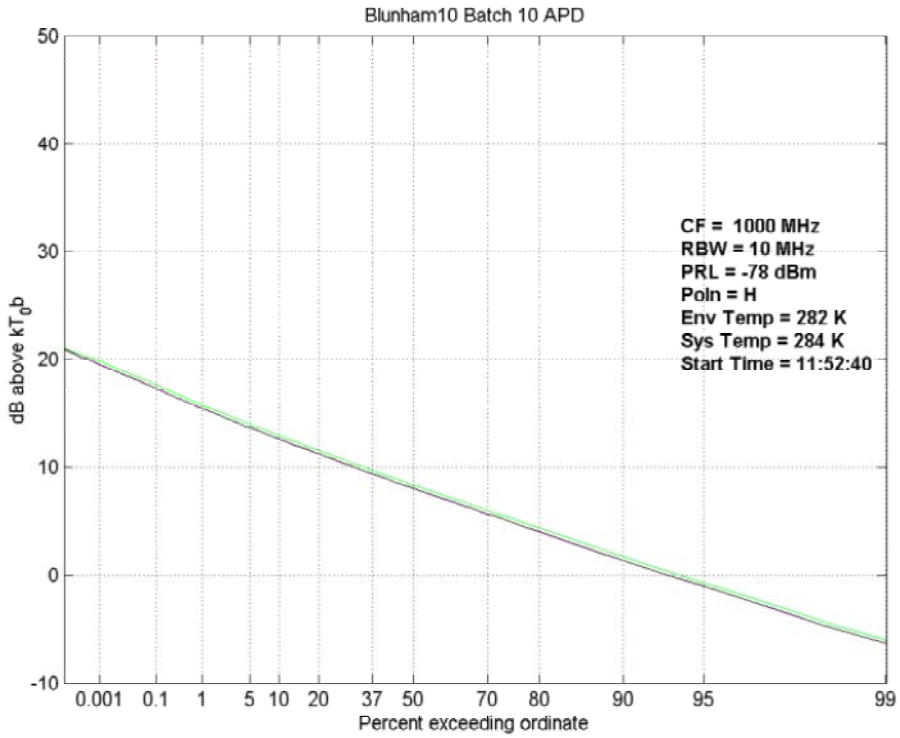

Figure 73 Rural APD (977 to 1010 MHz band)

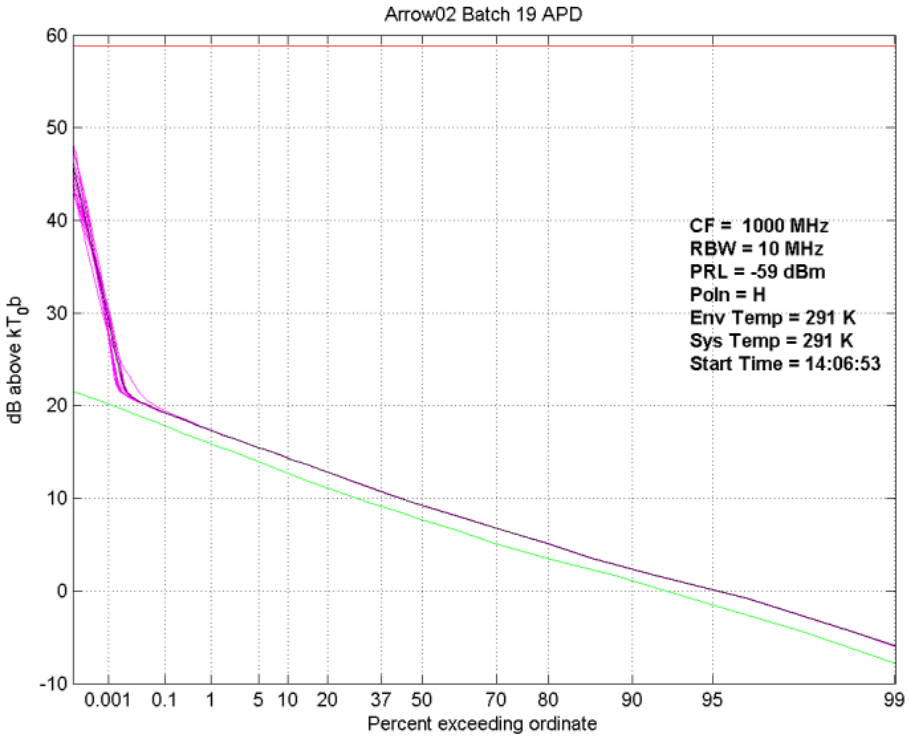

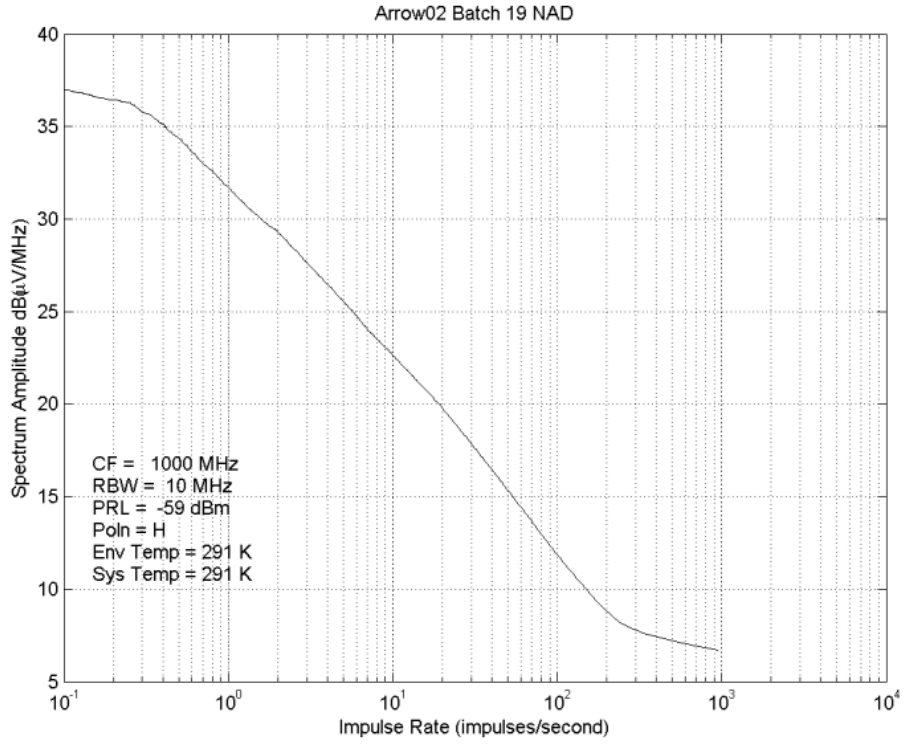

Figure 74 Factory Estate APD and NAD (977 to 1100 MHz band)